

Aus dem Institut für Kardiovaskuläre Physiologie und Pathophysiologie der Ludwig-Maximilians-Universität München



Dissertation
zum Erwerb des Doctor of Philosophy (Ph.D.)
an der Medizinischen Fakultät der
Ludwig-Maximilians-Universität zu München

**Localization and functional characterization of
renal dendritic cell subsets during steady state
and after acute kidney injury**

vorgelegt von:

Stephan Rambichler

aus:

Traunstein

Jahr:

2020

First supervisor: *Prof. Barbara Schraml-Schotta*

Second supervisor: *Prof. Gunnar Schotta*

Dean: **Prof. Dr. med. dent. Reinhard Hickel**

Datum der Verteidigung:

11.11.2020

Abstract

Dendritic cells (DCs) are important antigen-presenting cells, which can activate T cells after encounter of pathogens or tissue-damage and thereby bridge the innate and adaptive immune system. DCs can be split in two main subsets conventional DC1 (cDC1) and cDC2, each with their own unique role in the immune system. Interestingly, studies identified four major populations with DC origin in the kidney. In addition to cDC1 and cDC2 the kidney also contains F4/80^{hi} cells and CD11b^{hi} cells with a DC origin. Phenotypically, F4/80^{hi} cells resemble macrophages from other tissues and CD11b^{hi} cells are very similar to cDC2. Phenotypic overlap between DCs with other mononuclear phagocytes lead to conflicting data regarding the role of DCs in kidney injury. In this study we set out to better define the identity and function of renal DC subsets, in particular of F4/80^{hi} cells and CD11b^{hi} cells, using dendritic cell fate mapping, multicolour flow cytometry, confocal microscopy and RNA sequencing. We showed that CD11b^{hi} cells are closely related to cDC2 both in their localization but also their gene expression profile. Among differentially expressed genes between these cells we identified pattern-recognition receptors such as TLR7 and TLR8, which also correspond functional differences between cDC2 and CD11b^{hi} cells that were not known so far. We showed that F4/80^{hi} cells closely resemble splenic macrophages on a transcriptional level despite their DC origin. In addition, we demonstrated that F4/80^{hi} produce chemokines such as CXCL2, CCL17 and CCL2 after cisplatin-induced AKI and may thereby orchestrate the influx of monocytes, neutrophils and T-cells after kidney damage. Furthermore, we showed that F4/80^{hi} cells display major transcriptional changes after kidney injury, which causes downregulation of genes related to antigen-presentation and may be triggered by signalling through Prostaglandin E2 receptors. Using *Clec9a^{Cre}Rosa^{DTR}* depletion models we showed that cells with a DC origin may affect disease severity after cisplatin-induced kidney injury as evident by increased influx inflammatory cells and elevated serum markers for kidney damage. Interestingly, depletion of cDC1 using *XCR1^{Venus-DTR}* mice seemed to not affect the severity of cisplatin-induced AKI suggesting a minor role of cDC1 in early phases of AKI. Taken together, we were able to show that the kidney contains four phenotypically and functionally distinct dendritic cell subsets. We found that depletion of DCs prior to kidney injury exacerbates acute kidney injury, although cDC1 only play a minor role. Lastly, we showed that upon kidney injury F4/80^{hi} cells undergo a phenotypic and transcriptional switch, possibly mediated by Prostaglandin E2, which could hint at important functions of this subset in cisplatin-induced acute kidney injury.

Table of contents

Abstract	1
Table of contents	2
Table of Figures and Tables	6
Abbreviations	9
1. Introduction	10
1.1. Dendritic cell subsets and their functions	10
1.2. Ontogenetic differences define DCs, monocytes and macrophages.....	12
1.3. Genetically modified mouse models can be used to target specific mononuclear phagocyte subsets	14
1.4. The kidney contains a diverse mononuclear phagocyte network	16
1.5. Function and localization of DCs in the steady state kidney	17
1.6. The specific role of DCs in AKI is unclear	19
1.7. Research objectives.....	21
2. Materials and methods	22
2.1. Animal husbandry	22
2.2. Genotyping.....	22
2.3. Cell isolation for flow cytometry.....	23
2.3.1. Spleen and lymph nodes	23
2.3.2. Kidney.....	24
2.4. Flow cytometry	24
2.5. Cisplatin-induced acute kidney injury	25
2.6. Unilateral ischemia reperfusion injury	25
2.7. Diphtheria Toxin mediated cell depletion	25
2.8. RNA isolation and library construction	26
2.9. RNA sequencing analysis	26

2.10.	Immunofluorescence microscopy	27
2.11.	Histo-Cytometry.....	28
2.12.	Statistical Analysis.....	29
2.13.	Table of antibodies	29
2.14.	Analysis software	31
3.	Results	32
3.1.	Application of Histo-Cytometry to improve microscopic analysis of DC subsets in the kidney	32
3.1.1.	The adult kidney contains four distinct subsets of mononuclear phagocytes with DC origin	32
3.1.2.	Setup of Histo-Cytometry in lymph nodes to localize T cells and B cells	34
3.1.3.	Establishing Histo-Cytometry workflow in sections of early life kidney to identify DCs.....	36
3.1.4.	Localization of DC subsets in the kidney at different developmental time points	40
3.2.	The kidney contains four transcriptionally unique DC subsets	42
3.2.1.	Establishment of library preparation with low RNA input.....	42
3.2.2.	Sorting strategy to isolate splenic and renal DC subsets	43
3.2.3.	Characterization of transcriptional profiles of renal DC subsets.....	45
3.2.3.3.	F4/80 ^{hi} cells have a transcriptional profile similar to macrophages .	48
3.2.3.4.	CD11b ^{hi} cells are a unique DC subset with transcriptional characteristics of both macrophages and DCs.....	51
3.3.	F4/80 ^{hi} cells downregulate MHCII upon cisplatin-induced AKI and may orchestrate leukocyte infiltration through production of chemokines	54
3.3.1.	Disease induction after cisplatin-induced acute kidney injury	54
3.3.2.	YFP labelling remains restricted to DCs after cisplatin-induced acute kidney injury	55

3.3.3.	F4/80 ^{hi} cells downregulate MHCII on a protein level after cisplatin-induced kidney injury.....	58
3.3.4.	Ischemia reperfusion injury leads to influx of inflammatory cells and to a downregulation of MHCII on F4/80 ^{hi} cells.....	59
3.3.5.	YFP labelling remains restricted to DCs after ischemia-reperfusion-induced acute kidney injury	62
3.3.6.	Localization of DCs in the injured kidney	64
3.3.7.	F4/80 ^{hi} cells downregulate MHCII on a transcriptional level after cisplatin-induced acute kidney injury	66
3.4.	Depletion of cDCs using <i>Clec9a^{Cre}Rosa^{DTR}</i> exacerbates cisplatin-induced acute kidney injury	71
3.5.	cDC1 are dispensable for cisplatin-induced acute kidney injury	74
3.5.1.	Severity of acute kidney injury unchanged after depletion of XCR1 ⁺ cDC1	74
3.5.2.	cDC1 numbers are still decreased in the spleen 96h after depletion ..	75
3.5.3.	Mice with cDC1 depletion show a decreased infiltration of neutrophils	76
4.	Discussion.....	80
4.1.	Histo-Cytometry can be used to identify multiple DC subsets in the steady-state kidney	80
4.2.	Macrophages, monocytes or DCs – CD11b ^{hi} cells and F4/80 ^{hi} cells in the kidney	81
4.3.	F4/80 ^{hi} cells downregulate MHCII after acute kidney injury and may orchestrate recruitment of inflammatory cells to damaged areas	84
4.4.	Specific depletion of DCs with <i>Clec9a^{Cre}Rosa^{DTR}</i> may increase disease severity after cisplatin-induced AKI.....	86
4.5.	cDC1 are dispensable in cisplatin-induced AKI.....	87
4.6.	Outlook	88
	References.....	89

Acknowledgements	99
Appendix	100
Publications arising from this work:.....	100
Affidavit.....	101
Form of the “Münchner Universitätsgesellschaft”	102
Confirmation of congruency between printed and electronic version of the doctoral thesis	103
Curriculum vitae.....	104

Table of Figures and Tables

Figure 1. Commonly associated phenotypic markers and functional properties of DC subsets.....	10
Figure 2. Simplified developmental tree of mononuclear phagocytes.	13
Figure 3. Phenotypic characteristics of mononuclear phagocyte subsets in the kidney.	18
Figure 4. Schematic of the Histo-Cytometry workflow.	29
Figure 5: Gating strategy to identify DCs and YFP labelling in the kidney.....	32
Figure 6. Unsupervised clustering using tSNE analysis of renal leukocytes verifies specific labelling of renal DCs in <i>Clec9a^{Cre}Rosa^{YFP}</i> model.....	33
Figure 7. Microscopic image of murine lymph node stained for B220, CD3 and DAPI.	35
Figure 8. Histo-Cytometry in the lymph node.	35
Figure 9. Cell segmentation on immunofluorescence image of PND15 kidney based on Tomato expression.....	36
Figure 10. Watershed segmentation excludes cells with low F4/80 expression.	37
Figure 11. Combination of channels for efficient masking of cells.....	38
Figure 12. Multicolor immunofluorescence staining of adult kidney section.	39
Figure 13. Histo-Cytometry of adult kidney sections compared to flow cytometric data.	39
Figure 14. Histo-Cytometry of kidney sections at different developmental timepoints.	41
Figure 15. Histo-Cytometry of kidney sections at PND14.....	42
Figure 16. Sorting strategy for splenic cDCs and library preparation test with cDC1.	43
Figure 17. Sort purity of renal YFP ⁺ and YFP ⁻ F4/80 ^{hi} cells as well as CD11b ^{hi} cells.	44
Figure 18. PCA of renal and splenic DC populations as well as red pulp macrophages at steady state.....	46
Figure 19. Manual alignment of sequencing reads to identify <i>Cre</i> expression.	46
Figure 20. Comparison of normalized gene expression values between YFP ⁺ and YFP ⁻ populations.....	47
Figure 21. Clustering analysis between renal DC populations.	48

Figure 22. Expression of genes from cluster XI, XIII and XV.....	49
Figure 23. Core-macrophage and core-DC signature expression on renal DC subsets.	50
Figure 24. Pairwise comparison of CD11b ^{hi} cells to cDC2 and F4/80 ^{hi} cells.....	51
Figure 25. Heatmap of genes differentially expressed between cDC2 and CD11b ^{hi} cells.....	53
Figure 26. Differentially expressed pattern recognition receptors between renal DC subsets.....	54
Figure 27. Serum levels of BUN and creatinine.	55
Figure 28. Gating strategy to identify renal leukocyte populations after cisplatin- induced AKI.....	56
Figure 29. Quantification of renal leukocyte populations after cisplatin-induced AKI.	56
Figure 30. YFP labelling in renal leukocytes after cisplatin-induced AKI.....	57
Figure 31. tSNE analysis of renal leukocytes after cisplatin-induced AKI.....	58
Figure 32. F4/80 ^{hi} cells downregulate MHCII after cisplatin-induced AKI.....	59
Figure 33. Gating strategy to identify renal myeloid and lymphoid cell populations after IRI.....	60
Figure 34. Frequency of mononuclear phagocyte populations in the kidney after IRI.	61
Figure 35. Loss of MHCII expression on F4/80 ^{hi} cells after IRI.	62
Figure 36. YFP labelling in renal leukocyte populations.	63
Figure 37. tSNE analysis of renal leukocytes after IRI.	64
Figure 38. Analysis of CC3 staining after cisplatin-induced AKI.....	65
Figure 39. Quantification of MHCII ⁺ and MHCII ^{neg} F4/80 ^{hi} cells in the kidney.	66
Figure 40. Gating strategy and sort purity for transcriptional analysis of F4/80 ^{hi} cells.	67
Figure 41. PCA of F4/80 ^{hi} cells during steady state and after cisplatin-induced AKI.....	68
Figure 42. Pairwise comparisons of F4/80 ^{hi} cells after cisplatin-AKI.	69
Figure 43. Selected differentially expressed genes and expression of cytokines in F4/80 ^{hi} cells after cisplatin-induced AKI.	70
Figure 44. Upregulated expression of cytokines in F4/80 ^{hi} cells after cisplatin-induced AKI.	71

Figure 45. Disease severity and weight loss 48 h after cisplatin-induced AKI in <i>Clec9a^{Cre}Rosa^{DTR}</i> mice.	72
Figure 46. Quantification of lymphoid populations in the kidney after AKI in <i>Clec9a^{Cre}Rosa^{DTR}</i> mice.	73
Figure 47. Serum creatinine and BUN levels 72h after AKI in <i>XCR1^{Venus-DTR}</i> mice. .	75
Figure 48. cDC1 are decreased in kidney and spleen 96h after DT injection in <i>XCR1^{Venus-DTR}</i> mice.....	75
Figure 49. Myeloid populations in the kidney after AKI in <i>XCR1^{Venus-DTR}</i> mice.	76
Figure 50. Gating strategy to identify T cell subsets and ILCs in the kidney.	77
Figure 51. Quantification of lymphoid populations in the kidney after AKI in <i>XCR1^{Venus-DTR}</i> mice.....	78
Figure 52. Frequency of lymphoid cells in the kidney after AKI in <i>XCR1^{Venus-DTR}</i> mice.	78
<i>Table 1. List of used oligonucleotides</i>	22
<i>Table 2. Used PCR protocols for genotyping</i>	23
<i>Table 3. Preparation of Percoll dilutions</i>	24
<i>Table 4. List of used antibodies</i>	29
<i>Table 5. List of used software</i>	31

Abbreviations

Abbreviation	Full name
AKI	Acute kidney injury
bp	Base pairs
CC3	Cleaved Caspase 3
cDC1	Conventional dendritic cell type 1
cDC2	Conventional dendritic cell type 2
CDPs	Common dendritic cell progenitors
cMoPs	Common monocyte progenitor
CMPs	Common myeloid progenitor
DCs	Dendritic cells
DNA	Deoxyribonucleic acid
DT	Diphtheria toxin
DTR	Diphtheria toxin receptor
EMPs	Erythromyeloid progenitor
FACS	Fluorescence-activated cell sorting
GFP	Green fluorescent protein
HBSS	Hank's balanced salt solution
IFN γ	Interferon γ
ILC	Innate lymphoid cell
IRI	Ischemia reperfusion injury
MHCII	Major histocompatibility complex II
PBS	Phosphate buffered saline
PC	Principal component
PCA	Principal component analysis
PCA	Principal component analysis
pDCs	Plasmacytoid dendritic cells
PGE2	Prostaglandin E2
RNA	Ribonucleic acid
RNAseq	Bulk mRNA sequencing
TLR	Toll-like receptor
TPM	Transcripts per kilobase million
Treg	Regulatory T cell
WT	Wildtype
YFP	Yellow fluorescent protein

1. Introduction

1.1. Dendritic cell subsets and their functions

Dendritic cells (DCs) were discovered as a novel cell type in mouse lymphoid organs by Steinman and Cohn in 1973 (Steinman & Cohn, 1973). Even though the function of DCs was debated early on, they were later found to be the proposed ‘accessory cells’ for the induction of T cell responses (Steinman & Witmer, 1978; Nussenzweig, Steinman, Gutchinov, & Cohn, 1980). DCs are potent antigen-presenting cells, which are characterized by their ability to activate T cell responses, which allows DCs to bridge the innate and adaptive immune system (Nussenzweig et al., 1980; Nussenzweig et al., 1981; Steinman & Witmer, 1978). Later it was discovered that CD11c⁺MHCII⁺ DCs are a heterogeneous population consisting of two types of so called conventional DCs, CD8α⁺ cDC1 and CD11b⁺ cDC2. In addition, type I interferon producing plasmacytoid DCs (pDCs) can be found (Figure 1) (Asselin-Paturel et al., 2001; Schraml & Reis e Sousa, 2015; Vremec et al., 1992).




DC subset	pDC 	cDC1 	cDC2 
Phenotypic markers	CD11c ^{low} MHCII ^{low} B220 ⁺ Ly6C ⁺	CD11c ⁺ MHCII ⁺ CD103 ⁺ CD205 ⁺ XCR1 ⁺	CD11c ⁺ MHCII ⁺ CD11b ⁺ Clec4a4 ⁺ CD172a ⁺
Functions	Anti viral response	Defense against intracellular pathogens	Defense against extracellular pathogens

Figure 1. Commonly associated phenotypic markers and functional properties of DC subsets. pDCs, cDC1 and cDC2 can be distinguished by different phenotypic markers such as B220, CD103 and CD11b. It is necessary to distinguish between different DC subsets because each subset can possess unique functions which would be missed otherwise.

After their discovery, characterization of DC subsets especially in non-lymphoid tissue was complicated because a lot of surface markers, which were used to identify these cells in lymphoid tissue were not expressed in the non-lymphoid environment (del Rio, Rodriguez-Barbosa, Kremmer, & Förster, 2007). In non-lymphoid tissue cDC1 were discovered to express CD103 and/or XCR1 (del Rio et al., 2007; Dorner et al., 2009). A hallmark function of this subset is their ability to cross-present antigens on MHCI to activate CD8 α^+ T cells, which is an important mechanism for fighting intracellular pathogens (Haan, Lehar, & Bevan, 2000; Hildner et al., 2008). Activated cDC1 can produce high amounts of IL12 and thereby drive differentiation of naïve CD4 $^+$ T cells into Th1 cells (Reis e Sousa et al., 1997). Development of cDC1 is dependent on different transcription factors such as IRF8, Id2 and BATF3 (Aliberti et al., 2003; Hacker et al., 2003; Hildner et al., 2008). The second cDC subset cDC2 can be characterized by the expression of CD11b, CD172 α or Clec4a4 in most tissues (Crowley, Inaba, Witmer-Pack, & Steinman, 1989; Dudziak et al., 2007; Merad, Sathe, Helft, Miller, & Mortha, 2013; Metlay et al., 1990). Studies showed that cDC2s are itself a heterogeneous population containing Notch2-dependent ESAM^{hi} and Notch2-independent ESAM^{low} subsets (Lewis et al., 2011). Apart from Notch2 also IRF4, IRF2, RelB and RBP-J were shown to be important transcription factors controlling cDC2 development (Caton, Smith-Raska, & Reizis, 2007; Ichikawa et al., 2004; Lewis et al., 2011; Suzuki et al., 2004; Wu et al., 1998). cDC2 are very efficient activators of CD4 $^+$ T cells and were shown to drive differentiation of Th17 cells and Th2 cells (Dudziak et al., 2007; Persson et al., 2013; Schlitzer et al., 2013; Tussiwand et al., 2015). Additionally, it was demonstrated that cDC2 are necessary for induction of T follicular helper cells (Briseño et al., 2018; Shin et al., 2016). Plasmacytoid DCs are a completely separate subset with lower expression of CD11c and MHCII (Asselin-Paturel et al., 2001). They express other markers such as B220, Ly6C and SiglecH and can produce high amounts of interferon- α upon viral infection (Asselin-Paturel et al., 2001; Siegal et al., 1999). pDC development seems mainly regulated by the transcription factor E2-2 (Cisse et al., 2008). Characterization of DCs is complicated by their phenotypic and functional overlap with macrophages, monocytes and monocyte-derived cells, especially during inflammation (Mildner & Jung, 2014). Considering the limitations of phenotypic characterization of macrophages, DCs and monocytes it was suggested to define these cells by their ontogeny (Guilliams et al., 2014).

1.2. Ontogenetic differences define DCs, monocytes and macrophages

Most DCs are short-lived cells, which need constant replenishment from precursors in the bone marrow (Merad et al., 2013; Mildner & Jung, 2014). Due to an overlap of functional features and phenotypic characteristics DCs were grouped together with monocytes and macrophages in a so-called mononuclear phagocyte system, which was thought to derive from common progenitors in the bone marrow (van Furth, 1981). However, recent studies established DCs, monocytes and macrophages as ontogenetically and functionally distinct lineages with different developmental requirements (Guilliams et al., 2014; Schraml & Reis e Sousa, 2015). At the stage of the multipotent progenitor, cell development branches into common lymphoid progenitors, which can give rise to B cells, T cells and NK cells, or common myeloid progenitors (CMPs), which can ultimately give rise to monocytes, macrophages and DCs (Akashi, Traver, Miyamoto, & Weissman, 2000; Auffray et al., 2009; Kondo, Weissman, & Akashi, 1997). CMPs can further give rise to monocyte and DC committed precursors (MDPs), which can then differentiate to common monocyte progenitors (cMoPs), a precursor for monocytes and macrophages, or DC-lineage-committed common dendritic cell precursors (CDPs) (Auffray et al., 2009; Fogg et al., 2006; Hettinger et al., 2013; Onai et al., 2007). CDPs can give rise to pDCs and pre-DCs, which leave the bone marrow, seed different tissues and ultimately differentiate into the conventional DC subsets mentioned before (Figure 2) (K. Liu et al., 2009; Naik et al., 2006). Recent studies suggest that there is heterogeneity among pre-DCs and that there are subpopulations, which are pre-committed to specific cDC subsets before leaving the bone marrow (Grajales-Reyes et al., 2015; Schlitzer et al., 2015; See et al., 2017).

DC development largely depends on the growth factor receptor FLT3 and its ligand FLT3L (McKenna et al., 2000). Administration of FLT3L leads to an expansion of DCs in the tissue and studies utilizing *Flt3^{-/-}* and *Flt3l^{-/-}* mice showed a dramatic decrease of DCs (Maraskovsky et al., 1996; McKenna et al., 2000; Waskow et al., 2008). Moreover, FLT3 is expressed on CDPs and addition of FLT3L to BM cultures *in vitro* leads to the development of mature cDCs (Brasel, De Smedt, Smith, & Maliszewski, 2000; Kingston et al., 2009; Naik et al., 2005). Interestingly, monocytes and

macrophages are not affected by a loss of FLT3 signaling, making FLT3L-dependency a characteristic feature of DCs (Waskow et al., 2008).

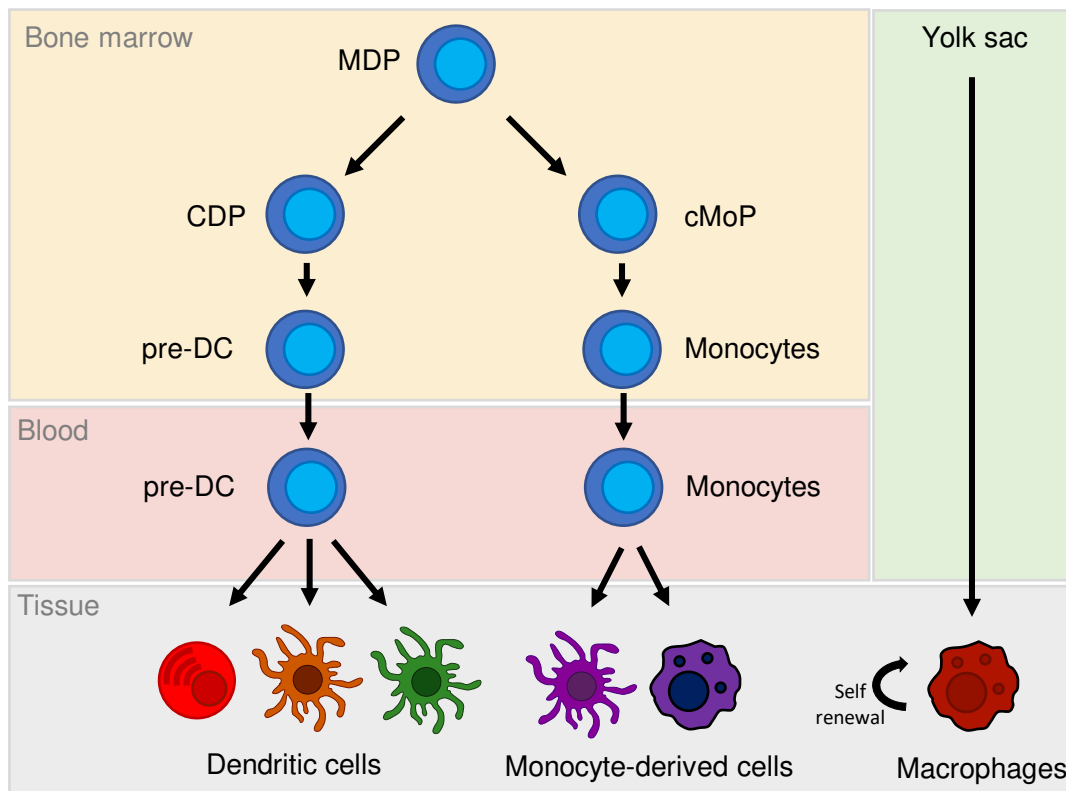


Figure 2. Simplified developmental tree of mononuclear phagocytes. Development of DCs and monocytes splits into two independent ontogenetic trees at the stage of the MDP, which gives rise to DC progenitor CDP and monocyte progenitor cMoP. Macrophages can develop independent of the bone marrow from yolk sac progenitors, are long-lived and can possess the ability to self renew.

In contrast to DCs and monocytes, which arise from definitive hematopoiesis, development of macrophages already begins in a first wave at embryonic day 7.25 (E7.25) from progenitors in the yolk sac (Ginhoux et al., 2010). Erythro-myeloid progenitors (EMPs) develop in the yolk sac in a second wave after E8.25 and are the major source of tissue-resident macrophages in various organs at this time point (Gomez-Perdiguero et al., 2015). From E10.5 onwards definitive hematopoiesis is established when hematopoietic stem cells (HSCs) develop in the aorto-gonad-mesonephros and migrate to the liver (Bertrand et al., 2010; Kissa & Herbomel, 2010). Definitive hematopoiesis later shifts to the bone marrow (Bertrand et al., 2010). Macrophages are usually long-lived cells, which have the ability to renew, therefore in

some tissues yolk sac-derived macrophages even persist in adulthood (Hashimoto et al., 2013; Schulz et al., 2012). With increased age the pool of yolk sac-derived macrophages gets diluted by monocytes which can also give rise to tissue resident macrophages (Gentek, Molawi, & Sieweke, 2014). Macrophages and monocytes are regulated through CSF-1 and IL-34, which bind to CSF-1R (CD115) (Cecchini et al., 1994; Y. Wang et al., 2012). Disruption of signaling through CSF-1R leads to an absence of monocytes and macrophages, but not DCs, across different tissues (Dai et al., 2002; Erblich, Zhu, Etgen, Dobrenis, & Pollard, 2011).

The origin of mononuclear phagocytes, even though complex, can be an important tool in understanding the function of these cells in different tissues. Moreover, mouse models were created, which utilized the different ontogeny of DCs, macrophages and monocytes to their advantage and thereby enabled a better characterization of these cells independent of phenotypic markers (Poltorak & Schraml, 2015).

1.3. Genetically modified mouse models can be used to target specific mononuclear phagocyte subsets

Many studies, which analyzed the phenotype, function and ontogeny of mononuclear phagocytes were only possible with the use of genetically modified mouse models. Systemic knockout of certain genes such as *Ccr2*^{-/-}, *Flt3l*^{-/-} or *Batf3*^{-/-} allowed to study developmental requirements or to achieve a cell depletion (Poltorak & Schraml, 2015). Another approach to study mononuclear phagocytes was with transgenic mice in which the expression of fluorescent reporters or diphtheria toxin receptor (DTR) (Poltorak & Schraml, 2015). Mice are not sensitive to diphtheria toxin (DT) and thereby cells expressing a human DTR can be conditionally depleted via injection of DT without major side effects (Saito et al., 2001). In addition, the rise of the *Cre-LoxP* system made studying mononuclear phagocyte function more efficient because mice with a CRE recombinase inserted in specific loci could be crossed to mice with either fluorescent reporters or DTR inserted in the *Rosa26* locus controlled by a promoter flanked with *lox-stop-lox* sites (Poltorak & Schraml, 2015; Vorhagen et al., 2015). Mice expressing DTR and green fluorescent protein (GFP) under the control of the CD11c promoter were used early on to study the function of DCs (Jung et al., 2002). However, since CD11c is also expressed by other cell types, such as macrophages or non-myeloid cells, conclusions from this model cannot be attributed specifically to DCs

(Probst et al., 2005; van Blijswijk, Schraml, & Reis e Sousa, 2013). A better alternative to CD11c as the driving promoter is the use of ZBTB46. ZBTB46 is expressed in the DC lineage and in endothelial cells but not in other myeloid populations at steady state, making *Zbtb46^{GFP}* and *Zbtb46^{DTR}* mice viable tools to study DC function (Meredith et al., 2012; Satpathy et al., 2012). However, because of ZBTB46 expression in endothelial cells DT injection in *Zbtb46^{DTR}* mice is lethal, making bone marrow chimeras a necessity for DC depletion experiments (Meredith et al., 2012). It also needs to be considered that activated monocytes upregulate expression of ZBTB46, which will lead to labelling in non-DCs during injury or disease (Satpathy et al., 2012). In addition, cDC1 specific *Xcr1^{Venus-DTR}* and *Clec9a^{DTR}* mice, cDC2 specific *Clec4a4^{DTR}* mice and other models allow to address the function of DC-subsets via subset-specific depletion through DT injection (Muzaki et al., 2016; Piva et al., 2012; Yamazaki et al., 2013). Monocytes and macrophages were routinely targeted using *Cx3cr1^{Cre}* or *LyzM^{Cre}* mouse models, however, same as with CD11c the expression of *Cx3cr1* and *LyzM* is not specific enough for these cell types to allow precise conclusions (Clausen, Burkhardt, Reith, Renkawitz, & Förster, 1999; Z. Liu et al., 2019; Yona et al., 2013). Even though some models have limitations, they nevertheless provide a powerful tool to unravel the role of the DC lineages or specific DC subsets during health and disease in various organs. Especially depletion models targeting subsets such as *XCR1^{Venus-DTR}* for cDC1 have the potential to shine light into subset-specific roles of DC subsets. The use of CRE recombinase expression also allowed to discern ontogenetic relationships or follow the fate of differentiated cells across tissues by choosing genes, which are only active in progenitor cells but not their progeny, or by utilizing tamoxifen-inducible CRE expression (Metzger, Clifford, Chiba, & Chambon, 1995; Poltorak & Schraml, 2015). DC development was addressed using the gene *Clec9a*, which was found to be specifically expressed in the DC-lineage by cDC1, DC progenitors in the bone marrow and by pDCs (Caminschi et al., 2008; Poulin et al., 2012; Sancho et al., 2008; Schraml et al., 2013). As such, the use of *Clec9a^{Cre}Rosa^{YFP}* mice allowed to trace DC progenitors and their progeny across lymphoid and non-lymphoid tissue (Schraml et al., 2013). For cells which do not express *Clec9a* the labelling in *Clec9a^{Cre}Rosa^{YFP}* is therefore a true indicator of DC origin. Crossing *Clec9a^{Cre}* to *Rosa^{DTR}* mice also allows DC-lineage specific cell depletion (Salvermoser et al., 2018; van Blijswijk et al., 2015). Additionally, a recent study by Liu *et al.* identified *Ms4a3* as a suitable model to identify monocyte-derived cells across tissues (Z. Liu et al., 2019).

Ms4a3 is expressed by GMPs and neutrophils and thereby allows the assessment of monocyte-contribution to myeloid cell populations without unspecific labelling in DC subsets (Z. Liu et al., 2019). Taken together, the wealth of established and new fate-mapping and depletion models can be utilized to further explore the functions of macrophages, monocytes and DC subsets especially during disease. However, because many models are not subset specific it may be necessary to use a combination of different models to reach precise conclusions.

1.4. The kidney contains a diverse mononuclear phagocyte network
Using different reporter lines, phenotyping via flow cytometry and single cell RNA sequencing it was shown that the murine kidney contains at least six different populations of mononuclear phagocytes at steady state (Guilliams et al., 2016; Kawakami et al., 2013; Schraml et al., 2013; Zimmerman et al., 2019). Five of these populations express classic DC markers, i.e. expression of CD11c and MHCII (Kawakami et al., 2013). Same as in other non-lymphoid organs the kidney contains CD103⁺XCR1⁺CD24⁺ cDC1 and CD11b⁺ cDC2, both of which express high levels of CD11c and MHCII (Ginhoux et al., 2009; Schraml et al., 2013; Zimmerman et al., 2019). Additionally, a small population of B220⁺Ly6C⁺ pDCs can be found (Deng et al., 2020; Zimmerman et al., 2019). However, the vast majority among CD11c⁺MHCII⁺ cells express CD64 and F4/80, markers which were used in other tissues to define monocyte-derived cells or macrophages (Austyn & Gordon, 1981; Langlet et al., 2012; Tamoutounour et al., 2012). These CD64⁺ cells were shown to include F4/80^{hi}CD11b^{low} as well as CD11b^{hi}F4/80^{low} cells (Kawakami et al., 2013; Schraml et al., 2013). CD11b^{hi}F4/80^{low} cells are phenotypically similar to cDC2 except for their expression of CD64 (Guilliams et al., 2016). In addition, they show classic DC features as their development depends on FLT3L same as for other cDCs and CDPs can give rise to this population in transfer experiments (Schraml et al., 2013). Although CD11b^{hi}F4/80^{low} cells are labelled in *Clec9a^{Cre}Rosa^{YFP}* mice, the amount of labelled cells is lower compared to cDC2, indicating additional heterogeneity in CD11b^{hi}F4/80^{low} cells (Salei et al., 2020; Schraml et al., 2013). Whether CD11b^{hi}F4/80^{low} cells and cDC2 differ in their transcriptional profile or their function has not been addressed yet. F4/80^{hi}CD11b^{low} cells resemble macrophages both in their expression of markers such as F4/80 and CD64, but also based on their

transcriptomic signature (Cao et al., 2015). However, the origin of these cells is complex. In early life F4/80^{hi}CD11b^{low} cells are derived from yolk sac progenitors or EMPs and were shown to be important for nephron formation (Hoeffel et al., 2015; Munro et al., 2019; Salei et al., 2020; Schulz et al., 2012). However, starting from around two weeks after birth F4/80^{hi}CD11b^{low} cells deriving from DC progenitors in the bone marrow start to appear as shown with the *Clec9a^{Cre}Rosa^{YFP}* model or from monocytes as demonstrated by the *Ms4a3* monocyte tracing model (Salei et al., 2020; Liu et al., 2019). In contrast to yolk sac-derived F4/80^{hi}CD11b^{low} cells, the bone marrow-derived cells express MHCII, which could hint at a different functional role more related to recognition of pathogens and antigen presentation (Lever et al., 2019; Salei et al., 2020). Interestingly, despite their possible DC origin, F4/80^{hi}CD11b^{low} cells are long-lived and do not depend on FLT3L for their development (Guilliams et al., 2016; Puranik et al., 2018; Schraml et al., 2013; Stamatiades et al., 2016). Current evidence suggests that the pool of F4/80^{hi}CD11b^{low} cells might consist of cells with different origin, but whether the origin of F4/80^{hi}CD11b^{low} cells has an impact on their function and whether all F4/80^{hi}CD11b^{low} cells share the same developmental requirements needs to be addressed in future studies.

1.5. Function and localization of DCs in the steady state kidney

Early localization studies in the kidney found that mononuclear phagocytes form a dense interstitial network across the whole kidney (Hume & Gordon, 1983; Soos et al., 2006). Localization of immune cells is important for efficient immune responses as shown in other organs (Germain et al., 2008). Therefore, the localization of DC subsets in the kidney could have important consequences for their functions during injury or disease. Most of the myeloid cells in the kidney are F4/80^{hi}CD11b^{low} cells found in the renal medulla, however, there is also a substantial number of F4/80^{hi} cells in the renal cortex (Hume & Gordon, 1983). Precise localization of DC subsets and monocyte-derived cells is difficult because of substantial phenotypic overlap in these populations (Figure 3) and the limited number of markers which can be used in fluorescent microscopy due to spectral overlap (Kawakami et al., 2013). New approaches utilizing imaging mass cytometry showed that both cDC1, cDC2 and monocytes seem to be mostly localized in the renal cortex close to major vessels and in close contact to T cells and B cells (Brähler et al., 2017). Same as in other organs, a major role of cDCs

is in the kidney is to monitor their surroundings and to induce T cell activation upon contact with an antigen (Yatim, Gosto, Humar, Williams, & Oberbarnscheidt, 2016). In addition, a recent study by Lu *et al.* demonstrated that cDCs are involved in mediating hypertension through activation of T-cells after chronic Angiotensin II infusion (X. Lu *et al.*, 2019).






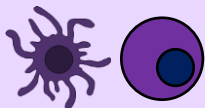
pDC	cDC1	cDC2	CD11b ^{hi}	F4/80 ^{hi}	Monocyte-derived cells
					
CD11c ^{low} MHCII ^{low} B220 ⁺ Ly6C ⁺	CD11c ⁺ MHCII ⁺ XCR1 ⁺ CD24 ⁺	CD11c ⁺ MHCII ⁺ CD11b ⁺ CD64 ⁻	CD11c ⁺ MHCII ⁺ CD11b ⁺ CD64 ^{low} F4/80 ^{low}	CD11c ⁺ MHCII ⁺ CD11b ^{low} CD64 ⁺ F4/80 ^{hi}	CD11c ⁺ MHCII ⁺ CD11b ⁺ Ly6C ⁺ F4/80 ^{low}

Figure 3. Phenotypic characteristics of mononuclear phagocyte subsets in the kidney.

Renal mononuclear phagocytes share the expression of many markers such as CD11c and MHCII. To distinguish these populations many additional markers, such as B220, CD24, CD11b, CD64, F4/80 and Ly6C, must be taken in consideration to ensure a proper identification of cells

F4/80^{hi}CD11b^{low} cells are not only localized in the interstitium, but also directly at the Bowman's capsule forming a ring around glomeruli (Hume & Gordon, 1983). In line with this, F4/80^{hi}CD11b^{low} cells were shown to process particles directly at the glomeruli through trans-endothelial processes and thereby mediate inflammatory responses (Stamatiades *et al.*, 2016). F4/80^{hi}CD11b^{low} cells are found in high numbers in the renal medulla, an observation that may be caused by a salt gradient in the kidney with highest salt concentrations in this area (Berry *et al.*, 2017). Consequently, F4/80^{hi}CD11b^{low} cells were shown to be crucial for protection against uropathogenic *Escherichia coli* which enter the renal medulla through the ureter (Berry *et al.*, 2017). Moreover, it was shown that yolk sac derived macrophages play an important role during kidney organogenesis by promoting endothelial cell growth and through clearance of apoptotic cells (Munro *et al.*, 2019).

1.6. The specific role of DCs in AKI is unclear

Two commonly used experimental acute kidney injury (AKI) models used on mice are ischemia reperfusion injury (IRI)-induced AKI and cisplatin-induced AKI (Rogers, Ferenbach, Isenberg, Thomson, & Hughes, 2014). Cisplatin is a common platinum-containing chemotherapeutic drug used against a variety of different cancers (Dasari & Tchounwou, 2014). Once taken up by a cell cisplatin binds to DNA and blocks cell division causing cell death (Dasari & Tchounwou, 2014). A common side-effect of cisplatin treatment is nephrotoxicity caused by cisplatin-uptake through organic cation transporter OCT2 and copper transporter Ctr1 in renal proximal tubular epithelial cells (Ciarimboli et al., 2010; Ozkok & Edelstein, 2014; Volarevic et al., 2019). Cisplatin-induced AKI causes an increase of CX3CL1 production in endothelial cells and upregulation of CXCL2 and CXCL1 leading to an influx of neutrophils and inflammatory monocytes (Chan et al., 2014; L. H. Lu et al., 2008; Tadagavadi & Reeves, 2010b). To induce ischemia-reperfusion injury blood flow to the kidney is blocked for a certain amount of time, which causes ischemia, hypoxia and leads to inflammation and organ damage (Malek & Nematbakhsh, 2015; Marschner, Schäfer, Holderied, & Anders, 2016). Additional murine AKI models which are used are unilateral ureteral obstruction and rhabdomyolysis-induced AKI caused by severe muscle damage (Bao, Yuan, Chen, & Lin, 2018). Kidney damage after AKI can be identified by the accumulation of waste products like blood urea nitrogen (BUN) and serum creatinine in the blood or through measurement of the glomerular filtration rate (GFR) (Holditch, Brown, Lombardi, Nguyen, & Edelstein, 2019).

Kidney injury models in combination with mouse models to deplete macrophages, DCs or DC subsets can be powerful tools to study the functions of these cells during AKI. However, because of considerable phenotypic overlap between DCs, macrophages and inflammatory monocytes entering the kidney upon injury (Figure 3) (Weisheit, Engel, & Kurts, 2015). As an alternative, clodronate liposomes can be used to deplete macrophages and DCs without the need of a specific mouse model (Ferenbach et al., 2012; Van Rooijen & Sanders, 1994). Once taken up by phagocytes via endocytosis, clodronate liposomes lead to apoptosis and cell death in these cells (Moreno, 2018). A downside of this method is that not only macrophages and DCs but also monocytes are affected by this method (Ferenbach et al., 2012). The use of different depletion

models, each with their own limitations, caused conflicting results about the function of DCs during AKI.

Ablation of phagocytes using clodronate liposomes before induction of cisplatin-induced AKI did not change the disease severity, however it can improve disease outcome after 24h IRI induction (Ferenbach et al., 2012; L. H. Lu et al., 2008). In contrast to this finding, depletion of CD11c⁺ cells using CD11c^{DTR/GFP} mice which targets the same cells as depletion via clodronate liposomes showed an exacerbation of cisplatin-induced AKI (Tadagavadi & Reeves, 2010b). A potential protective effect of CD11c⁺ cells during cisplatin-induced AKI may be explained by their production of IL10, however which of the CD11c⁺ subsets in the kidney produce this cytokine is not clear (Tadagavadi & Reeves, 2010a). A study by Tadagavadi *et al.* further demonstrated that the protective effect of CD11c⁺ cells is independent of neutrophils despite the observation of higher neutrophil infiltration after cisplatin-induced AKI in mice with depletion of CD11c⁺ cells (Tadagavadi, Gao, Wang, Gonzalez, & Reeves, 2015). Interestingly, depletion of phagocytes 24h after IRI surgery showed persistence of kidney damage and unresolved renal inflammation compared to controls, demonstrating a role of renal mononuclear phagocytes in the recovery after kidney injury (M.-G. Kim et al., 2010).

Renal toxicity of cisplatin is also caused by TNF α -production in different cell types including parenchymal cells but also macrophages, however experiments with chimeric mice suggest that TNF α produced in macrophages and DCs is negligible during AKI (Ramesh & Reeves, 2002; Zhang, Ramesh, Norbury, & Reeves, 2007). Contrary to this, Dong *et al.* showed that depletion of phagocytes before IRI using clodronate liposomes decreased TNF α -production both in myeloid and non-myeloid cells, revealing F4/80⁺ cells not parenchymal cells as the major source of TNF α in the early phases of kidney injury (Dong et al., 2007).

Apart from cytokine-production, DCs were shown to activate the adaptive immune response by taking up antigens in the kidney after IRI and trafficking to the renal lymph node resulting in activation of CD4⁺ T-cells (Dong et al., 2005). Whether activation of CD4⁺ T-cells or induction of regulatory T-cells by DCs during AKI plays a role in disease progression needs to be addressed in future studies.

Overall, the specific functions of renal mononuclear phagocyte subsets are largely unknown since most studies are based on models with a combined effect on most renal DC and macrophage populations. Some progress was seen in other kidney

disease models, e.g. it was shown that depletion of cDC1 during glomerular nephritis substantially increased neutrophil infiltration and lead to a worse disease progression (Brähler et al., 2017). Modern techniques such as (single-cell) RNA sequencing and kidney disease studies employing more DC subtype specific mouse models such as *Clec9a^{Cre}Rosa^{DTR}* or *XCR1^{Venus-DTR}* may help to understand the precise function of these populations during kidney disease.

1.7. Research objectives

Flow cytometric analyses of the kidney identified a novel CD11b^{hi} subset in the kidney, however the function of this subset was not addressed yet. Moreover, the ontogeny of F4/80^{hi}CD11b^{low} cells in the kidney is highly debated since they show characteristics of both cDCs and macrophages. Therefore, this study aimed to analyse the transcriptional identity of renal DC subsets both in steady state and after acute kidney injury to identify signs of ontogenetic relationships and to get clues about potential functional properties. In addition, multicolour confocal microscopy in combination with Histo-Cytometry for data analysis was employed to address the localization of DC subsets across renal cortex and medulla. Specific localization of different subsets could give insights into functional properties of these cells during steady state and disease.

Most studies analysing the function of mononuclear phagocytes during acute kidney injury are not addressing specific subsets but rather DCs, macrophages and monocytes combined. Therefore, this study aimed to use more specific depletion of DCs or DC subsets to improve knowledge about the function of these cells during cisplatin-induced acute kidney injury and IRI.

2. Materials and methods

2.1. Animal husbandry

Clec9a^{Cre} (Schraml et al., 2013), *Rosa26^{YFP}* (Srinivas et al., 2001), *Rosa26^{Tomato}* (Madisen et al., 2010), *Rosa26^{DTR}* (Buch et al., 2005), *XCR1^{Venus-DTR}* (Yamazaki et al., 2013) and *C57BL/6J* mice were bred at the Biomedical Center of the Ludwig-Maximilian's University in specific pathogen-free conditions with a 12 hour light/dark cycle. Adult mice were used at the age of 8-12 weeks. All animal procedures were performed according to institutional and national guidelines for animal welfare and approved by the Government of Upper Bavaria (Regierung von Oberbayern).

2.2. Genotyping

Ear snips for genotyping were taken by animal caretakers in the animal facility and transferred to 300 µl quick lysis buffer containing 10 mM Tris, 150 mM NaCl, 5 mM EDTA, 0.05 % NP-40 and 0.2 mg/ml Proteinase K. The samples were digested in a thermoshaker (Eppendorf) at 56 °C and 300 rpm for 3 hours and inactivated at 90 °C and 300 rpm for 10 min. Leftover mouse material was pelleted by centrifugation at 13000 g for 5min. 1 µL of the solution was used for genotyping.

Table 1. List of used oligonucleotides

Primer	Sequence 5' – 3'	PCR
Rosa1	AAA GTC GCT CTG AGT TGT TAT	DTR/YFP
Rosa3	GGA GCG GGA GAA ATG GAT ATG	DTR/YFP
iDTR-R BBO 0164	AAT AGG AAC TTC GTC GAG C	DTR
oIMR4982	AAG ACC GCG AAG AGT TTG TC	YFP
BS49	AAA AGT TCC ACT TTC TGG ATG ATG A	Cre
BS47	GGC TCT CTC CCC AGC ATC CAC A	Cre
A65	TCA CTT ACT CCT CCA TGC TGA CG	Cre
AKM 258	CTA TCT TAA GAT TTC TCA GGG CCA GTC TAC	XCR1
AKM 259	CAG GAC AAT GGT AGA GAT GGT GGA AAA G	XCR1
AKM 260	CTG CAG CCA GAA AGA GCT TCA G	XCR1

WT FOR	AAG GGA GCT GCA GTG GAG TA	tdTomato
WT REV	CCG AAA ATC TGT GGG AAG TC	tdTomato
Mut FOR	CTG TTC CTG TAC GGC ATG G	tdTomato
Mut REV	GGC ATT AAA GCA GCG TAT CC	tdTomato

Table 2. Used PCR protocols for genotyping

Locus	Primers	Annealing temperatur	Extension time	Expected bands
Clec9a-Cre	BS49, BS47, A65	60°C	40s	WT: 407 bp Mut: 597 bp
XCR1-Venus-DTR	AKM 258, AKM 259, AKM 260	62	30s	WT: 450 bp Mut: 450 bp
Rosa26-DTR	Rosa1, Rosa3, iDTR-R BBO 0164	61	60s	WT: 600 bp Mut: 845 bp
Rosa26-YFP	Rosa1, Rosa3, oIMR4982	60	60s	WT: 320 bp Mut: 600 bp
Rosa26-Tomato	WT FOR, WT REV, Mut FOR, Mut REV	61	30s	WT: 297 bp Mut: 196 bp

2.3. Cell isolation for flow cytometry

2.3.1. Spleen and lymph nodes

Spleens and lymph nodes were isolated from mice, transferred to 1 ml RPMI with 200 U/ml collagenase IV and 0.2 mg DNase I and then cut into small pieces. Organs were digested for 30 min in a heated shaker at 37 °C and 120 rpm. Digested organs were passed through a 70µm strainer and washed with FACS Buffer. Red blood cell lysis was performed with 2 ml Red Blood Cell Lysing Buffer Hybri-Max (Sigma Aldrich) for 2 min at room temperature. Cells were washed once and then resuspended in FACS buffer (PBS containing 1 % FCS (Sigma-Aldrich), 2.5 mM EDTA (Invitrogen) and 0,02% sodium azide) for further analysis.

2.3.2. Kidney

Kidneys were perfused with ice-cold PBS before isolation, transferred to 2 ml RPMI with 200U/ml collagenase IV and 0.2 mg DNase I and then cut into small pieces. Digested kidneys were passed through a 70 µm strainer, washed once with FACS Buffer and resuspended in 4ml 70 % Percoll for enrichment. The resuspended cells were overlaid with additional 37 % Percoll and 30 % Percoll layer to create a gradient and centrifuged at 2000rpm for 30min at room temperature without brakes. Enriched leukocytes were collected at the interface of the 70 % and 37 % layers and washed once with FACS buffer. Isotonic Percoll was prepared by adding 1 part of 10x PBS to 9 parts of Percoll (Sigma-Aldrich). Percoll dilutions were prepared according to Table 3. FACS buffer without sodium azide was used for RNA sequencing.

Table 3. Preparation of Percoll dilutions

Percoll dilution %	Amount Percoll	isotonic	Additive
70	28 ml		12 ml Hank's balanced salt solution (HBSS, Sigma-Aldrich)
37	14,8 ml		25.2 ml PBS
30	6 ml		14 ml HBSS

2.4. Flow cytometry

Before staining, cells were incubated with 50 µl F_c-block containing purified anti-mouse CD16/32 in FACS Buffer for 10min at 4 °C. Antibodies for surface antigens for were combined in a master mix in FACS buffer and added to the samples for a final staining volume of 100 µl at 4 °C for 20 min. Stained cells were washed twice in FACS buffer to remove unbound antibodies and then resuspended for flow cytometric analysis. Dead cells were identified using 4',6-diamidino-2-phenylindole (DAPI) (Sigma-Aldrich) or Fixable Viability Dye eFluor™ 780 (Thermo Fisher Scientific). For staining of intranuclear antigens the Foxp3 transcription factor staining set (Thermo Fisher Scientific) was used according to the manufacturer's instructions. Flow cytometry was performed on a LSR Fortessa (BD Biosciences) and data were analyzed using FlowJo software (FlowJo LLC). For cell sorting an Aria III Fusion (BD Biosciences) sorter was

used. CountBright™ Absolute Counting Beads (Thermo Fisher Scientific) were used for cell quantification.

2.5. Cisplatin-induced acute kidney injury

Acute kidney injury was induced in adult female *Clec9a^{cre/cre}Rosa^{YFP}* mice by i.p. injection of 15 mg/kg body weight cisplatin. Control mice were injected with an equal amount of NaCl. Organs and blood were collected 72h after injection of cisplatin or when the mice reached a high disease score. Blood serum was used for creatinine and blood urea nitrogen (BUN) measurements using a Cobas Integra 400 plus analyser (Roche). Serum BUN was identified with a cobas c pack UREAL (Roche) and creatinine levels were measured using a cobas c pack CREP2 (Roche). Kidneys and spleen were isolated and analyzed as described above.

2.6. Unilateral ischemia reperfusion injury

Unilateral ischemia reperfusion injury was performed in collaboration with the group of Prof. HJ Anders as previously described (Marschner et al., 2016). 10-week-old male *Clec9a^{cre/cre}Rosa^{YFP}* mice were anesthetized prior to surgery using a mixture containing medetomidine, midazolam and fentanyl and online rectal temperature recording was installed for each mouse. Anesthetized mice were placed on a heating plate to maintain body temperature between 36.5-38.5 °C and a flank incision was performed and the renal hilum of the left kidney was clamped for 25 min using a micro aneurysm clamp (Medicon, Germany). Body temperature was monitored with a rectal probe. After clamping, successful ischemia was indicated by a pale color of the kidney, which changed back to its original color. Both the peritoneal and cutaneous layer were stitched with absorbable sutures (Ethicon) to close the wound. Mice were supplemented with 200 µl saline to maintain fluid balance. 72 h after surgery kidneys and spleen were isolated and analyzed as described above.

2.7. Diphtheria Toxin mediated cell depletion

DCs were depleted in 10-12-week-old *XCR1^{Venus-DTR}* or *Clec9a^{Cre}Rosa^{DTR}* mice by i.p. injection of 25 ng/kg diphtheria toxin. Control mice without DTR were injected with the same concentration of DT to exclude DT-mediated side-effects. 24 h after injection the

mice were either analyzed or subsequently injected with cisplatin to induce acute kidney injury.

2.8. RNA isolation and library construction

DCs for RNAseq were directly sorted in Extraction Buffer using an Aria III Fusion (BD Biosciences). PicoPure™ RNA Isolation Kit (Thermo Fisher Scientific) was used to extract total mRNA from sorted cells according to manufacturer's instructions. RNA quantity and quality were analyzed using a 2100 Bioanalyzer (Agilent) and only samples with a RNA Integrity Number (RIN) > 8 were considered for further steps. cDNA synthesis of isolated mRNA was performed with the ultra-low input RNA SMART-seq v4 kit (Clontech) according to the manufacturer's instructions. Purified cDNA was transferred to 6x16 mm microTUBEs (Covaris) and sheared by sonication with a Covaris S220. Sheared cDNA was cleaned using ethanol precipitation and successful sonication was confirmed using DNA High Sensitivity chips on a 2100 Bioanalyzer. Libraries for RNA sequencing were created with the MicroPlex Library Preparation kit v2 (Diagenode) and a maximum of 10 ng sheared cDNA. Next, libraries were amplified for 4 cycles and DNA amount was quantified by Qubit 2 DNA quantification (Thermo Fisher Scientific). Additional cycles were added until a DNA amount of 5 ng/μl was reached. AMPure XP beads (Beckman Coulter) were used to clean amplified libraries according to the SMART-seq v4 kit (Clontech) protocol. Quality and amount of the finished libraries were analyzed by using a 2100 Bioanalyzer (Agilent). Sequencing of finished libraries was performed at LAFUGA (Gene Center LMU) on an Illumina HiSeq1500 sequencer. 50 base pair (bp) single read sequencing in combination with a sequencing depth of 20 million reads was chosen to reach an adequate sequencing depth.

2.9. RNA sequencing analysis

Sequenced cDNA libraries were demultiplexed and reads were mapped to the mouse genome (mm10) using STAR (Dobin et al., 2013). Normalized gene expression was calculated in transcripts per kilobase million (TPM) with RSEM (B. Li & Dewey, 2011). RNA-seq analysis was performed in R (Version 3.4.3) with R-Studio (R-Studio Inc, Version 1.1.414). The DESeq2 R-package (Version 1.18.1) was used for differential gene expression analysis and principal component analysis (PCA). Genes with

average gene counts lower than 1 were discarded and Apeglm (A. Zhu, Ibrahim, & Love, 2018) as used for log₂ fold change shrinkage. *iCre* and *Gapdh* DNA sequences were loaded in R using Biostrings (Version 2.50.1) and manual alignment was performed with Shortread (Version 1.40.0). pheatmap (Version 1.0.10) was used to make heatmaps and graphs were plotted with the ggplot2 package (Version 2.2.1). Sequencing data have been deposited in the Gene Expression Omnibus under accession numbers GSE131751 and GSE135921.

2.10. Immunofluorescence microscopy

Organs were fixed overnight at 4 °C in 1% paraformaldehyde according to (Bajénoff, Glaichenhaus, & Germain, 2008) and then transferred to 30% sucrose at 4 °C. Once the organs were equilibrated with sucrose they were transferred to Tissue-Tek O.C.T. (Sakura) and frozen on dry ice. 10-12 µm thick sections were cut on a Leica CM3050S cryostat at -20 °C. After thawing the sections were dried and then rehydrated in PBS and permeabilized with PBS + 0.2 % Triton-X (Sigma-Aldrich) or Acetone (Sigma-Aldrich). For staining the sections were circled with a PAP Pen (Kisker Biotech GmbH) and blocked for at least 1 hour at room temperature (RT) in a dark humidified chamber with blocking buffer containing 10 % goat serum in PBS. During the blocking step antibodies were diluted in blocking buffer and sections were subsequently stained for two hours at RT in the dark with the staining solution. After staining the sections were washed with PBS twice and mounted with ProLong™ Diamond Antifade Mountant (Thermo Fisher Scientific), cured in a dark chamber at RT for 24 hours and stored at 4°C until imaging. Microscopy was performed at the Core Facility Bioimaging of the Biomedical Center with an upright Leica SP8X WLL microscope, equipped with 405nm laser, WLL2 laser (470 - 670nm) and acusto-optical beam splitter. Images were acquired with a 20x0.75 objective, image voxel size was 180nm in x/y direction and 0.5-1.3µm in z direction. The following detector settings were used for acquisition: AF647 (excitation 646nm; emission 656-718nm), AF594 (excitation 592nm; emission 605-640nm), tdTomato/AF555 (excitation 553nm; emission 563-591nm), AF488 (excitation 500nm; emission 510-542nm) and DAPI/BV421 (excitation 405nm; emission 415-470nm). Channels were recorded sequentially to avoid bleed-through. BV421, AF488, AF555, AF594, AF647 and tdTomato were recorded with hybrid photo detectors, DAPI with a conventional photomultiplier tube. Tile-scans were merged in

LAS X (Leica) and deconvolved using Huygens Professional (Scientific Volume Imaging). After deconvolution z-stacks were imported in Fiji (Schindelin et al., 2012) to adjust brightness/contrast, create maximum projections and to add scale bars. For quantification of MHCII⁺/MHCII^{neg} F4/80^{hi} cells in tissue sections 300 x 300µm cutouts were randomly chosen from renal cortex and medulla out of deconvoluted tile-scans. F4/80^{neg} cells were excluded using a mask created with the Interactive Watershed plugin on a thresholded F4/80 channel. Cells with high expression of CD11b were not counted.

2.11. Histo-Cytometry

Histo-Cytometry was adapted from Gerner *et al.* (Gerner, Kastenmuller, Ifrim, Kabat, & Germain, 2012) and Li *et al.* (W. Li, Germain, & Gerner, 2017). Deconvoluted tile-scans were opened in Fiji and a maximum projection was performed. The images were split in their channels and each channel was thresholded with the Auto Threshold Plugin and Default settings. The thresholded channels of an image were recombined and transformed to RGB to allow a mask creation on combined signal. Small noise was removed with the Despeckle plugin and the image was blurred with a Gaussian Blur filter and a 2-pixel radius. The Interactive Watershed plugin (Version 1.2.1) was used to perform the segmentation and to import the selections of all segmented cells from the LabelMap to the ROIManager. The selections were applied to the original deconvoluted tile-scan and mean fluorescent intensity for every channel as well as area, position and shape descriptors were exported for each segmented cell. Finally, results were combined to a comma separated value files and opened in Flowjo software to create flow cytometry standard files for analysis (Workflow see Figure 4).

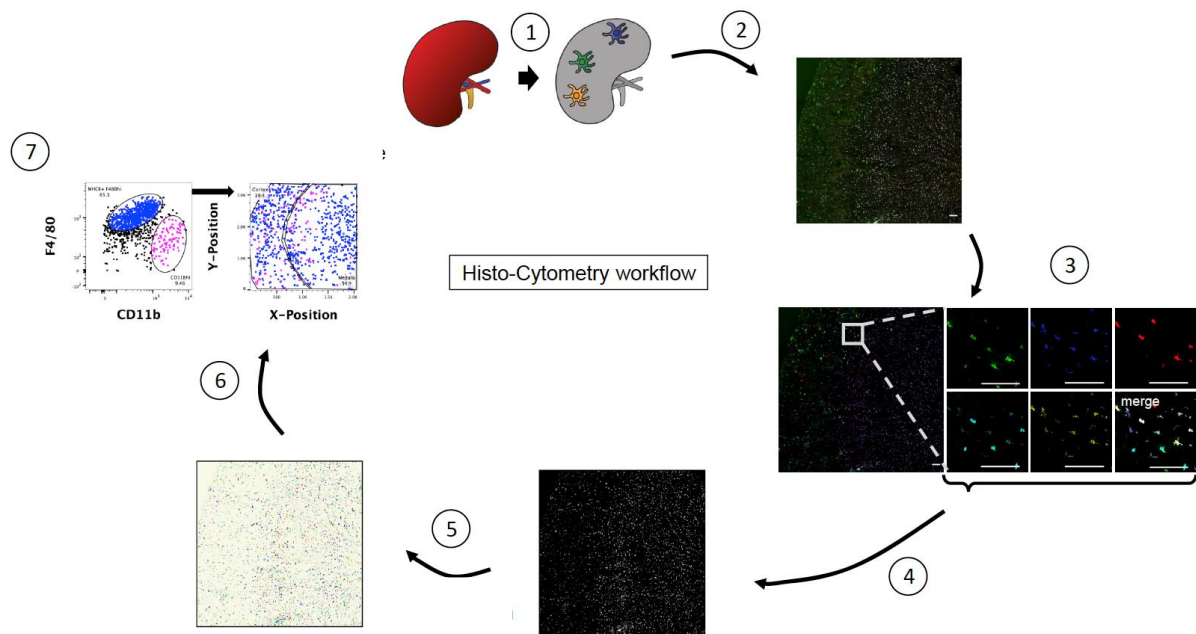


Figure 4. Schematic of the Histo-Cytometry workflow. (1) Staining of 12 µm tissue sections (2) Confocal imaging of 2 µm z-stack (3) Deconvolution and maximum projection of each channel (4) Thresholding and channel combination (5) Cell segmentation (6) Export of fluorescent intensities, location and shape descriptors (7) Analysis in flow cytometry software. (Modified from Salei *et al.* (Salei *et al.*, 2020))

2.12. Statistical Analysis

Statistical significance was calculated using two-tailed t test in Prism 7 software (GraphPad). One-way ANOVA was used for multiple comparisons. A p-value < 0.05 was considered significant.

2.13. Table of antibodies

Table 4. List of used antibodies

Antigen	Clone	Conjugates	Company
CD3	17A2	AF594	Biologend
CD3ε	145-2C11	PE-Cy5, purified	BV421, Biologend
CD4			
CD8			

CD11b	M1/70	BV421, APC-Cy7, AF647, purified	Biolegend
CD11b	ICRF44	BUV737	BD Biosciences
CD11c	N418	PerCP-Cy5.5, BV421, BV785	Biolegend
CD16/CD32	2.4G2	purified	BD Biosciences
CD19	6D5	BV650, APC	Biolegend
CD24	M1/69	BUV395	BD Biosciences
CD24	M1/69	BV605	Biolegend
CD31	MEC13.3	AF488, AF594, AF647	Biolegend
CD45.2	104	PE-Cy7, PB, AF700, FITC	Biolegend
CD45R/B220	RA3-6B2	PE, AF647	Biolegend
CD64	X54-5/7.1	APC, PE, PE-Cy7	Biolegend
CD64	27	purified	Sino Biological
CD90.1	OX-7	AF700, PE-Cy7	Biolegend
CD103			
CD127	SB/199	BUV737	BD Biosciences
F4/80	BM8	BV785, AF647, AF594	Biolegend
I-A/I-E (MHCII)	M5/114.15.2	BV510, AF488, AF647, AF594, AF700, BV421	Biolegend
Ly6C	HK1.4	BV605, PerCP-Cy5.5	Biolegend
Ly6G	1A8	PerCP-Cy5.5, PB	Biolegend
XCR1	ZET	BV650, BV421	Biolegend
Cleaved caspase-3	D3E9	purified	Cell Signaling Technologies
Foxp3	150D	AF647	Biolegend
Gata3	16E10A23	PE	Biolegend
Roryt	Q31-378	BV421	Biolegend

Rabbit IgG	goat polyclonal	AF555	ThermoFisher
Rabbit IgG	goat polyclonal	AF488	Jackson ImmunoResearch
Hamster IgG	goat polyclonal	Cy3	Jackson ImmunoResearch

2.14. Analysis software

Table 5. List of used software

Software	Version	Company
Flowjo	10.5.3	Becton Dickinson
GraphPad PRISM	7.0c	GraphPad Software
Fiji	2.0.0-rc-69/1.52p	-
LAS X	3.4.1.17670	Leica
Huygens Professional	17.10.0p2.64b	Scientific Volume Imaging
R Studio	1.1.414	R Studio Inc
Imaris	8.2.0	Bitplane

3. Results

3.1. Application of Histo-Cytometry to improve microscopic analysis of DC subsets in the kidney

3.1.1. The adult kidney contains four distinct subsets of mononuclear phagocytes with DC origin

To confirm that the *Clec9a^{Cre}Rosa^{YFP}* model is indeed only labelling DCs in the kidney and not other myeloid or lymphoid cells an in depth phenotypic analysis by flow cytometry was performed (Figure 5).

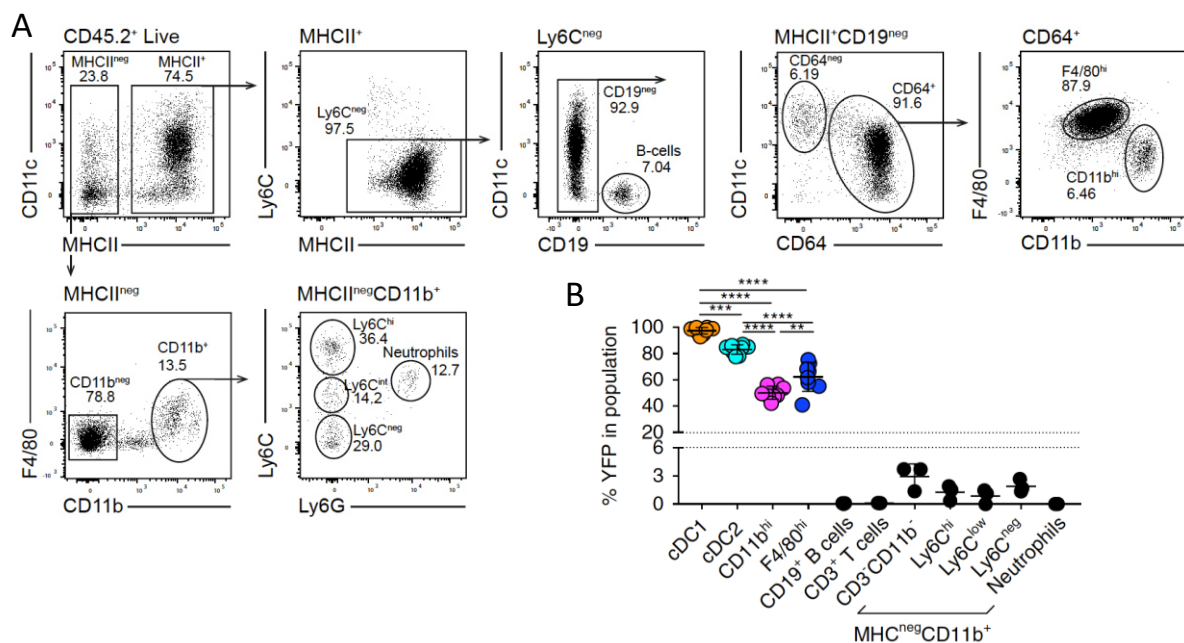


Figure 5: Gating strategy to identify DCs and YFP labelling in the kidney. (A) Renal leukocytes isolated from kidneys of *Clec9a^{Cre}Rosa^{YFP}* mice were analysed by flow cytometry. CD45.2⁺Live cells were divided in MHCII⁺ and MHCII^{neg} cells. The majority of cells in the MHCII⁺ gate is CD64⁺. CD64⁻CD11c⁺ gate contains XCR1⁺ cDC1 and CD11b⁺ cDC2. In the CD64⁺ gate two populations can be identified, F4/80^{hi}CD11b^{low} and CD11b^{hi}F4/80^{low} cells. (B) YFP labelling percentage in leukocyte populations in the kidney of *Clec9a^{Cre}Rosa^{YFP}* mice. Each dot represents one mouse. Horizontal bars indicate mean, error bars indicate SD. ** p-value < 0.01, *** p-value < 0.001, **** p-value < 0.0001 (Modified from Salei *et al.* (Salei *et al.*, 2020))

Renal leukocytes were identified as live cells expressing CD45 and further segregated in MHCII⁺ and MHCII^{neg} cells. Next, Ly6C⁺ cells contaminating the MHCII⁺ gate were removed and the remaining cells analysed for their CD11c and CD64 expression. The remaining MHCII⁺ cells can be split in a prominent CD64⁺ population as well as CD11c⁻ CD64⁻ B cells and CD11c⁺ CD64⁻ cells. CD11c⁺ cells can be further divided in the two main cDC subsets XCR1⁺/CD24⁺ cDC1 and CD11b⁺ cDC2. Within the CD64⁺ cells two populations can be identified, F4/80^{hi}CD11b^{low} cells (Referred to as F4/80^{hi} cells from here on out) and CD11b^{hi}F4/80^{low} cells (Referred to as CD11b^{hi} cells from here on out). The MHCII^{neg} cells were subdivided in a CD11b⁺ and CD11b⁻ fraction, wherein the latter contained CD3⁺ T cells. The CD11b⁺ cells were further subdivided in Ly6C^{hi} monocytes, Ly6C^{int} cells, Ly6C⁻ cells and Ly6G⁺ neutrophils. To identify cells with CDP origin in the aforementioned populations the percentage of YFP-expressing cells was determined.

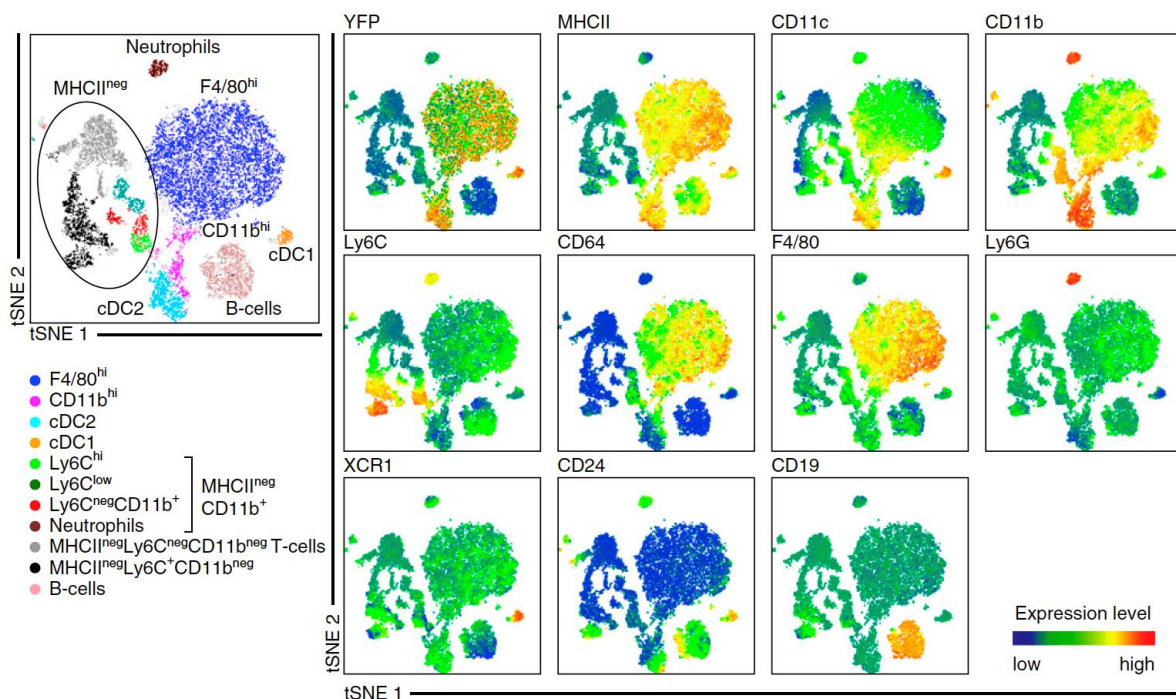


Figure 6. Unsupervised clustering using tSNE analysis of renal leukocytes verifies specific labelling of renal DCs in *Clec9a*^{Cre}*Rosa*^{YFP} model. Representative tSNE of kidney leukocytes from *Clec9a*^{Cre}*Rosa*^{YFP} mice. Cells were clustered independently of their YFP labelling and manually gated populations were overlaid on the tSNE plot in the indicated colors. Blue-to-red gradient indicates increasing intensity of marker expression. (Modified from Salei *et al.* (Salei *et al.*, 2020))

As expected, cDC1 were almost completely labelled as they express *Clec9a* in their differentiated state (Caminschi et al., 2008). For other cells the amount of YFP labelling is a true indicator of CDP origin, except for pDCs which also express low levels of *Clec9a* (Schraml et al., 2013). As previously described (Schraml et al., 2013), apart from cDC1 three more populations showed a significant contribution from DC progenitors, namely cDC2 (labelling $83.1 \pm 3.6\%$), CD11b^{hi} ($50.2 \pm 5.0\%$) and F4/80^{hi} ($62.3 \pm 11.0\%$) cells. Other cell types did not show YFP labelling. To confirm that we did not exclude any populations with a DC origin using the previously described gating strategy we employed t-Distributed Stochastic Neighbour Embedding (tSNE) as an unsupervised method to cluster cells during flow cytometric analysis (Figure 6).

3.1.2. Setup of Histo-Cytometry in lymph nodes to localize T cells and B cells

An important role of mononuclear phagocytes in the kidney during development and disease was shown by many studies (Munro & Hughes, 2017; Munro et al., 2019; Rogers et al., 2014; Weisheit et al., 2015), however there is only little known about the localization of macrophages and DC subsets in the kidney. After having confirmed the specificity of the *Clec9a^{Cre}Rosa^{YFP}* model for tracing CDP-derived cells in the kidney we wanted to study the precise localization of renal DC subsets in the kidney using this model. We hypothesized that analysis of the localization of renal DC subsets in steady state tissue or after acute kidney injury would allow us to correlate specific DC subsets to potentially protective or damaging functions.

To identify the localization of DC subsets in the kidney we aimed to employ confocal microscopy with a multiplex immunofluorescence in combination with a method called Histo-Cytometry (Gerner et al., 2012; W. Li et al., 2017). This method utilises multiple cell surface markers to segment cells in the tissue. Size, shape descriptors, x/y-position and mean channel intensity of each segmented cell are subsequently exported for analysis in flow cytometry software. In this way, DC subsets can be identified by gating on the expression of DC specific markers and localization of these cells can be retraced to the microscopy image.

To establish the Histo-Cytometry workflow in our hands we stained sections of murine lymph nodes with DAPI, CD3 and B220 (Figure 7).

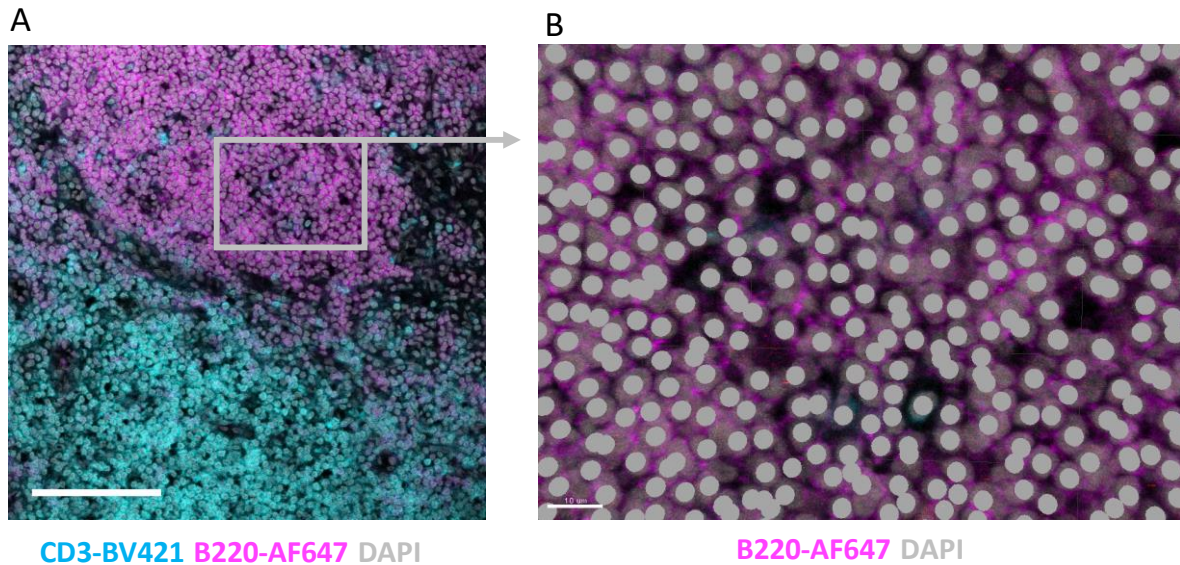


Figure 7. Microscopic image of murine lymph node stained for B220, CD3 and DAPI. (A) Immunofluorescence image of WT murine inguinal lymph node section stained to reveal T cells (CD3, Cyan), B cells (B220, AF647) and nuclei (DAPI, gray); scale bar 100 μm . (B) Magnification of area in B cell zone. Selections of nuclei based on segmentation performed in imaris are overlaid as filled gray circles; scale bar 50 μm .

The goal was to use these markers for identification of B220⁺ B cells and CD3⁺ T cells. Segmentation was performed with Imaris software on the DAPI signal using the surface creation tool as described by Gerner *et al.* (Gerner *et al.*, 2012) (Figure 7B). Mean channel fluorescence was exported for each exported nucleus and exported for analysis in FlowJo (Figure 8).

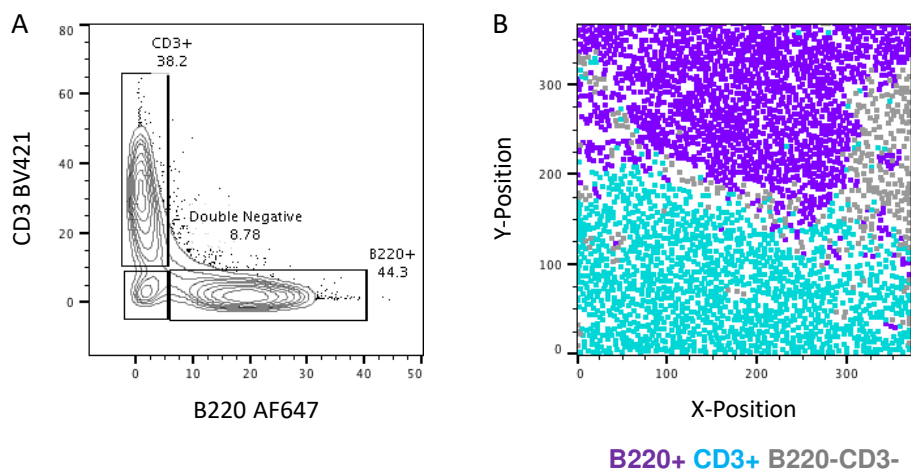


Figure 8. Histo-Cytometry in the lymph node. (A) Flow cytometric analysis of exported mean fluorescent values exported from microscopic image using segmentation in Imaris.

T cells are identified as $CD3^+B220^-$, B cells as $B220^+CD3^-$. (B) Dot plot showing the X/Y-position of cells gated in (A).

Since the membrane staining of B220/CD3 was partly overlapping with DAPI this allowed segmentation of round cells as for example B cells and T cells. CD3 and B220 are mutually exclusive markers, however, as soon as cells with different marker expression were in close contact, we saw an overlap of membrane signal, which caused $B220^+CD3^+$ cells. In addition, since this approach has limitations when trying to identify cells with dendritic cell shape because most of the membrane staining in the dendrites will not overlap with the nuclear DAPI staining, we resorted to a different segmentation approach based on membrane staining rather than DAPI as described in Li *et al.* (W. Li et al., 2017). Moreover, we decided to test this approach in kidneys of *Clec9a^{Cre/+}Rosa^{Tomato}* reporter mice with the reasoning that it would be our tissue of interest later on and that DCs in the kidney are usually not in close contact with other immune cells and we thereby expected an easier segmentation.

3.1.3. Establishing Histo-Cytometry workflow in sections of early life kidney to identify DCs

For establishing a different Histo-Cytometry workflow we chose kidney sections from 2-week-old *Clec9a^{Cre/+}Rosa^{Tomato}* mice because at this timepoint the amount of fluorescently labelled $F4/80^{hi}$ cells is relatively low (Salei et al., 2020). Therefore, we expected only few $Tomato^+$ cells in close contact to each other, which would help in identifying single cells. Kidney section were stained with DAPI to identify nuclei, F4/80 and MHCII (Figure 9).

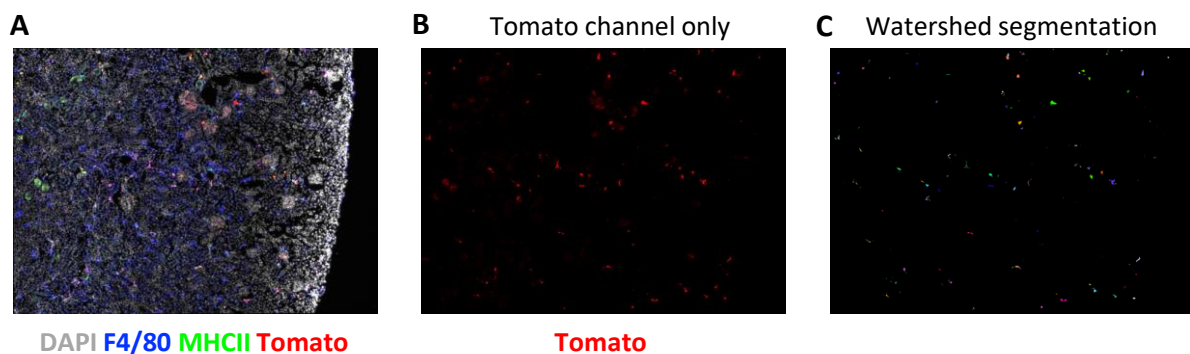


Figure 9. Cell segmentation on immunofluorescence image of PND15 kidney based on Tomato expression. (A) Kidney section from *Clec9a^{Cre/+}Rosa^{Tomato}* kidney isolated at PND15

stained for nuclei (DAPI, gray), F4/80 (blue), MHCII (green) and Tomato (red). (B) Isolated Tomato channel from (A). (C) Tomato channel after segmentation using a watershed algorithm. Each individual cell was randomly assigned a color.

We segmented cells based on their expression of Tomato using the SCF watershed plugin in Fiji. With this method, we saw that the algorithm reliably called all Tomato expressing cells (Figure 9). In addition, cells in relatively close proximity still seemed to be segmented (Figure 9). Next, we wanted to test whether we could improve the number of cells, which we segmented by using F4/80 as the base for the algorithm. From our phenotypic analysis with flow cytometry we knew that the kidney contains cells with high expression of F4/80 (F4/80^{hi}) and cells with low expression of F4/80 (CD11b^{hi} DCs or monocytes).

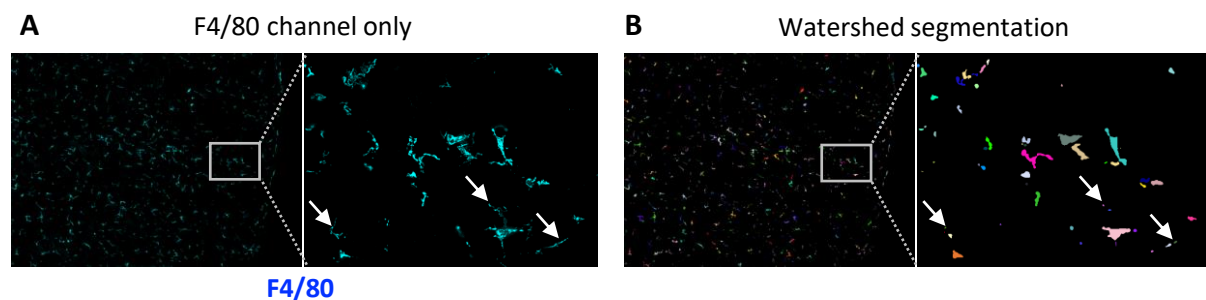


Figure 10. Watershed segmentation excludes cells with low F4/80 expression. (A) Isolated F4/80 channel from Figure 9A. Magnification illustrates cells with low F4/80 expression (White arrows). (B) F4/80 channel after segmentation using a watershed algorithm. Each individual cell was randomly assigned a color. Magnification illustrates cells with low F4/80 expression (White arrows).

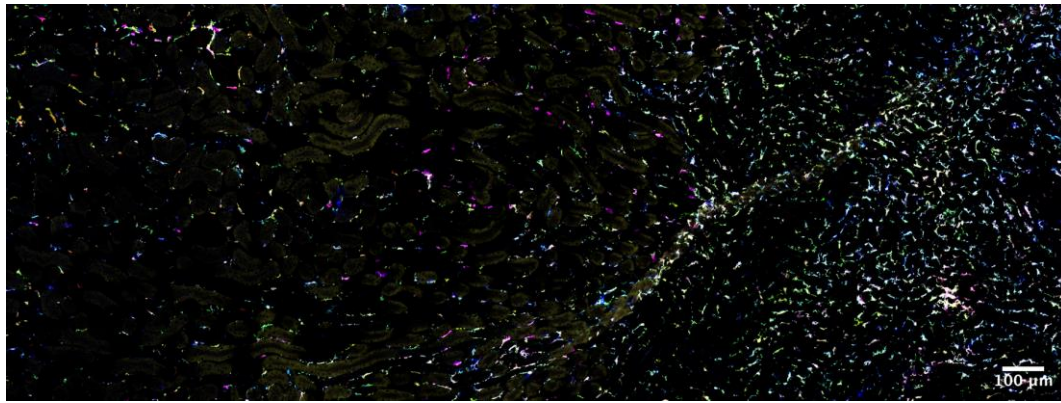
After running the algorithm, we noticed that even though many cells were correctly identified, cells with low expression of F4/80 were more likely to be excluded since the algorithm needs a bright and clear signal for good segmentation results (Figure 10). To circumvent this problem, we decided to combine the signal of multiple channels to one 'masking channel' (Figure 11).



Figure 11. Combination of channels for efficient masking of cells. (A) F4/80 channel after segmentation using a watershed algorithm from Figure 10B. (B) Tomato channel after segmentation using a watershed algorithm from Figure 9C. (C) Results of watershed segmentation on a 'masking channel' consisting of F4/80 and Tomato channels. Each individual cell was randomly assigned a color.

The reasoning behind this approach was that with the combination of more markers we would be able to identify more cells, e.g. through combination of Tomato and F4/80 signals we would ultimately be able to also identify Tomato⁻F4/80⁺ cells and *vice versa*. We noticed that segmentation of cells was still very good, even with many more cells being called based on the combined signal (Figure 11). The combination of these two markers also helped with the segmentation of cells with low F4/80 signal because many of them were overlapping with Tomato signal and thus segmented with the algorithm. We concluded that combination of a cytoplasmatic marker like Tomato in our case with one or more cell surface markers like F4/80, MHCII etc. would give us a good enough coverage on DCs in the kidney so that we would be able to identify our cells of interest. Of course, successful segmentation was supported by a lower percentage of dendritic cells in kidneys isolated from young mice compared to adult tissue.

Therefore, we next turned to kidney sections from adult *Clec9a^{Cre/+}Rosa^{Tomato}* mice, in which DCs are more frequent. In adult *Clec9a^{Cre/+}Rosa^{Tomato}* mice DCs are highly labelled with the Tomato reporter, which we expected to lead to a very good coverage after the segmentation algorithm. We stained these sections with antibodies against MHCII, CD64, CD11b and F4/80 (Figure 12). Visualization as overlays and analysis of such images gets very complex because of a limited amount of distinguishable colors, but with the use of Histo-Cytometry we hoped to solve these problems (Figure 12).



MHCII CD64 Tomato CD11b F4/80

Figure 12. Multicolor immunofluorescence staining of adult kidney section. Section of adult kidney isolated from a *Clec9a^{Cre/+}Rosa^{Tomato}* mouse. Multicolor staining against MHCII (blue), CD64 (green), Tomato (red), CD11b (magenta) and F4/80 (yellow) to identify multiple renal DC subsets.

From our flow cytometry data, we knew that with these markers in combination with Tomato we should be able to identify all 4 of the DC subsets in the tissue (Figure 13). Gating on all MHCII⁺ cells we were able to find CD64⁺ and CD64⁻ cells same as in flow cytometric data (Figure 13). The CD64⁺ cells we split F4/80^{hi} (blue) and CD11b^{hi}F4/80^{low} (magenta). CD64⁻ cells we split in CD11b⁺ cDC2 (cyan) and CD11b⁻ cells, which should mostly be cDC1 (orange) (Figure 13).

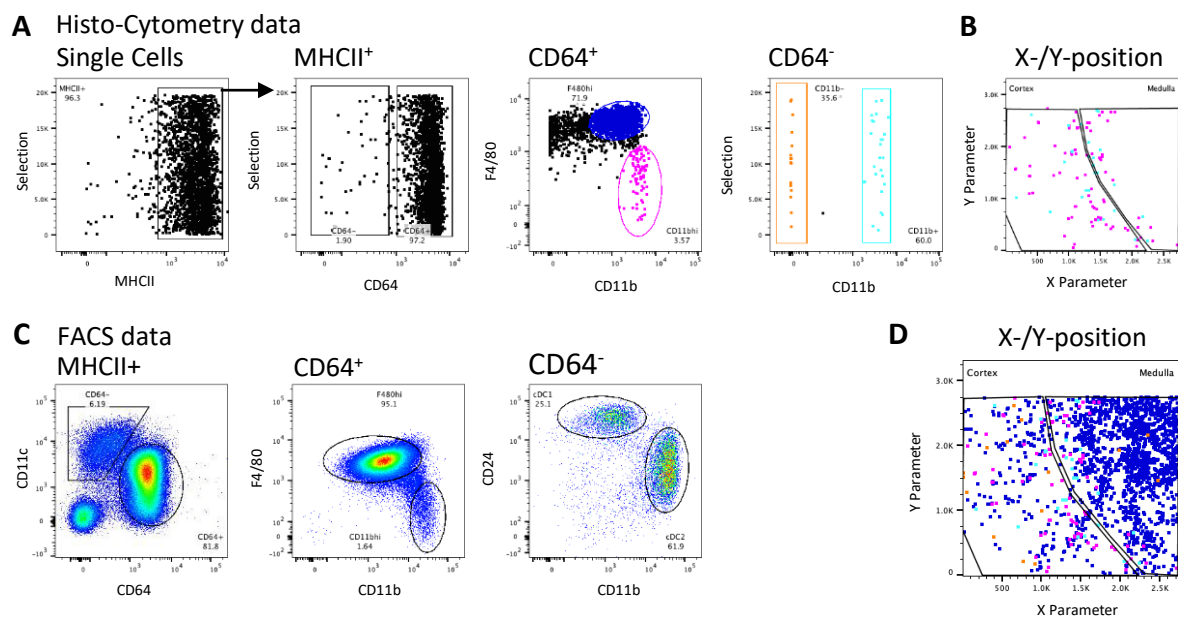


Figure 13. Histo-Cytometry of adult kidney sections compared to flow cytometric data. (A) Representative gating strategy for Histo-Cytometry data obtained from murine adult kidney

sections of *Clec9a^{Cre/+}Rosa^{Tomato}* mice. Single cells were identified based on area of the selection. The majority of cells was MHCII⁺ as expected based on a combined masking channel of MHCII, F4/80, CD64, CD11b and Tomato. MHCII⁺ cells were split in CD64⁻ and CD64⁺ cells. The latter population contained F4/80^{hi} (Blue) and CD11b^{hi} (Magenta) cells. CD64⁺ were split into CD11b⁺ cDC2 (Cyan) and CD11b⁻ cDC1 (Orange). (B) X/Y-position of cDC2 and CD11b^{hi} cells in the section. Cortex and medulla are indicated as gates on the dot plot. (C) Flow cytometric data for comparison to Histo-Cytometry analysis. Live CD45.2⁺MHCII⁺ cells were split into CD64⁻ and CD64⁺ cells. The latter population contained F4/80^{hi} and CD11b^{hi} cells. CD64⁻ cells were split into CD24⁺ cDC1 and CD11b⁺ cDC2 (D) X/Y-position of previously gated F4/80^{hi} (Blue), CD11b^{hi} (Magenta), cDC2 (Cyan) and cDC1 (Orange) populations in the tissue as assessed by Histo-Cytometry.

As mentioned previously, another advantage of using Histo-Cytometry is that the X/Y-position of cells gets preserved during the analysis. We therefore checked where the four DC subsets actually localize in our case. In line with previously published reports, we saw that F4/80^{hi} cells mostly localized in the renal medulla whereas cDC1, cDC2 and CD11b^{hi} cells were mostly found in the renal cortex (Figure 13) (Berry et al., 2017; Brähler et al., 2017). Despite the phenotypic differences we showed for cDC2 and CD11b^{hi} cells, these subsets did not localize in an obviously different manner. What was noticeable however was that cDC1 were almost exclusively found in the cortex, whereas cDC2 and CD11b^{hi} cells seemingly clustered at the interface between cortex and medulla.

3.1.4. Localization of DC subsets in the kidney at different developmental time points

It was recently recognized that there are dynamic changes in the renal mononuclear phagocyte compartment of mice during development (Lever et al., 2019). In the early days the kidney harbours a prominent population of MHCII^{neg}F4/80^{hi} cells, which is later replaced by phenotypically similar MHCII⁺F4/80^{hi} cells, possibly with a DC origin. Seeing that the Histo-Cytometry approach with a combination of multiple markers worked well at post-natal day 14 (PND14) we decided to analyse the localization of DCs during development. We sought out investigate the localization of F4/80^{hi} cells in young mice and during development. For this we isolated kidneys from *Clec9a^{Cre/+}Rosa^{Tomato}* mice at PND2, PND14 and PND28 days after birth and after 3 months as an adult timepoint. Next, we stained sections from these tissues with

MHCII, F4/80 and CD11b to identify our cells of interest and subjected them to the Histo-Cytometry workflow (Figure 14). In our Histo-Cytometry data we nicely saw that at PND2 and PND14 we still had a prominent population of MHCII^{neg}F4/80^{hi} cells (Figure 14). These cells were confined to the renal medulla, same as MHCII⁺F4/80^{hi} cells in adult mice. At PND14 we also saw an influx of MHCII⁺F4/80^{hi} cells, however it seemed that at this point these cells were not exclusively found in the medulla but also in the cortex. At PND28 we saw an increase of MHCII⁺F4/80^{hi} cells in the medulla and MHCII^{neg}F4/80^{hi} cells were basically absent from the tissue. Only at the adult timepoint did we notice this accumulation of CD11b^{hi} cells at the corticomedullary junction (Figure 14).

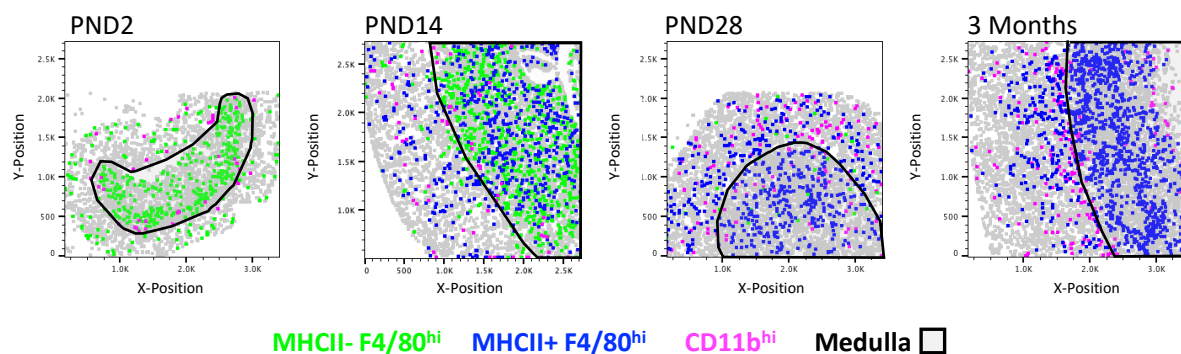


Figure 14. Histo-Cytometry of kidney sections at different developmental timepoints.

Representative histo-cytometric analysis of kidney sections from *Clec9a*^{Cre/+}*Rosa*^{Tomato} mice isolated PND2, PND14, PND28 and at 3 months of age. Sections were stained for MHCII, F4/80, CD11b and Tomato. Renal medulla is depicted as a gate on the X/Y-position dot plots.

To confirm our observation that MHCII⁺ and MHCII^{neg}F4/80^{hi} cells seemed to show a difference in localization we isolated additional kidneys from *Clec9a*^{Cre}*Rosa*^{Tomato} mice at PND14 and stained sections with MHCII, CD11b, F4/80 and CD64. We performed Histo-Cytometry on these sections and quantified the localization of these cells in the renal cortex or medulla (Figure 15).

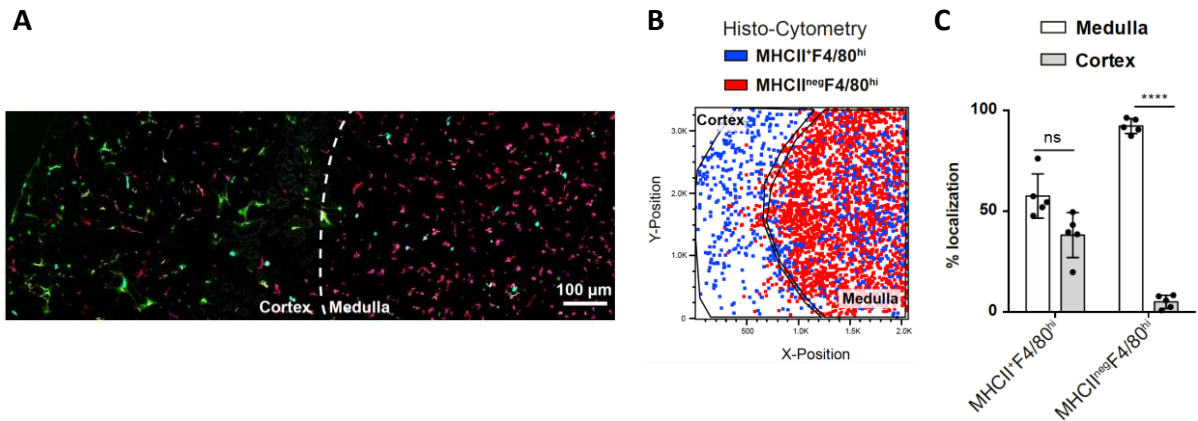


Figure 15. Histo-Cytometry of kidney sections at PND14. (A) Representative section of PND14 *Clec9a^{Cre}Rosa^{Tomato}* kidney section stained against MHCII (green), CD64 (blue), CD11b (cyan) and F4/80 (red) to identify MHCII^{neg}F4/80^{hi} cells and MHCII⁺F4/80^{hi} cells. (B) Representative histo-cytometric analysis of microscopic images of PND14 kidney overlaying the X/Y-position of MHCII^{neg}F4/80^{hi} cells (blue) and MHCII⁺F4/80^{hi} cells (red) in the kidney. Renal cortex and medulla are depicted as gates on the dot plot. Each dot represents one mouse. Horizontal bars indicate mean, error bars indicate SD. **** p-value < 0.0001 (Modified from Salei *et al.* (Salei et al., 2020))

Confirming our previous findings, we again saw a preferential localization of the MHCII^{neg}F4/80^{hi} cells in the renal medulla. The MHCII⁺F4/80^{hi} cells however seemed to be evenly spread across the cortex and medulla. Only with time the MHCII⁺F4/80^{hi} cells become the dominating subset in the kidney and are mostly found in the medulla.

3.2. The kidney contains four transcriptionally unique DC subsets

3.2.1. Establishment of library preparation with low RNA input

Next, we decided to utilize transcriptomic profiling by mRNA sequencing (RNAseq) to further characterize DC subsets in the kidney and to understand why F4/80^{hi} cells derive from DC progenitors but also possess a macrophage phenotype. However, because the number of CD11b^{hi} cells, cDC2 and cDC1, which can be isolated from the kidneys of one mouse was very limited (~1000-2000 cells), we first needed to verify the library preparation protocol for low inputs. For this we sort purified CD24⁺CD205⁺cDC1 from the spleen (Figure 16) and isolated RNA as described as described before.

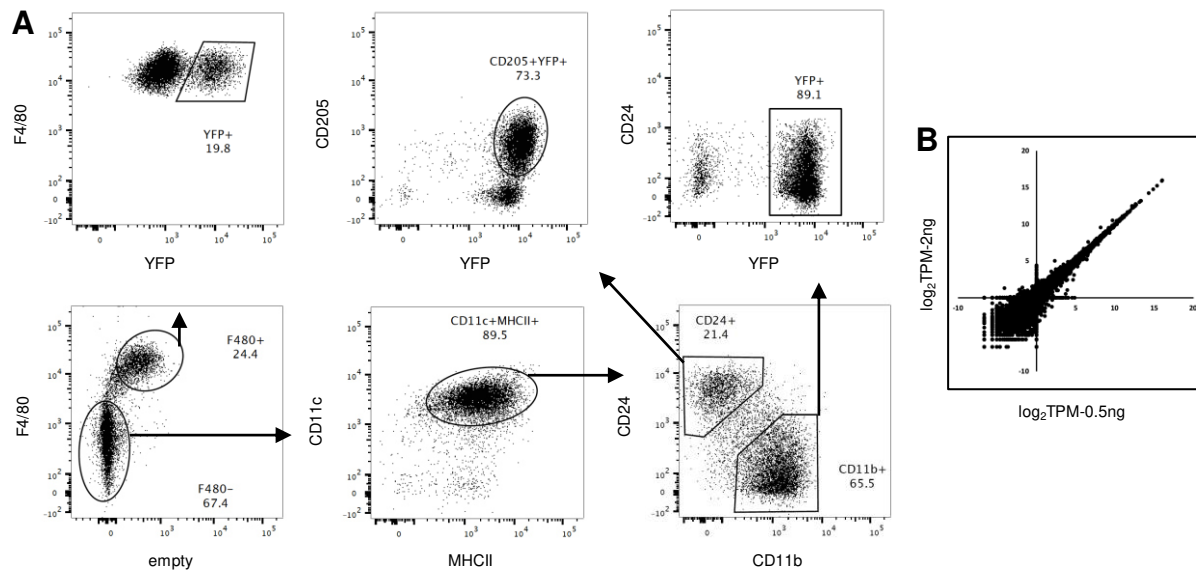


Figure 16. Sorting strategy for splenic cDCs and library preparation test with cDC1. (A) Sorting strategy for purification of splenic DC populations and macrophages from *Clec9a^{Cre}Rosa^{YFP}* mice. Red pulp macrophages were identified as Autofluorescence⁺F4/80⁺YFP⁺ cells. DCs were identified as Autofluorescence^{neg}CD11c⁺MHCII⁺ cells and then split into CD24⁺ cDC1 and CD11b⁺ cDC2. Only CD205⁺YFP⁺ cDC1 and YFP⁺ cDC2 were sorted. (B) Dot plot of TPM values after sequencing of CD205⁺YFP⁺ cDC1 libraries prepared from different starting amounts of RNA (2 ng and 0.5 ng).

From the purified RNA of this sample we used 0.5 ng and 2 ng as input for the library preparation as described above.

We sequenced the finished libraries as 50 bp single-read with a depth of 20 million reads per sample. We took normalized gene expression from both samples and plotted them against each other (Figure 16). Since most of the genes were falling on a 45° axis, which indicates equal gene expression values, we concluded that there is no qualitative difference between the two RNA input amounts in this protocol.

3.2.2. Sorting strategy to isolate splenic and renal DC subsets

To analyse the transcriptomic profile of DC subsets in the kidney we sort purified cDC1, cDC2, F4/80^{hi} cells and CD11b^{hi} cells from the kidney to perform RNAseq (Example of gating strategy and sort purity for F4/80^{hi} cells see Figure 17).

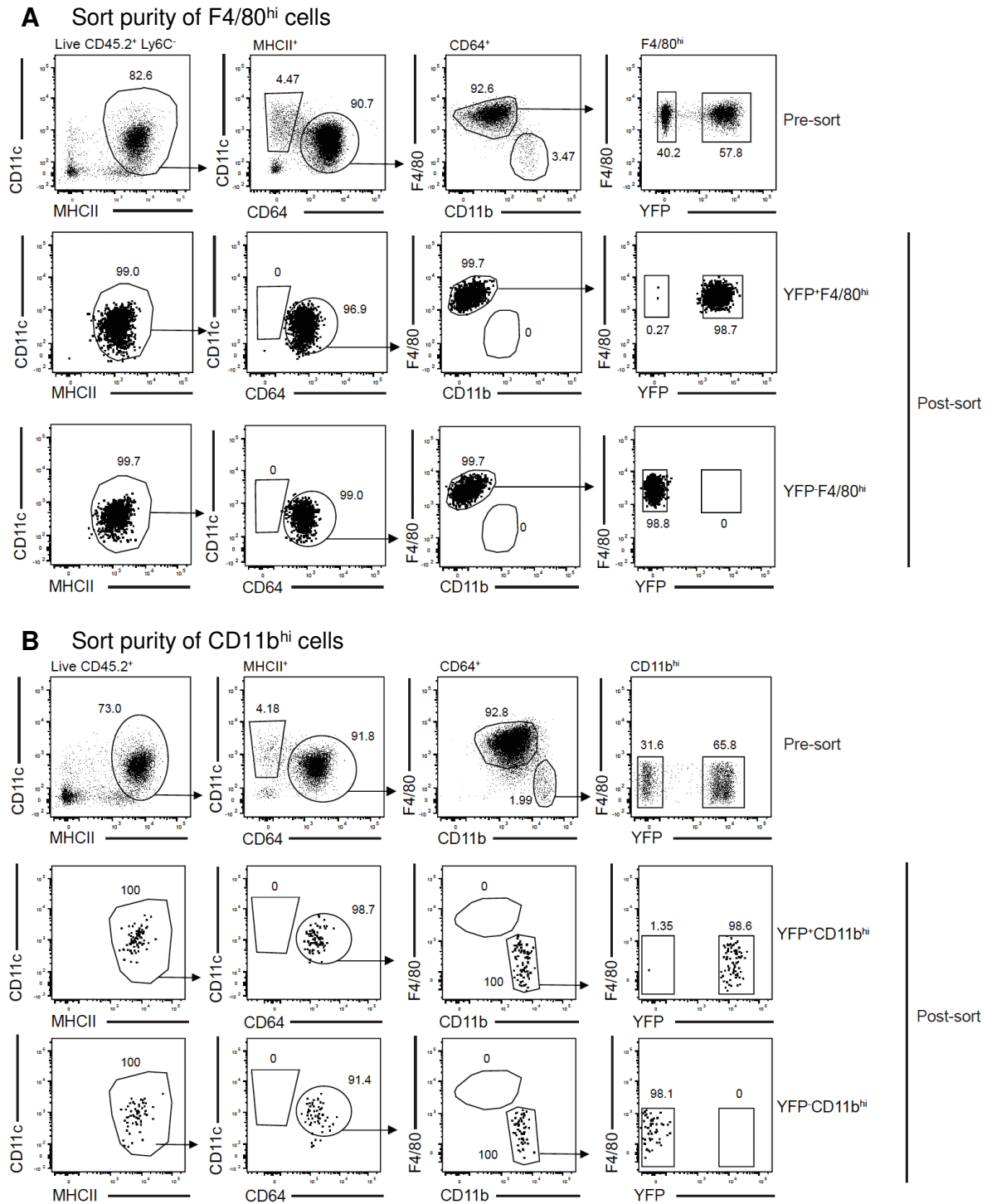


Figure 17. Sort purity of renal YFP⁺ and YFP⁻ F4/80^{hi} cells as well as CD11b^{hi} cells. (A) Example of sorting strategy and purity check for renal F4/80^{hi} cells isolated from *Clec9a^{Cre}Rosa^{YFP}* mice. F4/80^{hi} cells were identified as MHCII⁺CD64⁺F4/80^{hi}CD11b^{low} and then sorted as YFP⁺ or YFP⁻ for RNA sequencing. (B) Example of sorting strategy and purity check for renal CD11b^{hi} cells. CD11b^{hi} cells were identified as MHCII⁺CD64⁺CD11b^{hi}F4/80^{low} and then sorted as YFP⁺ or YFP⁻ for RNA sequencing (Modified from Salei *et al.*, 2020)

In addition, we sorted YFP⁺ cDC1, YFP⁺ cDC2 and YFP⁻ red pulp macrophages from the spleen as control populations for DCs and macrophages. We did this to be able to show, which DC subsets from the kidney have transcriptomic similarities to other DCs or macrophages. Because the labelling in cDC2, CD11b^{hi} cells and F4/80^{hi} cells is not complete we sorted both YFP⁺ and YFP⁻ fractions of these cells. By comparing the transcriptome of YFP⁺ and YFP⁻ cells from the same subset we wanted to address whether there is any evidence for different gene expression profiles caused by a different ontogenetic background.

3.2.3. Characterization of transcriptional profiles of renal DC subsets

3.2.3.1. Principal component analysis of DC subsets from the spleen and kidney

Sequencing of the finished libraries was performed by the Laboratory for Functional Genome Analysis (LAFUGA, Gene Center LMU). Finished runs were demultiplexed and aligned to the mm10 mouse genome using the STAR aligner as mentioned before. We used principal component analysis (PCA) of the top 5000 most variable genes across all sequenced samples to get a first glance at which population cluster together. We saw two major trends which organized the PCA, principal component 1 (PC1) segregated different DC subsets and macrophages from another and PC2 showed differences between related subsets/cell types which were isolated from different organs (Figure 18). As expected, renal cDC1 and cDC2 clustered close to their respective counterparts isolated from the spleen, which indicates a core DC signature and subset specific expression of genes which is conserved across organs. F4/80^{hi} cells clustered close to red pulp macrophages, further confirming that F4/80^{hi} cells from the kidney do not only resemble macrophages based on phenotypic markers but also based on their transcriptomic signature. Notably, YFP⁺ and YFP⁻ F4/80^{hi} cells do not show any obvious transcriptomic differences despite the fact that they may be derived from different progenitors. CD11b^{hi} cells localized between F4/80^{hi} cells and renal cDC2 indicating that they are indeed a unique subset in the kidney distinct from both cDC2 and F4/80^{hi} cells. Same as for F4/80^{hi} cells also CD11b^{hi} cells did not show a big difference between YFP⁺ and YFP⁻ fractions.

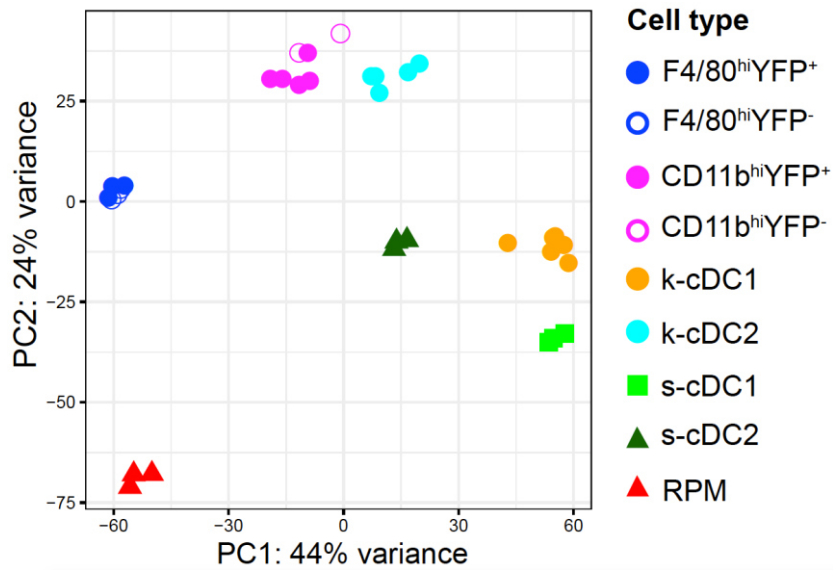


Figure 18. PCA of renal and splenic DC populations as well as red pulp macrophages at steady state. PCA based on top 500 genes with highest variance across sequenced samples. Each dot represents one biological replicate. Each dot represents one mouse. (Modified from Salei *et al.*, 2020)

To confirm previous results by Schraml *et al.*, 2013 that CD11b^{hi} cells and F4/80^{hi} cells are not YFP labelled because of *Clec9a* expression in their differentiated state we manually aligned the samples isolated from the kidney to the *iCre* sequence (GenBank ID: AY056050.1) (Figure 19) (Schraml *et al.*, 2013).

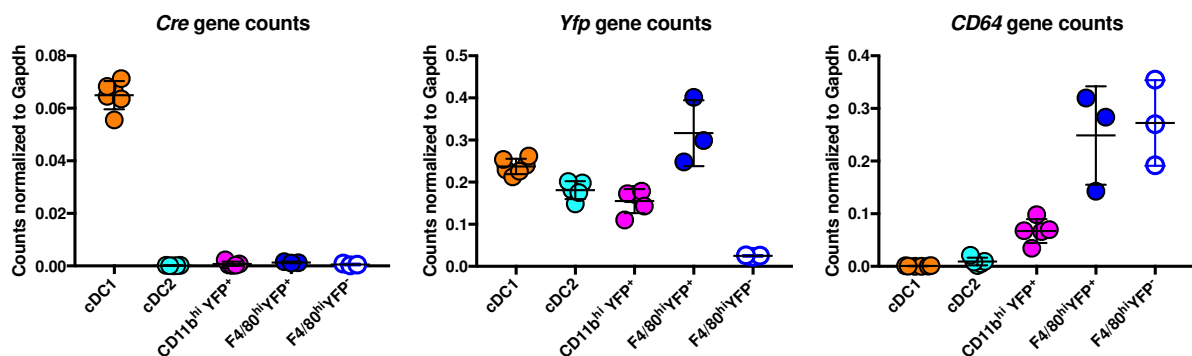


Figure 19. Manual alignment of sequencing reads to identify *Cre* expression. RNA sequencing reads of renal DC populations were manually aligned to *Cre*, *Yfp* and *CD64* sequences using Shortread and Biostrings packages in R-Studio. Each dot represents one mouse. Horizontal bars indicate mean, error bars indicate SD. (Modified from Salei *et al.*, 2020)

Our results clearly showed that we were not able to detect any *Cre* reads in our RNAseq data, strengthening the specificity of the *Clec9a^{Cre}* model and confirming previous qPCR results from Schraml *et al.* (Schraml *et al.*, 2013). To confirm the validity of our approach we also performed manual alignment of other markers such as CD64 and YFP. F4/80^{hi} cells showed high expression of CD64 as expected and we detected low CD64 levels in CD11b^{hi} cells but not cDC1 or cDC2. In addition, all samples which were sorted as YFP⁺ also showed YFP mRNA, thereby confirming our manual alignment approach.

Pairwise comparison of YFP⁺ and YFP⁻ F4/80^{hi} cells or YFP⁺ and YFP⁻ CD11b^{hi} cells with a log₂foldchange > 4 and an adjusted p-value < 0.05 yielded almost no differentially expressed genes (Figure 20).

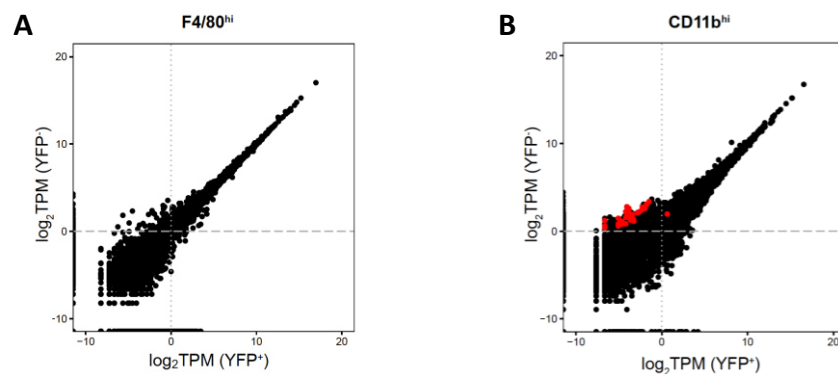


Figure 20. Comparison of normalized gene expression values between YFP⁺ and YFP⁻ populations. (A) log₂TPM values of YFP⁺F4/80^{hi} cells plotted against YFP⁻F4/80^{hi} cells. (B) log₂TPM values of YFP⁺CD11b^{hi} cells plotted against YFP⁻CD11b^{hi} cells. (Modified from Salei *et al.*, 2020)

We therefore concluded that YFP labelling could not be used to reveal ontogenetic differences in these two populations on a transcriptomic level and focused on YFP⁺ cells for further analyses.

3.2.3.2. K-means clustering of renal DC subsets

We performed pairwise comparisons between renal cDC1, cDC2, CD11b^{hi} cells and F4/80^{hi} cells to get an initial idea about transcriptional differences between these populations and to maybe identify defining markers for each subset. K-means clustering on the results of these comparisons yielded 15 clusters with distinct gene expression patterns across the four populations (Figure 21).

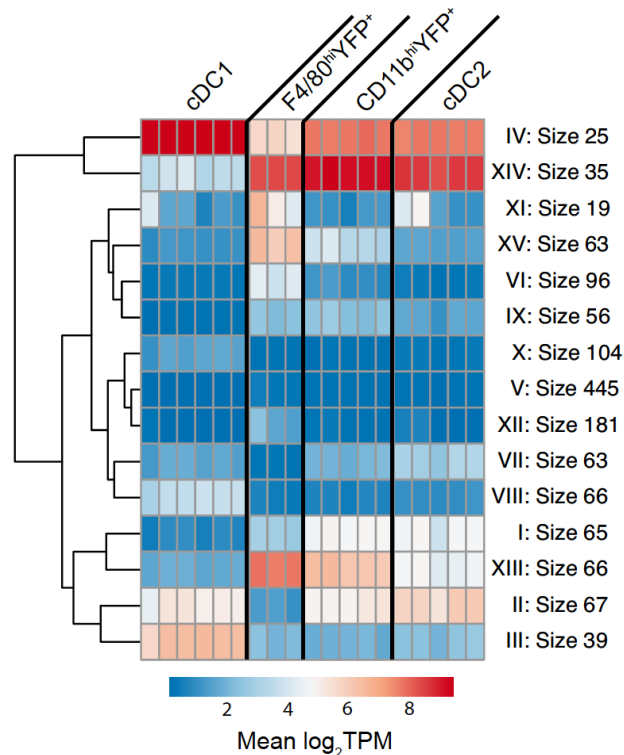


Figure 21. Clustering analysis between renal DC populations. K-means clustering of differentially expressed genes between renal DC subsets with a \log_2 foldchange > 4 and an adjusted p-value < 0.05 . (Modified from Salei *et al.*, 2020)

Clusters XI, XV, XIII contained genes higher expressed in F4/80^{hi} cells although clusters XIII and XV also seemed to be characteristic for CD11b^{hi} cells. Clusters XII and XV also contained genes, which were used to identify these populations, namely *Fcgr1* (CD64), *Emr1* (F4/80) and *Itgam* (CD11b). Moreover, these clusters contained many more genes commonly associated to macrophages, such as *C5ar1*, *C3r1*, *Fcgr4*, *Matb*, *Tmem119*, *C1qa*, *Apoe*, *Cx3cr1* (Cronk *et al.*, 2018; Zimmerman *et al.*, 2019). Clusters IV and II contained genes expressed in cDC1, cDC2 and CD11b^{hi} cells but not in F4/80^{hi} cells including known markers of conventional DCs such as *Flt3*, *Ccr7*, *Zbtb46* or *Amica1* (Miller *et al.*, 2012).

3.2.3.3. F4/80^{hi} cells have a transcriptional profile similar to macrophages

Considering that renal F4/80^{hi} cells showed expression of many genes associated to macrophages we analysed the expression of genes from clusters XI, XV and XIII and compared them to red pulp macrophages sorted from the spleen (Figure 22).

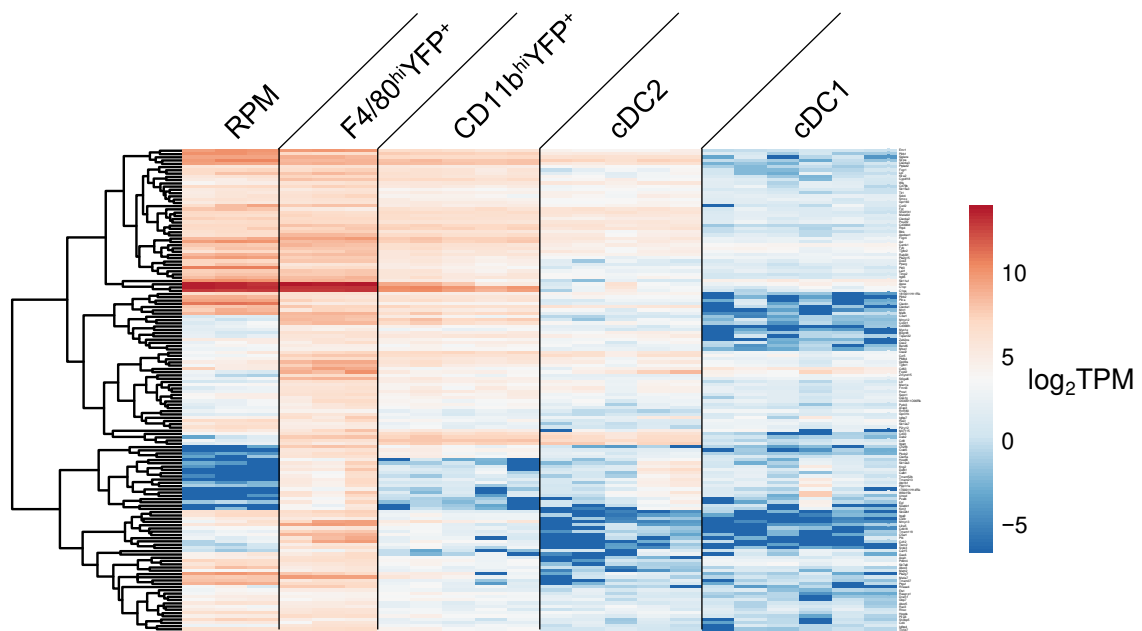


Figure 22. Expression of genes from cluster XI, XIII and XV. Expression of genes from F4/80^{hi} specific clusters XI, XIII and XV in renal DC subsets and splenic red pulp macrophages. Gene expression depicted as log₂TPM values.

As visualized by the blue-to-red gradient most genes from clusters which are highly expressed by renal F4/80^{hi} cells were also expressed in splenic red pulp macrophages. This further confirmed that F4/80^{hi} cells resemble macrophages on a transcriptional level. Interestingly, CD11b^{hi} cells showed intermediate expression of many of the shown genes indicating that it has a mixed transcriptomic signature, harbouring characteristic genes of both macrophages and DCs. Many studies tried to assign a core-signature of genes to conventional DCs or to macrophages (Cronk et al., 2018; Gautier et al., 2012; Miller et al., 2012; Scott et al., 2018). While these signatures are not perfect, we thought it could give us a hint whether there is any ontogenetic evidence of a DC origin for F4/80^{hi} cells. We chose a core-macrophage signature from Gautier et al. and a core-cDC signature from Miller et al. and analysed the expression of those genes in our renal DC populations (Figure 23) (Gautier et al., 2012; Miller et al., 2012).

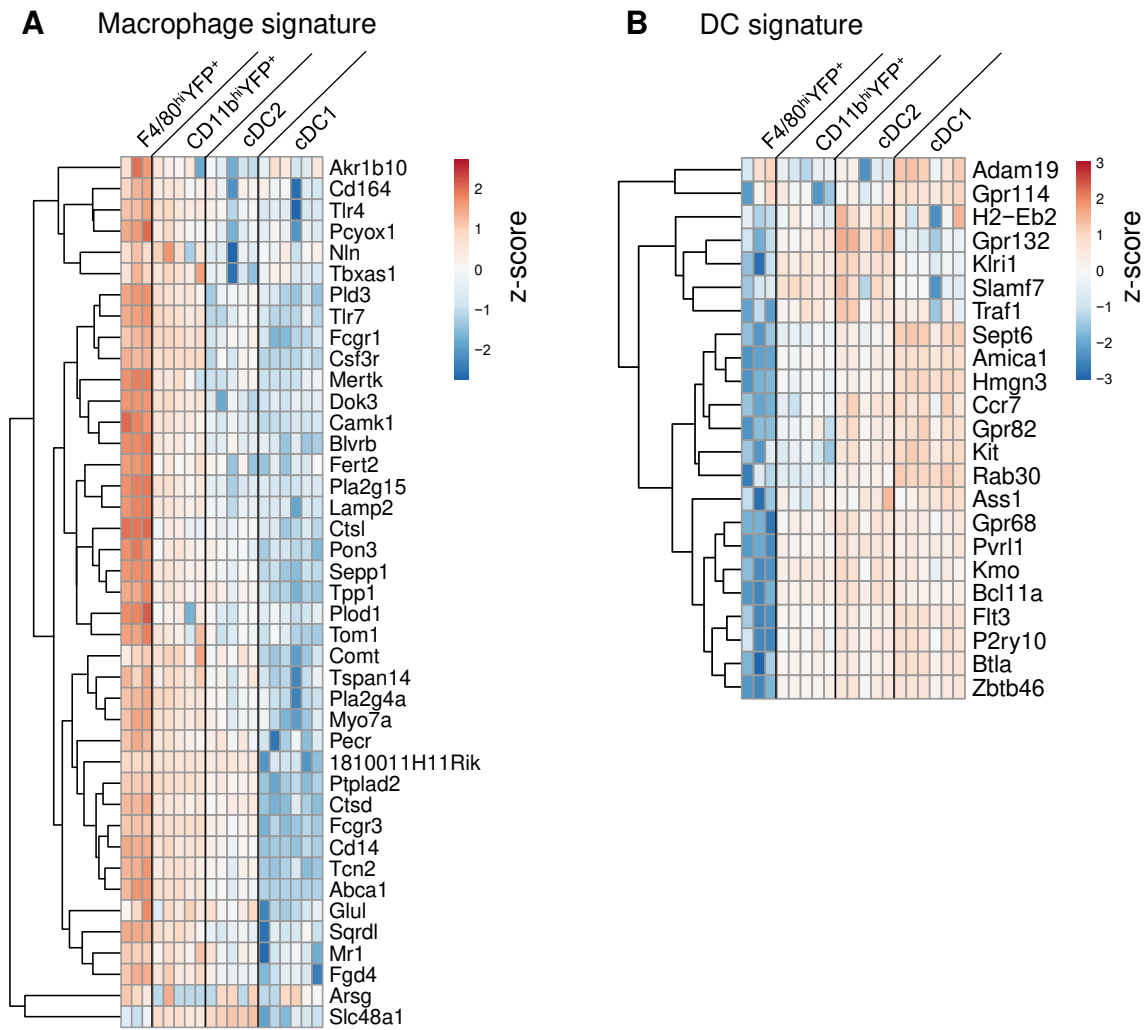


Figure 23. Core-macrophage and core-DC signature expression on renal DC subsets. (A) Expression of genes from a core-macrophage signature described in Gautier et al. on renal DC subsets (Gautier et al., 2012). (B) Expression of genes from a core-cDC signature described in Miller et al. on renal DC subsets (Miller et al., 2012).

Expression of genes from the core-macrophage signature was clearly enriched in F4/80^{hi} cells, strengthening the observation that this population is very much related to macrophages from other tissue based on its transcriptional profile (Figure 23B). CD11b^{hi} cells and to a lesser extent cDC2 also expressed genes from this list. In line with this observation, F4/80^{hi} cells expressed core-cDC genes to a lesser compared to CD11b^{hi} cells, cDC2 and cDC1 (Figure 23B). This both shows the macrophage-like transcriptional profile of F4/80^{hi} cells and it also demonstrates that CD11b^{hi} are also related to the DC lineage on a transcriptional level.

3.2.3.4. CD11b^{hi} cells are a unique DC subset with transcriptional characteristics of both macrophages and DCs

To analyse transcriptional differences between CD11b^{hi} cells and cDC2 or F4/80^{hi} cells we performed pairwise comparison using DESeq2. As cutoffs for differentially expressed genes we chose a log₂foldchange > 4 and an adjusted p-value < 0.05.

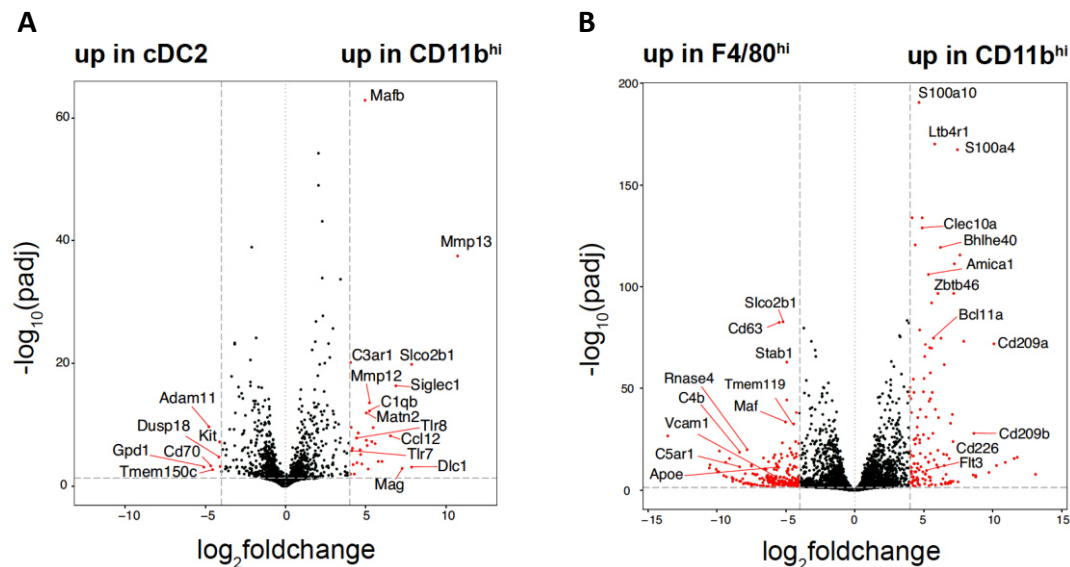


Figure 24. Pairwise comparison of CD11b^{hi} cells to cDC2 and F4/80^{hi} cells. (A) Pairwise comparison of renal cDC2 with CD11b^{hi} cells. Genes with a log₂foldchange > 4 and an adjusted p-value < 0.05 are depicted as red dots. (B) Pairwise comparison of renal F4/80^{hi} cells with CD11b^{hi} cells. Genes with a log₂foldchange > 4 and an adjusted p-value < 0.05 are depicted as red dots. (Modified from Salei *et al.*, 2020)

The comparison between cDC2 and CD11b^{hi} cells only identified 38 differentially expressed genes (Figure 24). Lowering the cutoff to log₂foldchange > 3 increased the number to 95 differentially expressed genes (Figure 25). Among differentially genes we found potential targets for studies addressing functional differences between these two populations, e.g. toll-like receptors (*Tlr* 7 and *Tlr*8). Some genes higher expressed in CD11b^{hi} cells compared to cDC2 included genes, which are commonly associated with macrophages such as *Mafb*, *C1qb* or *C3ar1* (Figure 24). This shows a transcriptional overlap between CD11b^{hi} cells and macrophages, an observation, which was also visible in the core-signature analysis (Figure 23). In line with this, a heatmap containing genes differentially expressed between cDC2 and CD11b^{hi} cells

with a \log_2 foldchange > 3 illustrates that many genes higher expressed in CD11b^{hi} cells are also expressed in F4/80^{hi} cells (Figure 25).

Whereas the differences between cDC2 and CD11b^{hi} cells are few as expected, we identified 362 differentially expressed genes with a \log_2 foldchange > 4 between CD11b^{hi} cells and F4/80^{hi} cells. Interestingly, in this comparison the CD11b^{hi} cells showcased their close relationship to cDC2s and the DC lineage. Many of the genes higher expressed in CD11b^{hi} cells like *Zbtb46*, *Flt3*, *Amica1* or *Bcl11a* are commonly associated with cDCs (Figure 24B) (Miller et al., 2012). As expected, F4/80^{hi} cells were enriched with genes usually attributed to macrophages such as *Tmem119*, *Maf*, *ApoE* or *C5ar1* (Figure 24B) (Gautier et al., 2012).

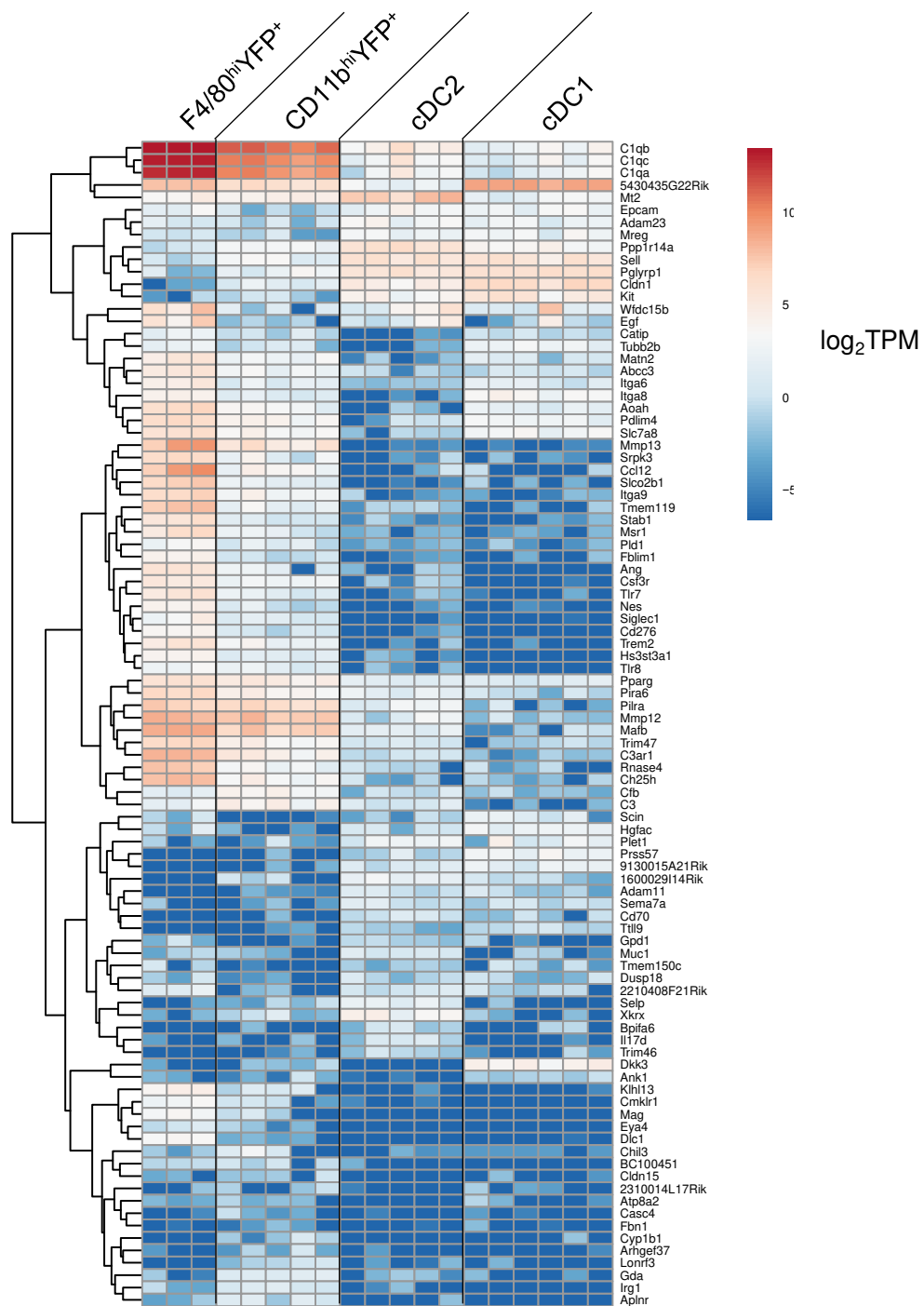


Figure 25. Heatmap of genes differentially expressed between cDC2 and CD11b^{hi} cells.

Heatmap depicting differentially expressed genes between renal cDC2 and CD11b^{hi} cells with a log₂foldchange > 3 and an adjusted p-value < 0.05. Gene expression is shown as log₂TPM values.

Intrigued by our findings that *Tlr7* and *Tlr8* were differentially expressed between CD11b^{hi} cells and cDC2 we looked at other potential targets for functional studies. This analysis revealed that also other pathogen-recognition receptors such as

Dectin1, TLR2 and TLR4 are differentially expressed between renal DC subsets (Figure 26). This provides a valuable tool for future studies and was already used to confirm functional differences between cDC2 and CD11b^{hi} cells in response to TLR ligands (Salei et al., 2020).

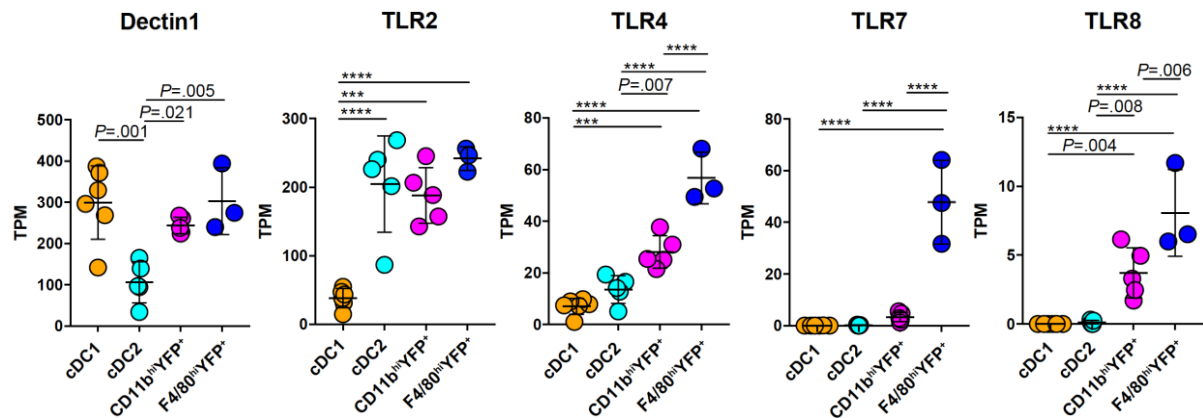


Figure 26. Differentially expressed pattern recognition receptors between renal DC subsets. TPM expression values of pattern-recognition receptors Dectin1, TLR2, TLR4, TLR7 and TLR8 in renal cDC1 (orange), cDC2 (cyan), CD11b^{hi} cells (magenta) and F4/80^{hi} cells (blue). Each dot represents one mouse. Horizontal bars indicate mean, error bars indicate SD. *** p-value < 0.001, **** p-value < 0.0001 (Modified from Salei *et al.*, 2020)

Overall the transcriptional analysis of renal DC subsets clearly showed that CD11b^{hi} cells are a unique DC subset with characteristics of both macrophages and DCs. These analyses further demonstrated that F4/80^{hi} cells – despite their DC origin – strongly resemble macrophages from other tissues.

3.3. F4/80^{hi} cells downregulate MHCII upon cisplatin-induced AKI and may orchestrate leukocyte infiltration through production of chemokines

3.3.1. Disease induction after cisplatin-induced acute kidney injury

Having established that *Clec9a*^{Cre} faithfully traces DC subsets in steady state we wanted to analyse the dynamics and function of DCs after kidney injury. From multiple kidney injury models established in the field we chose to use cisplatin-induced acute kidney injury because it is a fast model with established doses of cisplatin for reliable results. In this model a high dose of cisplatin is injected *i.p.* and leads to kidney damage through cisplatin-uptake in proximal tubular epithelial cells (Ozkok &

Edelstein, 2014). We again used *Clec9a^{Cre}Rosa^{YFP}* mice to be able to identify cells with DC origin after disease induction. Mice were sacrificed 72 h after cisplatin injection and spleen, kidneys and blood were collected. Kidney damage was assessed by the concentration of blood urea nitrogen (BUN) and creatinine in the blood serum. Cisplatin injection lead to a significant increase of BUN and creatinine levels in the serum compared to control mice injected with NaCl indicating a stable induction of kidney injury (Figure 27).

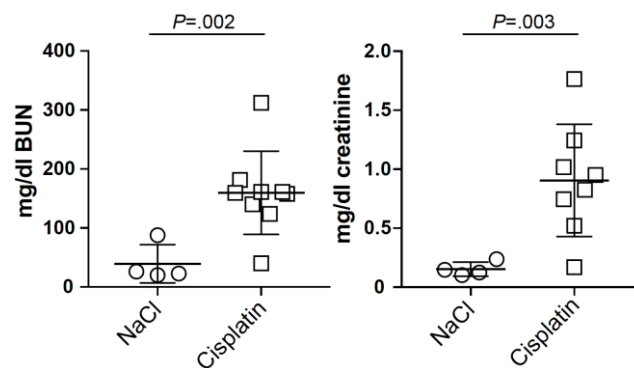


Figure 27. Serum levels of BUN and creatinine. BUN and Creatinine levels of *Clec9a^{Cre}Rosa^{YFP}* mice with cisplatin-induced AKI and *Clec9a^{Cre}Rosa^{YFP}* mice injected with NaCl. Each dot represents one mouse. Horizontal bars indicate mean, error bars indicate SD. (Modified from Salei *et al.*, 2020)

3.3.2. YFP labelling remains restricted to DCs after cisplatin-induced acute kidney injury

Using flow cytometry, we were able to identify the same populations as in IRI (Gating strategy see Figure 28). We again noticed a downregulation of MHCII, which lead to the appearance of MHCII^{neg}F4/80^{hi} cells. Same as in IRI we saw a large influx of inflammatory cells, with Ly6G⁺ neutrophils being the major infiltrating populations (Figure 29). The MHCII⁺ gate contained the four populations with DC origin as defined at steady state. Notably, we saw a decrease of cDC1 and cDC2 after cisplatin-induced AKI, a dynamic, which we could not observe in IRI (Figure 29). We found a slight decrease in F4/80^{hi} cells, which was accompanied by a decrease in MHCII^{neg}F4/80^{hi} cells, however the increase of MHCII^{neg}F4/80^{hi} cells was not as pronounced as we saw in IRI.

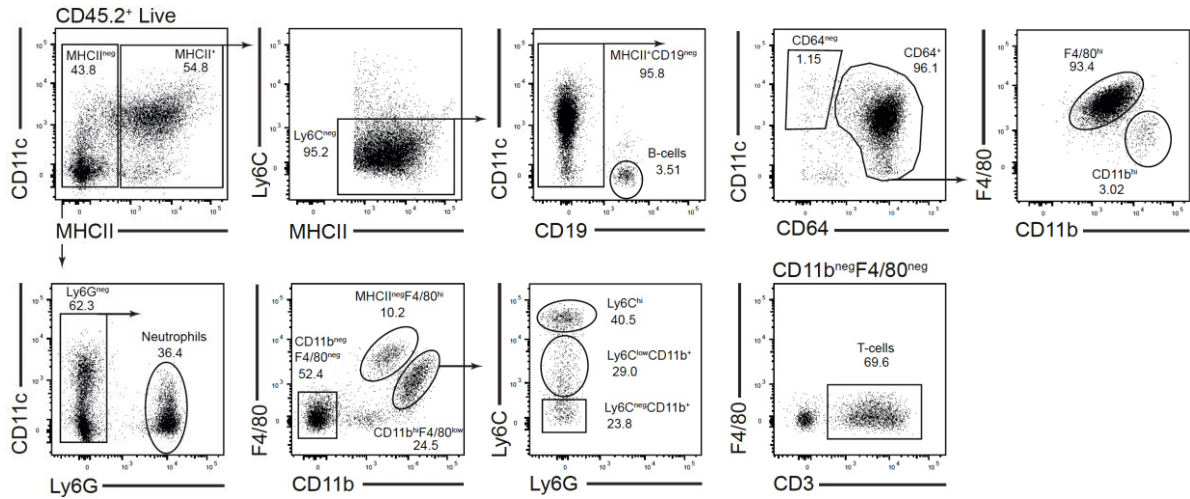


Figure 28. Gating strategy to identify renal leukocyte populations after cisplatin-induced AKI. Flow cytometric analysis of renal leukocyte populations isolated from *Clec9a^{Cre}Rosa^{YFP}* mice after cisplatin-induced kidney injury. Live CD45.2⁺ cells were split into MHCII⁺ and MHCII^{neg} cells. Ly6C⁺ inflammatory cells and CD19⁺ B cells were excluded from the MHCII⁺ populations. Remaining MHCII⁺ cells were split into CD64⁺ and CD64⁻. CD64⁺ cells contained F4/80^{hi} cells and CD11b^{hi} cells. CD24⁺ cDC1 and CD11b⁺ cDC2 were identified in CD64⁻ cells. MHCII^{neg} cells contained Ly6G⁺ neutrophils. Remaining Ly6G⁻ cells were split into MHCII^{neg}F4/80^{hi} cells, CD11b⁺F4/80⁺ cells and CD11b^{neg}F4/80^{neg} cells. The latter contained CD3⁺ T cells. CD11b⁺F4/80⁺ cells contained Ly6C^{hi} monocytes as well as Ly6C^{int}CD11b⁺ and Ly6C^{neg}CD11b⁺ cells (Modified from Salei *et al.*, 2020)

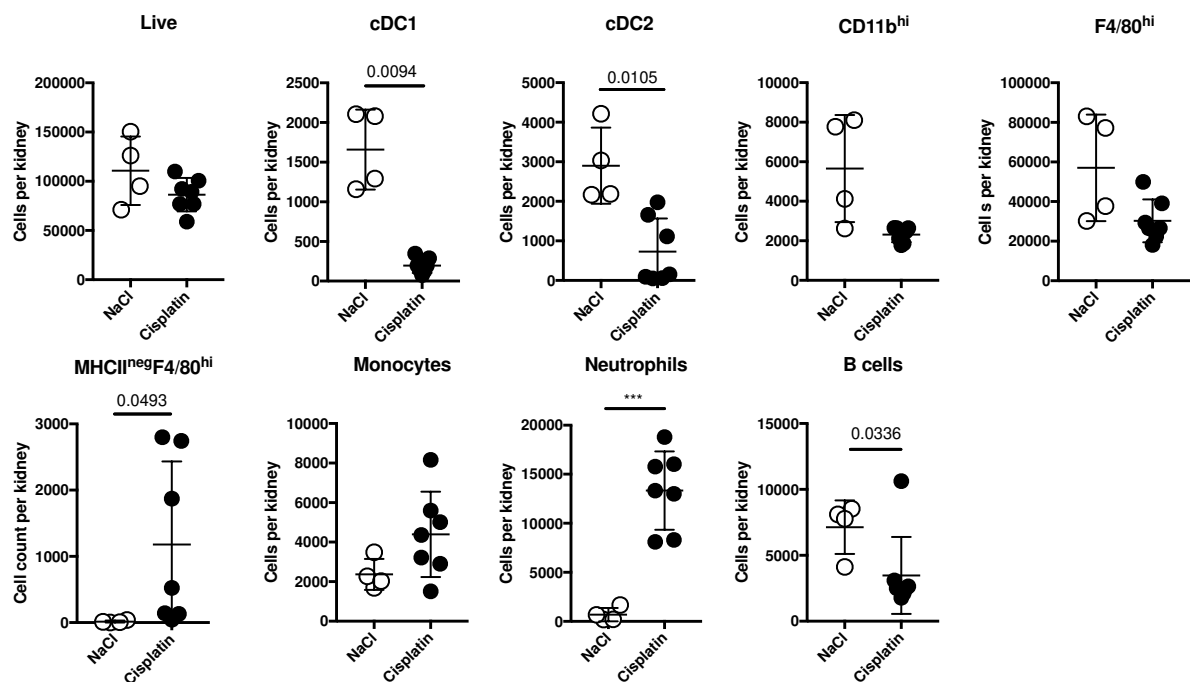


Figure 29. Quantification of renal leukocyte populations after cisplatin-induced AKI. Number of renal leukocyte populations per kidney isolated after cisplatin-induced AKI (black)

or control NaCl injection (white) in *Clec9a^{Cre}Rosa^{YFP}* mice. Each dot represents one mouse. Horizontal bars indicate mean, error bars indicate SD. *** p-value < 0.001

When we looked at YFP labelling the renal leukocyte populations we found that the four DC populations we found at steady state were still labelled with YFP after cisplatin-induced AKI. The remaining cDC1 were almost completely labelled as expected (95±5%). But also cDC2 (83±5%), CD11b^{hi} cells (68±3%) and F4/80^{hi} cells (62±10%) were highly labelled in the *Clec9a^{Cre}* model after kidney injury (Figure 30). Notably, the labelling percentage of cDC2, CD11b^{hi} cells and F4/80^{hi} cells was comparable to steady state conditions, indicating that in the cisplatin-induced AKI model there is substantially less influence of inflammatory cells on the dynamics of DC populations. Apart from the before mentioned populations only MHCII^{neg}F4/80^{hi} cells were highly labelled with YFP, suggesting a DC origin, all other tested cell types were not labelled above background levels.

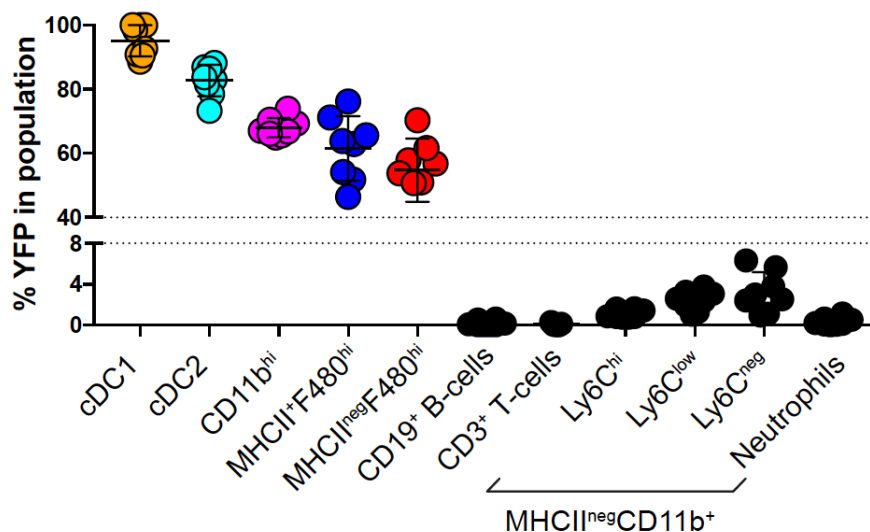


Figure 30. YFP labelling in renal leukocytes after cisplatin-induced AKI. YFP labelling percentage in the indicated populations after cisplatin-induced AKI in *Clec9a^{Cre}Rosa^{YFP}* mice. Each dot represents one mouse. Horizontal bars indicate mean, error bars indicate SD. (Modified from Salei *et al.*, 2020)

Same as with the IRI model, we wanted to confirm for the cisplatin-induced AKI model that we were not excluding YFP labelled populations based on the gating strategy we chose. Therefore, we performed tSNE analysis on the flow cytometry data and overlaid our manually gated populations on the resulting plot (Figure 31). This analysis clearly

demonstrated that YFP labelling could only be observed in four DC populations and MHCII^{neg}F4/80^{hi} cells.

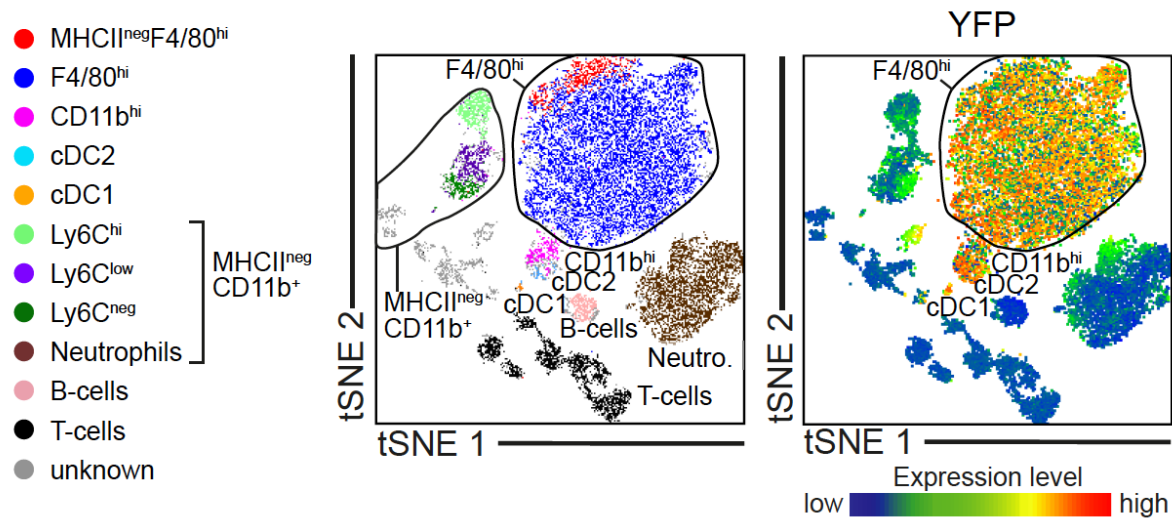


Figure 31. tSNE analysis of renal leukocytes after cisplatin-induced AKI. Representative tSNE analysis of renal leukocytes isolated from kidney of *Clec9a*^{Cre}*Rosa*^{YFP} mice with cisplatin-induced AKI. Left plot shows manually gated populations (see Figure 28) overlaid on tSNE plot in the indicated colors. Right plots shows YFP expression among renal leukocytes. (Modified from Salei *et al.*, 2020)

3.3.3. F4/80^{hi} cells downregulate MHCII on a protein level after cisplatin-induced kidney injury

For analysing the changes in MHCII signal on F4/80^{hi} cells we employed a different gating strategy. Starting from CD45.2⁺ live cells we excluded Ly6C⁺ cells and identified F4/80^{hi} cells as F4/80^{hi}CD64⁺ cells independent of MHCII expression. We then compared the MHCII expression on these cells between the control group (Blue) and the group with cisplatin injection (Red) (Figure 32). Same as in IRI this analysis shows a clear downregulation of MHCII on F4/80^{hi}CD64⁺ cells, which leads to the appearance of MHCII^{neg}F4/80^{hi} cells in our standard gating strategy.

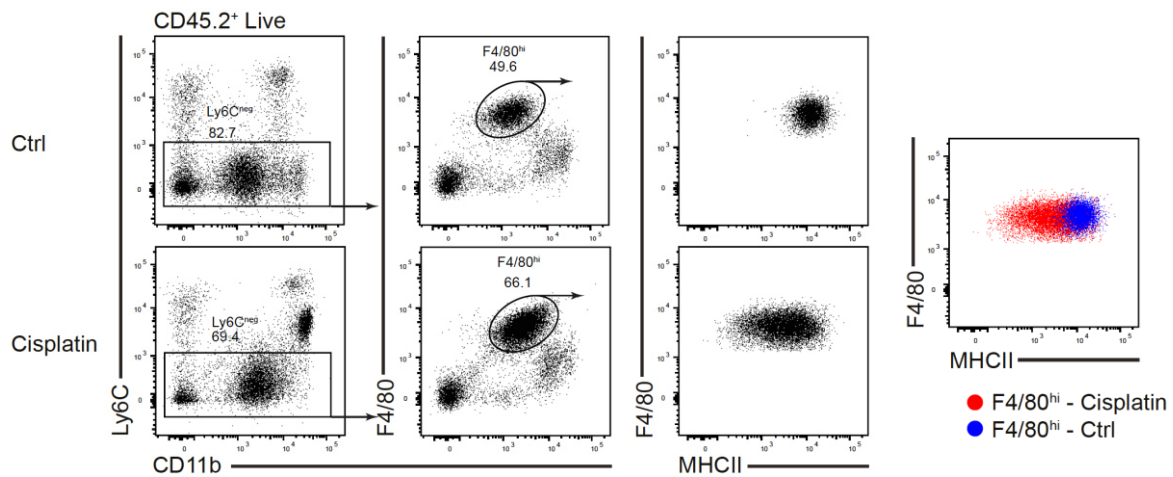


Figure 32. F4/80^{hi} cells downregulate MHCII after cisplatin-induced AKI. Flow cytometric analysis of kidneys isolated from control-injected *Clec9a^{Cre}Rosa^{YFP}* mice (top row) or *Clec9a^{Cre}Rosa^{YFP}* mice with cisplatin-induced AKI (bottom row). F4/80^{hi} cells were identified independent of MHCII expression among live CD45.2⁺ cells as Ly6C^{res}F4/80^{hi}CD11b^{low}. The third column of dot plots shows MHCII expression on F4/80^{hi} cells in sham-operated or injured kidney. An overlay of these two plots shows F4/80^{hi} cells from IRI kidney as red dots and from sham-operated kidney in blue dots. (Modified from Salei *et al.*, 2020)

3.3.4. Ischemia reperfusion injury leads to influx of inflammatory cells and to a downregulation of MHCII on F4/80^{hi} cells

To confirm our observation that F4/80^{hi} cells downregulate MHCII after kidney injury we decided to utilize the unilateral ischemia reperfusion injury model. It is another well-established kidney injury model and similar to cisplatin-induced AKI it was shown that DCs or macrophages play important roles in this model (Rogers *et al.*, 2014). IRI was performed with *Clec9a^{Cre}Rosa^{YFP}* mice in collaboration with Prof. Anders (LMU) as described above. For each mouse the artery of one kidney was clamped for 25 minutes, the second kidney was not operated. We isolated kidneys 72h after IRI and analysed population dynamics and labelling using flow cytometry (Gating strategy see Figure 33).

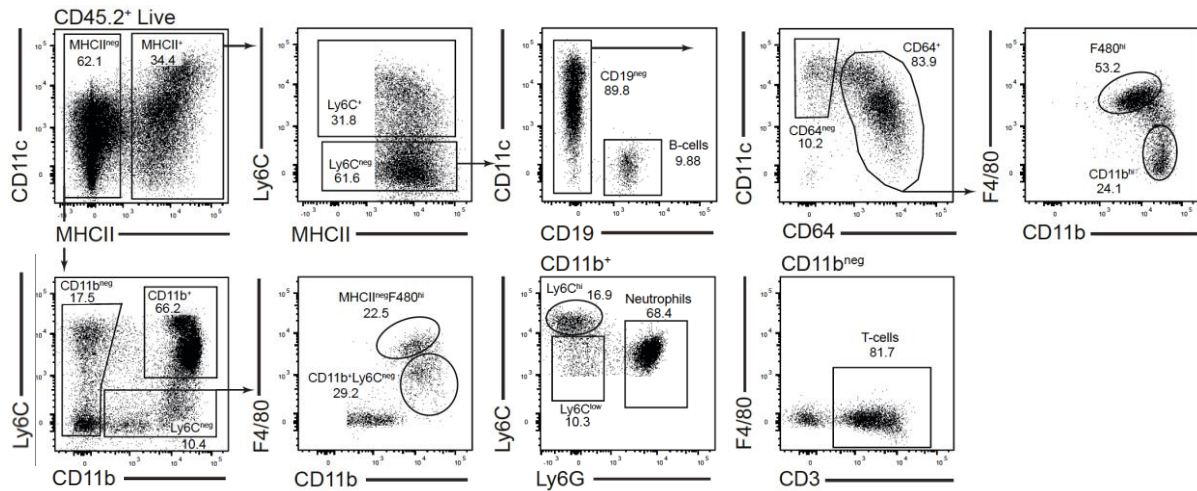


Figure 33. Gating strategy to identify renal myeloid and lymphoid cell populations after IRI. Flow cytometric analysis of renal leukocyte populations after IRI-induced kidney injury in *Clec9a^{Cre}Rosa^{YFP}* mice. Live CD45.2⁺ cells were split into MHCII⁺ and MHCII^{neg} cells. Ly6C⁺ inflammatory cells and CD19⁺ B cells were excluded from the MHCII⁺ populations. Remaining MHCII⁺ cells were split into CD64⁺ and CD64⁻. CD64⁺ cells contained F4/80^{hi} cells and CD11b^{hi} cells. CD24⁺ cDC1 and CD11b⁺ cDC2 were identified in CD64⁻ cells. MHCII^{neg} cells were split into CD11b^{neg}, CD11b⁺Ly6C⁺ and CD11b⁺Ly6C^{neg} populations. CD3⁺ T cells were identified among the CD11b^{neg} cells. CD11b⁺Ly6C^{neg} cells contained MHCII^{neg}F4/80^{hi} cells and CD11b⁺ cells with intermediate expression of F4/80. Ly6C^{hi} monocytes and Ly6C⁺ neutrophils were identified in the CD11b⁺Ly6C⁺ population. (Modified from Salei *et al.*, 2020)

We noticed a striking influx of inflammatory CD11b⁺ cells in the ischemic kidney, mostly comprised of Ly6C⁺ neutrophils and Ly6C^{hi} monocytes (Figure 34). We further noticed a decrease of F4/80^{hi} cells in the damaged kidneys compared to the control organs (Figure 34). This decrease of F4/80^{hi} cells was accompanied by an increase of MHCII^{neg}F4/80^{hi} cells as described by Lever *et al.* (Lever *et al.*, 2019) (Figure 34).

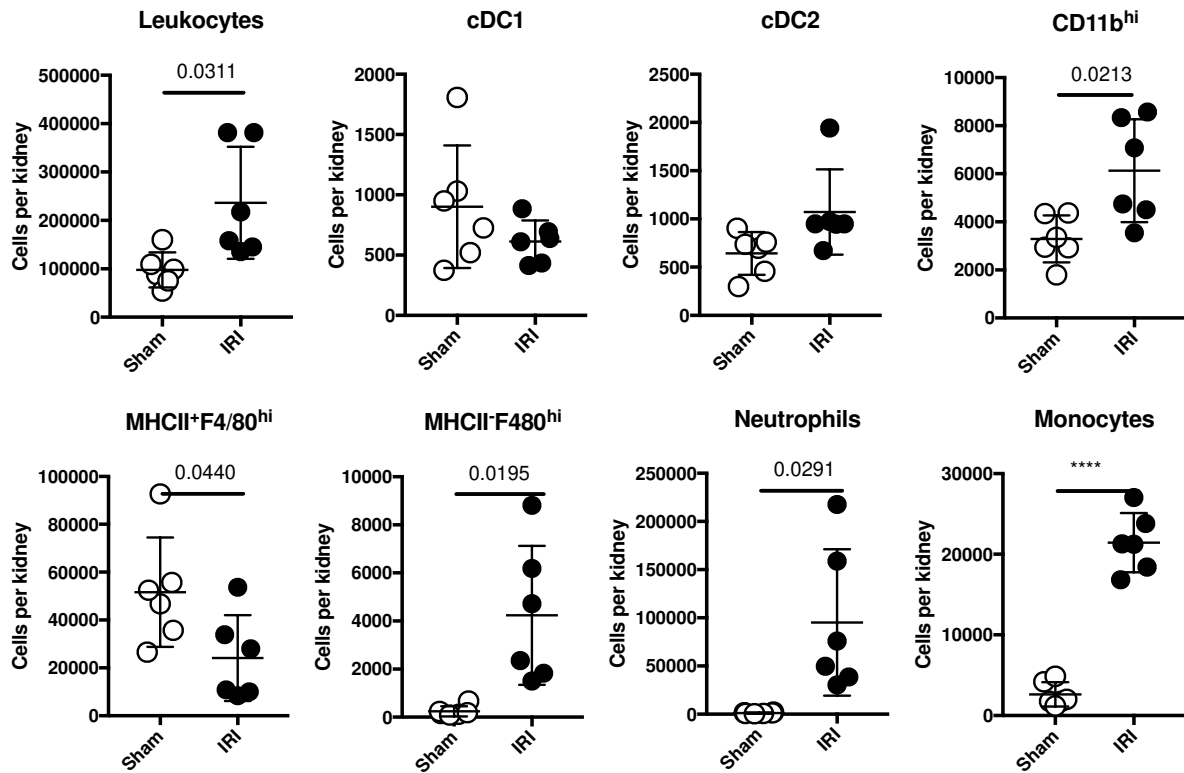


Figure 34. Frequency of mononuclear phagocyte populations in the kidney after IRI. Number of renal leukocyte populations per kidney isolated after IRI-induced AKI (black) or from sham operated *Clec9a^{Cre}Rosa^{YFP}* mice (white). Each dot represents one mouse. Horizontal bars indicate mean, error bars indicate SD. **** p-value < 0.0001

Interestingly, when we gated on F4/80^{hi} cells independent of MHCII based on the expression of CD11b and F4/80 we had two observations. On the one hand some cells showed a complete loss of MHCII signal on F4/80^{hi} cells in the ischemic kidney compared to control (Figure 35). On the other hand, a part of the F4/80^{hi} population in ischemic kidney had intermediate expression levels of MHCII indicating a gradual loss of MHCII expression on F4/80^{hi} cells (Figure 35). Both of these observations lead to the increase of MHCII^{neg}F4/80^{hi} cells.

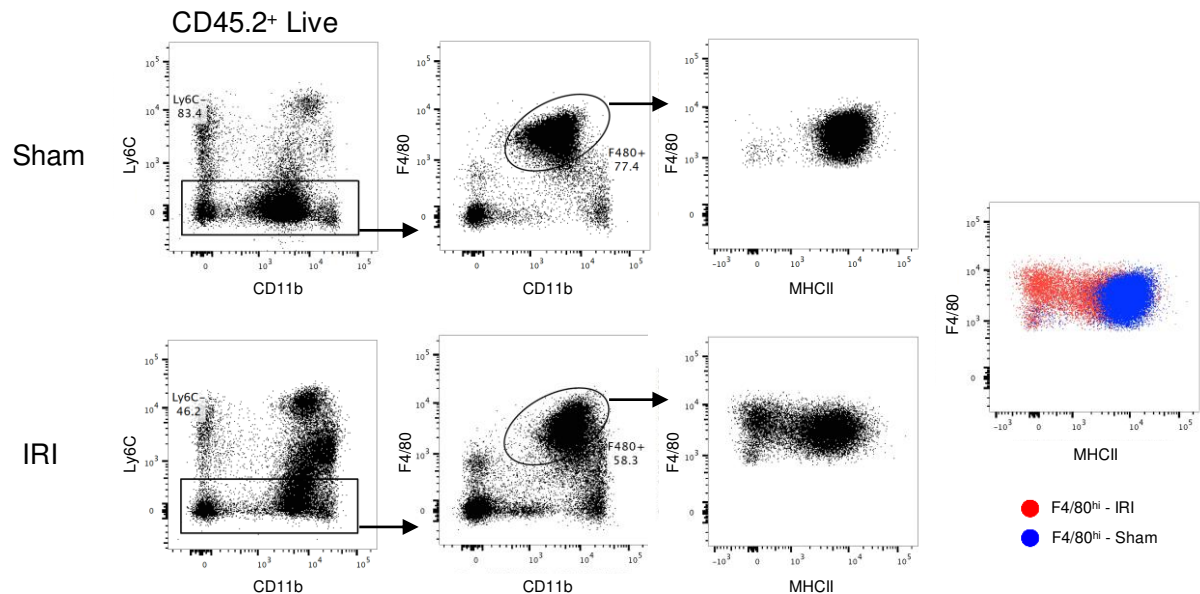


Figure 35. Loss of MHCII expression on F4/80^{hi} cells after IRI. Flow cytometric analysis of kidney from *Clec9a^{Cre}Rosa^{YFP}* mice with IRI-induced kidney damage (bottom row) and sham-operated control (top row). F4/80^{hi} cells were identified independent of MHCII expression among live CD45.2⁺ cells as Ly6C⁻F4/80^{hi}CD11b^{low}. The third column of dot plots shows MHCII expression on F4/80^{hi} cells in sham-operated or injured kidney. An overlay of these two plots shows F4/80^{hi} cells from IRI kidney as red dots and from sham-operated kidney in blue dots.

3.3.5. YFP labelling remains restricted to DCs after ischemia-reperfusion-induced acute kidney injury

Since *Clec9a^{Cre}Rosa^{YFP}* mice were used for IRI we were also able to analyse, which cells are of DC origin in the injured kidney based on their YFP labelling. We noticed that the DC subsets in the kidney were mostly unaffected in IRI. cDC1 were almost completely labelled (98±1%) as expected because of their *Clec9a* expression. cDC2 (63±3%), CD11b^{hi} cells (43±7%) and F4/80^{hi} cells (57±5%) were still highly labelled, although to a lower extent compared to steady state conditions (Figure 5, Figure 36). MHCII^{neg}F4/80^{hi} cells were also YFP labelled (33±10%) but to a significantly lower extent compared to MHCII⁺F4/80^{hi} cells from the same organ, indicating another source for MHCII^{neg}F4/80^{hi} cells apart from loss of MHCII expression in F4/80^{hi} cells (Figure 36).

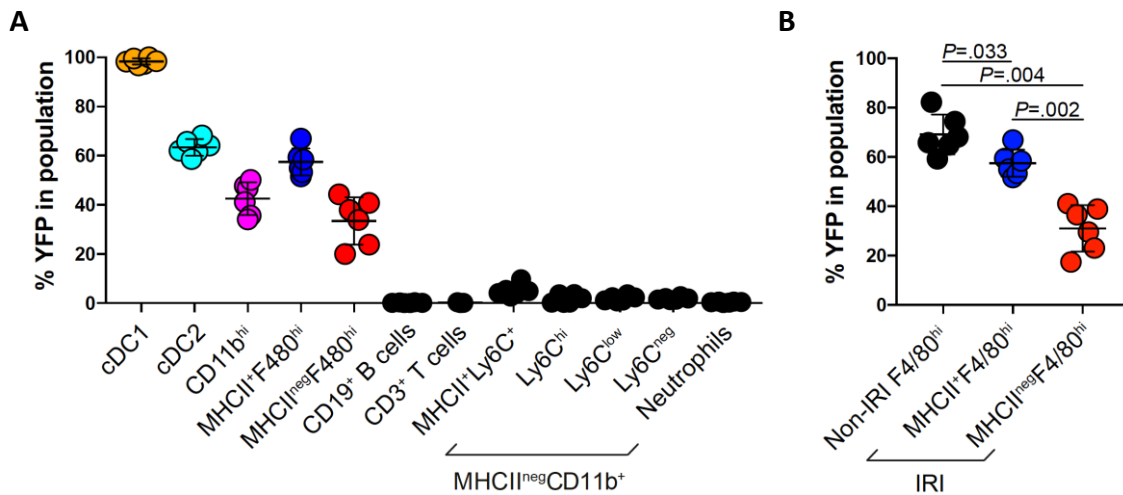


Figure 36. YFP labelling in renal leukocyte populations. (A) YFP labelling percentage in the indicated populations after IRI-induced acute kidney injury in *Clec9a^{Cre}Rosa^{YFP}* mice. (B) Comparison of YFP labelling percentage in F4/80^{hi} cells from sham-operated (black) or IRI kidneys (blue) as well as MHCII^{neg}F4/80^{hi} cells isolated from kidneys with IRI (red). Each dot represents one mouse. Horizontal bars indicate mean, error bars indicate SD. (Modified from Salei *et al.*, 2020)

Other cell types did not show YFP labelling and the *Clec9a^{Cre}Rosa^{YFP}* model stayed faithful to DCs (Figure 36). To exclude that we missed YFP labelled populations with our gating strategy we performed tSNE analysis on the flow cytometry data and overlaid the manually gated populations on the tSNE plot (Figure 37). This analysis further confirmed that YFP labelling was only present in our manually gated DC populations but not in any other cells.

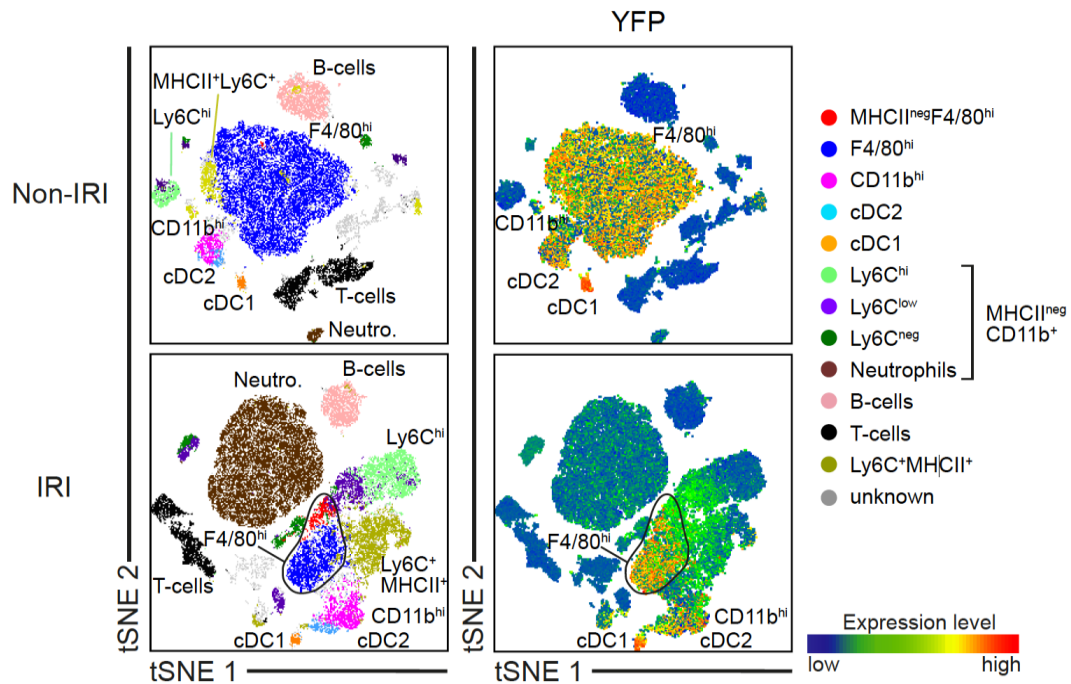


Figure 37. tSNE analysis of renal leukocytes after IRI. Representative tSNE analysis of renal leukocytes isolated from kidneys of *Clec9a^{Cre}Rosa^{YFP}* mice with IRI-induced kidney damage (bottom) or sham-operated control (top). Left plots show manually gated populations (see Figure 33) overlaid on tSNE plot in the indicated colors. Right plots show YFP expression among renal leukocytes. (Modified from Salei *et al.*, 2020)

3.3.6. Localization of DCs in the injured kidney

The loss of MHCII expression on F4/80^{hi} cells intrigued us and we wanted to know whether this might be caused by the localization of these cells. Since in our flow cytometric analysis we isolated cells from whole kidneys we were not able to determine whether MHCII^{neg}F4/80^{hi} cells are localized in the renal medulla or cortex. Therefore, we froze kidneys from mice with cisplatin-induced AKI and stained tissue sections with antibodies against MHCII, CD64, F4/80, CD11b and cleaved Caspase 3 (CC3). With CD64, F4/80 and CD11b we were able to find F4/80^{hi} cells and determine their MHCII expression. CC3 is a marker for apoptotic cells and was previously used to assess kidney damage (S. Chen *et al.*, 2019). As expected, most of the kidney damage marked by CC3 was found in the renal cortex as expected because of cisplatin uptake in proximal tubular cells (Ozkok & Edelstein, 2014). Kidney sections of NaCl injected mice did not show any CC3 signal (Figure 38). Notably, cells seemed to cluster around the areas with strong CC3 staining (as seen in dotted circles on image Figure 38).

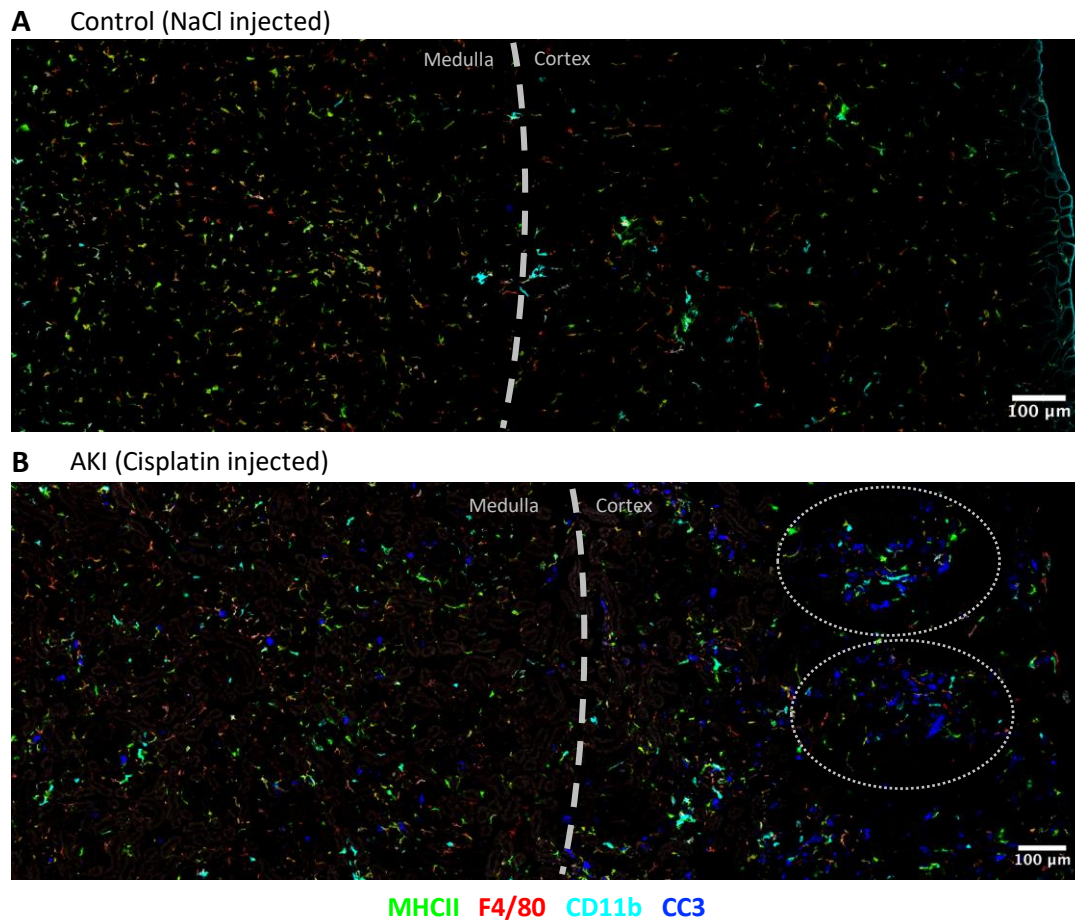


Figure 38. Analysis of CC3 staining after cisplatin-induced AKI. Confocal tile-scans of *Clec9a^{Cre}Rosa^{YFP}* kidneys isolated after NaCl injection (A) or after cisplatin induced-AKI (B). Section was stained for MHCII (green), F4/80 (red), CD11b (cyan) and CC3 (blue). (B) Dotted areas indicate regions with accumulation of CC3, F4/80 and CD11b signal.

We next wanted to analyse the localization of F4/80^{hi} cells and MHCII^{neg}F4/80^{hi} cells in kidney sections after cisplatin-induced AKI. Because of the close interaction of cells at the damaged areas in the renal cortex after cisplatin injection we found that cell segmentation by Histo-Cytometry not to be feasible. Therefore, we made multiple random cutouts from the cortex and medulla and manually identified F4/80^{hi} cells and MHCII^{neg}F4/80^{hi} cells as cells with high expression of CD64 and F4/80 and low expression of CD11b (Figure 39). To our surprise we were able to find MHCII^{neg}F4/80^{hi} cells both in the cortex and the medulla, even though CC3 signal seemed to be mostly restricted to the cortex. This indicates that the downregulation of MHCII on F4/80^{hi} cells is not triggered by direct contact to tissue injury in the cortex but rather through a compartment-independent tissue-wide effect.

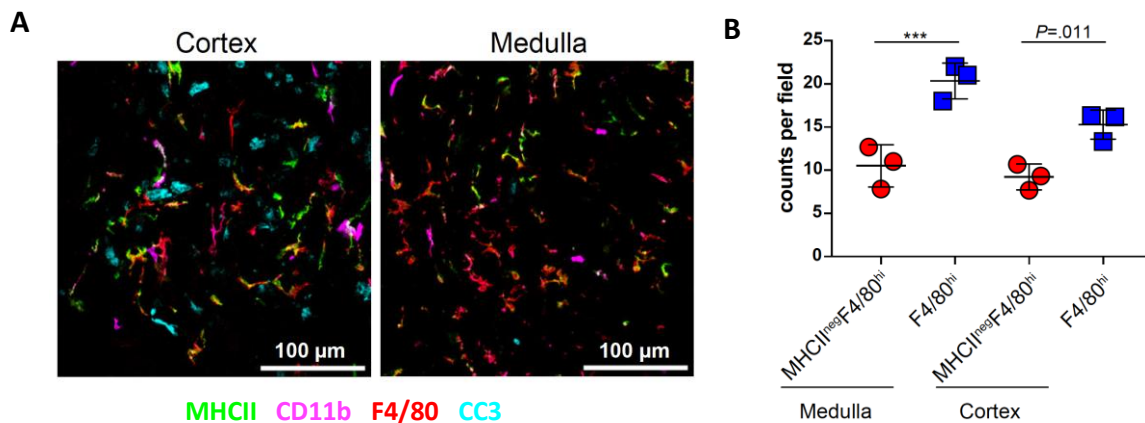


Figure 39. Quantification of MHCII⁺ and MHCII^{neg}F4/80^{hi} cells in the kidney. (A) Representative cutouts from microscopic images of *Clec9a^{Cre}Rosa^{YFP}* kidneys with cisplatin-induced kidney damage. Section was stained for MHCII (green), CD11b (magenta), F4/80 (red) and CC3 (cyan). (B) Manual quantification of MHCII^{neg}F4/80^{hi} cells and MHCII⁺F4/80^{hi} cells in cortical and medullary cutouts similar to (A). Each dot represents the average of one biologic replicate. Horizontal bars indicate mean, error bars indicate SD. *** p-value < 0.001 (Modified from Salei *et al.*, 2020)

3.3.7. F4/80^{hi} cells downregulate MHCII on a transcriptional level after cisplatin-induced acute kidney injury

In order to identify possible mechanisms behind the downregulation of MHCII in renal F4/80^{hi} cells after cisplatin induced acute kidney injury, we performed transcriptional analysis from sorted F4/80^{hi} cells and MHCII^{neg}F4/80^{hi} cells 72h after cisplatin-induced AKI. F4/80^{hi} cells from NaCl-injected mice were sorted as control at the same timepoint. For sorting of cells we used a more strict gating strategy, excluding F4/80^{hi} cells with intermediate expression of MHCII (Example of gating strategy and sort purity see Figure 40).

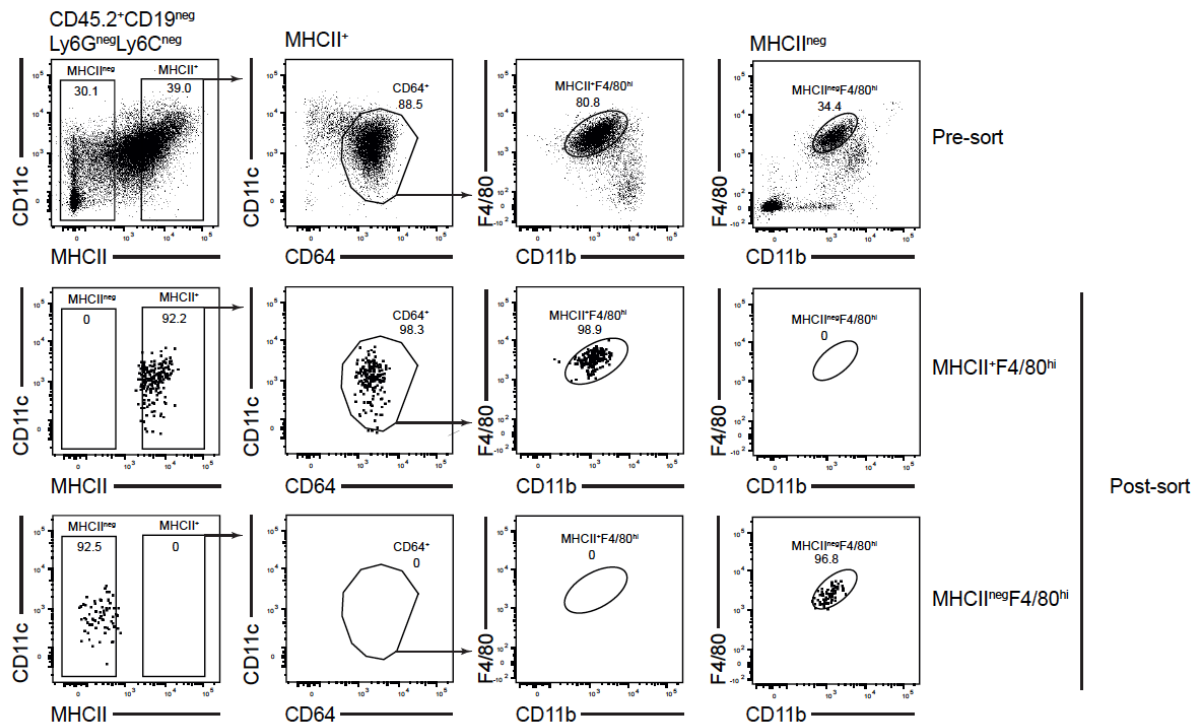


Figure 40. Gating strategy and sort purity for transcriptional analysis of F4/80^{hi} cells. Example of sorting strategy and purity check for renal MHCII^{neg}F4/80^{hi} and MHCII⁺F4/80^{hi} cells after cisplatin-induced AKI in *Clec9a^{Cre}Rosa^{YFP}* mice. MHCII⁺F4/80^{hi} cells were identified as MHCII⁺CD64⁺F4/80^{hi}CD11b^{low} and MHCII^{neg}F4/80^{hi} cells as MHCII^{neg}F4/80^{hi}CD11b^{low}. (Modified from Salei *et al.*, 2020)

We again performed a principal component analysis to quickly get an idea about differences between the populations. PC1 separated the control populations from the cells sorted after kidney injury (Figure 41). A potential transcriptional difference between F4/80^{hi} cells and MHCII^{neg}F4/80^{hi} cells sorted after cisplatin-induced AKI was highlighted by their segregation on PC2 (Figure 41). We performed pairwise comparison between F4/80^{hi} cells and MHCII^{neg}F4/80^{hi} cells after cisplatin-induced AKI to identify genes which could potentially hint at a different role of these cells during kidney injury. Based on the PCA we only expected minimal differences between F4/80^{hi} cells and MHCII^{neg}F4/80^{hi} cells, which is why we chose a log₂foldchange > 1 with an adjusted p-value < 0.05 to identify differentially expressed genes between these two populations. This analysis identified 56 genes, which were higher expressed in F4/80^{hi} cells and only 10 genes, which were higher expressed in MHCII^{neg}F4/80^{hi} cells (Figure 42A).

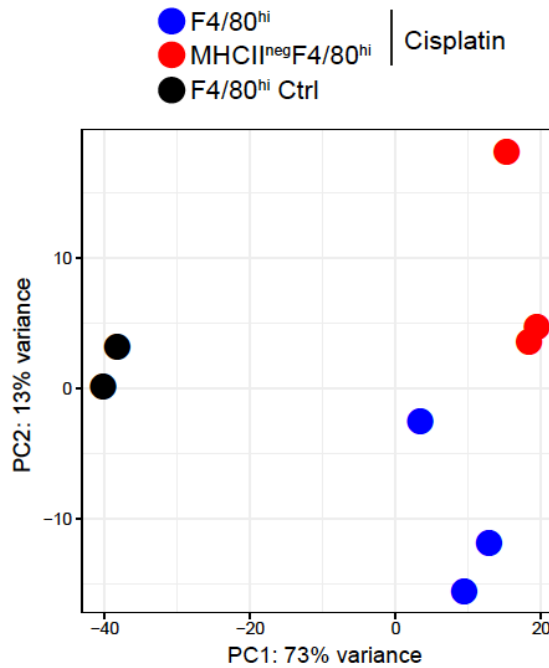


Figure 41. PCA of F4/80^{hi} cells during steady state and after cisplatin-induced AKI. PCA based on top 5000 genes with highest variance across sequenced samples. Each dot represents one biological replicate. (Modified from Salei *et al.*, 2020)

As expected, most of the genes which were higher expressed in F4/80^{hi} cells compared to MHCII^{neg}F4/80^{hi} cells were related to the expression of MHCII, such as *H2-Ab1*, *Cd74* and *Ciita* (Figure 42A). Since this analysis did not reveal many genes, we decided to compare F4/80^{hi} cells from control-injected mice with F4/80^{hi} cells after AKI independent of their MHCII expression. We identified 635 genes upregulated in F4/80^{hi} cells after AKI with a \log_2 foldchange > 1 and an adjusted p-value < 0.05. Moreover, in this comparison we found 691, which were higher expressed in F4/80^{hi} cells from control mice compared to AKI (Figure 42B). Notably, we still found many MHCII-related genes differentially expressed, with a higher expression in F4/80^{hi} cells sorted from control-treated mice. This suggested that MHCII is already downregulated on a transcriptional level in F4/80^{hi} cells after cisplatin injection, even though it is still present on protein level.

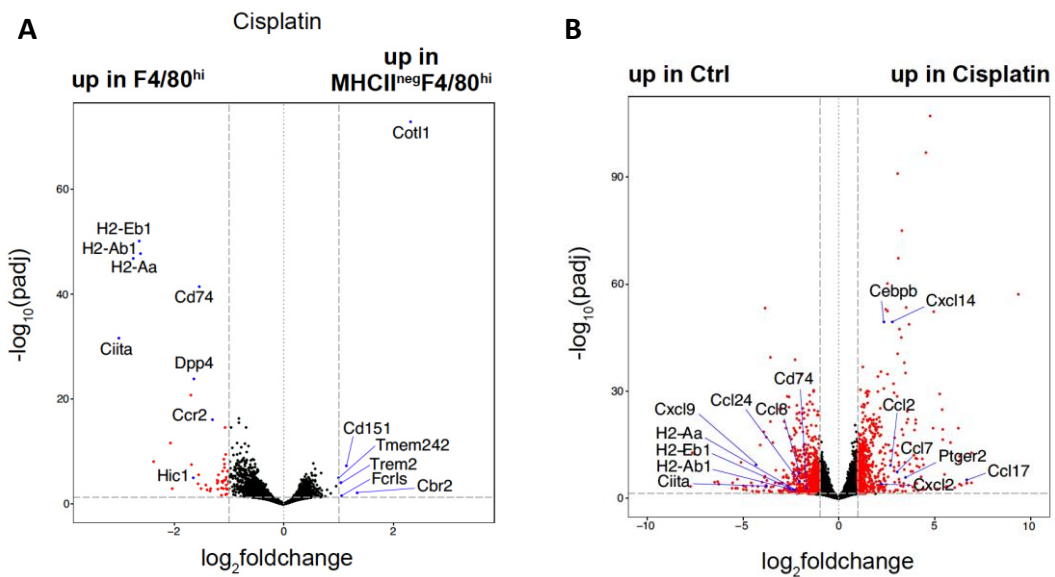


Figure 42. Pairwise comparisons of F4/80^{hi} cells after cisplatin-AKI. (A) Pairwise comparison of renal MHCII⁺F4/80^{hi} cells with MHCII^{neg}F4/80^{hi} cells after cisplatin-induced AKI. Genes with a log₂foldchange > 1 and an adjusted p-value < 0.05 are depicted as red. Differentially expressed genes of interest are labelled as blue dots. (B) Pairwise comparison of renal F4/80^{hi} cells from control-treated mice with F4/80^{hi} cells after cisplatin-induced AKI independent of MHCII expression. Genes with a log₂foldchange > 1 and an adjusted p-value < 0.05 are depicted as red dots. Differentially expressed genes of interest are labelled as blue dots. (Modified from Salei *et al.*, 2020)

The transcriptional downregulation of MHCII after cisplatin-induced AKI in F4/80^{hi} cells intrigued us, since it could indicate a functional switch in these cells in response to kidney damage. In search for a mechanism behind the downregulation of the antigen-presentation machinery we noticed that the major activator of MHCII transcription *Ciita* was downregulated during AKI. Additional activators of MHCII expression, such as *Irf1*, *Stat1* or *Ep300*, were also downregulated in F4/80^{hi} cells isolated from mice with AKI (Figure 43A) (Boss & Jensen, 2003). Coincidentally, we identified prostaglandin E2 receptor 2 (*Ptger2*) among the genes which were upregulated in F4/80^{hi} cells after AKI (Figure 42B). It was shown that Prostaglandin E2 (PGE2) levels in the kidney are elevated upon cisplatin induced acute kidney injury where it is produced by renal tubular cells through induction of *Ptges* and *Ptgs2* (Jia *et al.*, 2011). Binding of PGE2 to EP2 or EP4 causes an increase of cellular cAMP levels (Aronoff, Canetti, & Peters-Golden, 2004) which can inhibit the function of *Ciita*, the main activator of MHCII expression (Ivashkiv, Ayres, & Glimcher, 1994; G. Li, Harton, Zhu, & Ting, 2001).

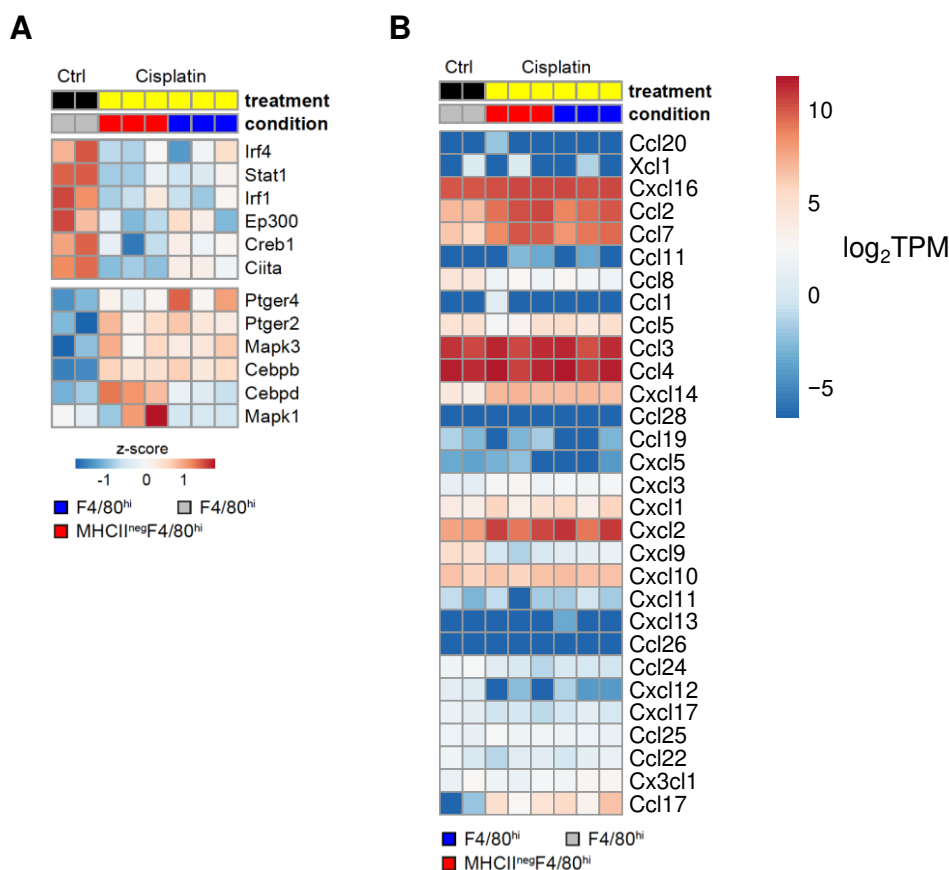


Figure 43. Selected differentially expressed genes and expression of cytokines in F4/80^{hi} cells after cisplatin-induced AKI. (A) Heatmap depicting expression of selected genes connected to activation of MHCII expression (top box) or inhibition of MHCII expression (bottom box). (B) Heatmap depicting expression of various genes encoding known chemokines. Gene expression depicted as log₂TPM value. (Modified from Salei *et al.*, 2020)

Additionally, other known factors which can lead to falling MHCII levels such as *Cebpb*, *Cebpd* or *Mapk1/3* were also upregulated after cisplatin-induced AKI (Figure 43A, Figure 42B). *Cepdb* and *Cebpd* are activated upon increased cAMP levels in the cell, caused for example by binding of PGE2 to its surface receptors EP2 and EP4, and were shown to directly inhibit expression of *Ciita* by binding to its promoter region (Côté, Pasvanis, Bounou, & Dumais, 2009; Pennini *et al.*, 2007). This further indicated that, indeed, MHCII is downregulated on a transcriptional level in F4/80^{hi} cells after cisplatin-induced AKI, possibly regulated through prostaglandin E2 signalling. In addition to MHCII downregulation we found many chemokines which were differentially regulated after kidney injury, e.g. *Ccl2*, *Cxcl9*, *Ccl7*, *Cxcl2* and *Ccl17* (Figure 42, Figure 43B, Figure 44).

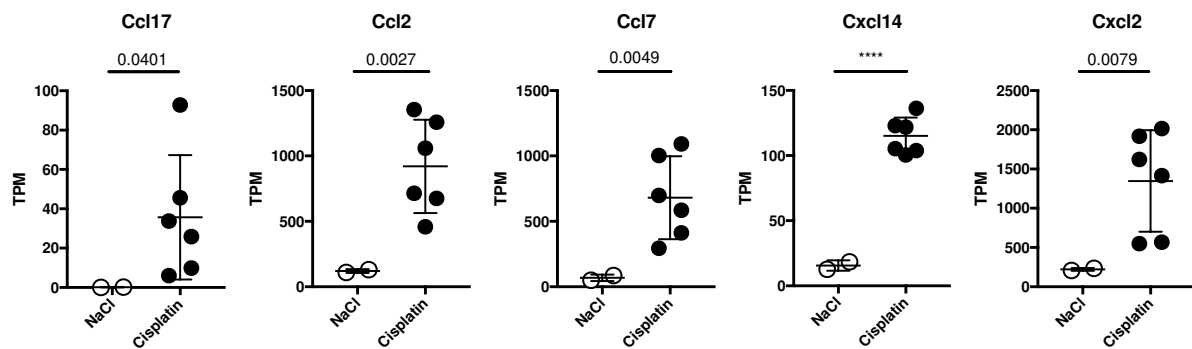


Figure 44. Upregulated expression of cytokines in F4/80^{hi} cells after cisplatin-induced AKI. TPM expression values of differentially expressed cytokines upregulated in F4/80^{hi} cells after cisplatin-induced AKI compared to controls. Each dot represents one mouse. Horizontal bars indicate mean, error bars indicate SD. **** p-value < 0.0001

Most of these chemokines were higher expressed after induction of kidney damage. This suggests that F4/80^{hi} cells have an important role in recruiting and positioning inflammatory cells during disease.

3.4. Depletion of cDCs using *Clec9a^{Cre}Rosa^{DTR}* exacerbates cisplatin-induced acute kidney injury

To identify the specific role of dendritic cells during cisplatin-induced AKI we decided to use cell depletion mouse models. Many studies aiming to address the function of DCs in the kidney relied on the use of either depletion of mononuclear phagocytes using clodronate liposomes or DT induced depletion with mouse lines such as *CD11c^{DTR}* (Rogers et al., 2014). As previously mentioned, these models affect a variety of cells in addition to DCs. Therefore, we aimed to repeat cisplatin-induced AKI utilizing *Clec9a^{Cre}Rosa^{DTR}* mice which allows depletion of DCs with high specificity (Schraml et al., 2013). *Rosa^{DTR}* mice without expression of CRE were used as controls. We injected 10-12-week-old male mice with 15 mg/kg cisplatin to induce AKI as mentioned above. Unfortunately, mice with a systemic depletion of DCs showed an even increased weight loss forcing an early termination of this experiment 48 h after cisplatin injection (Figure 45B).

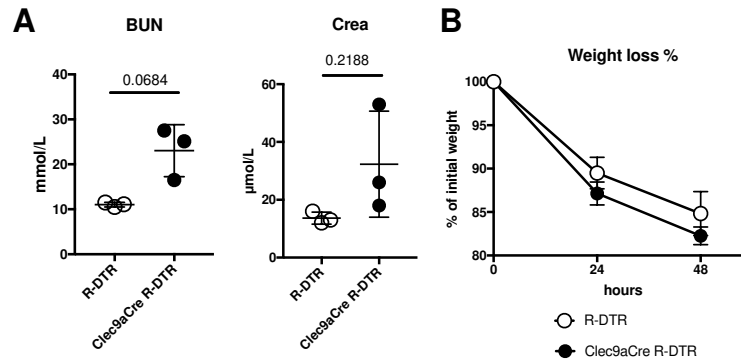
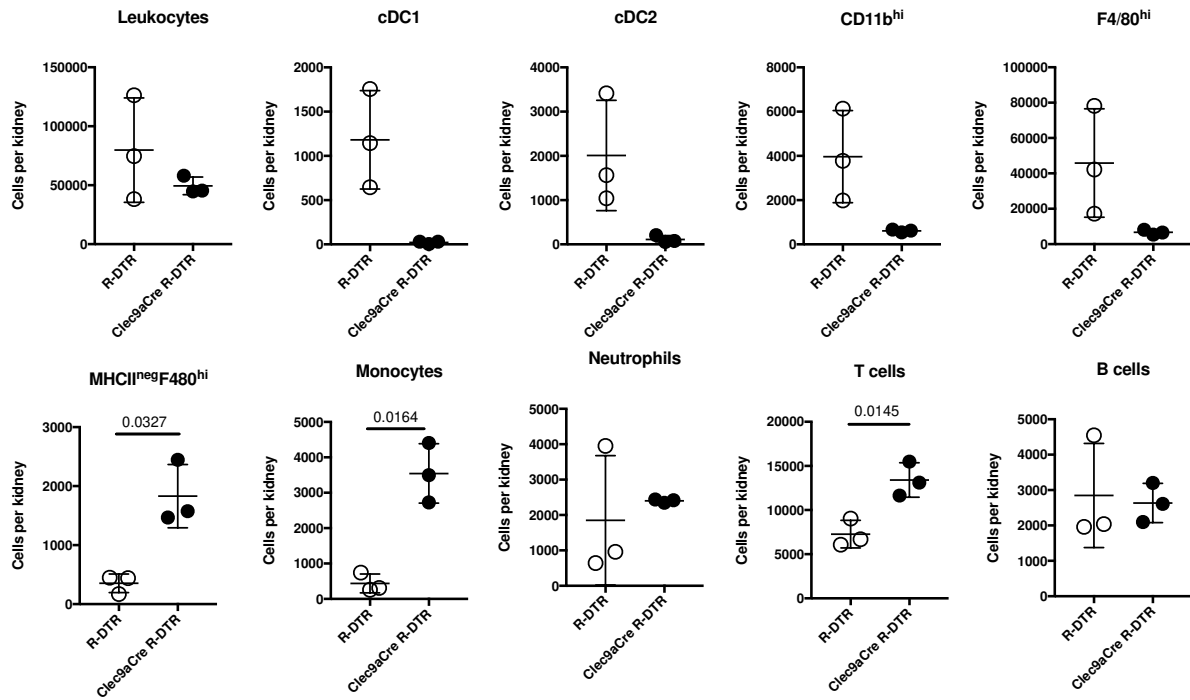


Figure 45. Disease severity and weight loss 48 h after cisplatin-induced AKI in *Clec9a^{Cre}Rosa^{DTR}* mice. (A) BUN and creatinine levels in blood serum isolated from DT treated *Rosa^{DTR}* or *Clec9a^{Cre}Rosa^{DTR}* mice 48h after cisplatin-induced AKI. Each dot represents one mouse. Horizontal bars indicate mean, error bars indicate SD. (B) Average weight loss in *Rosa^{DTR}* or *Clec9a^{Cre}Rosa^{DTR}* mice. Dots represent mean weight loss at each time point, error bars indicate SD.

Phenotypic analysis of myeloid and lymphoid cell population was performed via flow cytometry. Blood serum was collected to measure BUN and Creatinine for an assessment of kidney damage. We did not see a significant elevation of BUN or creatinine levels in *Clec9a^{Cre}Rosa^{DTR}* mice, indicating that there was no difference in disease severity (Figure 45A).

A Cells per kidney



B Frequency of cell populations among live cells

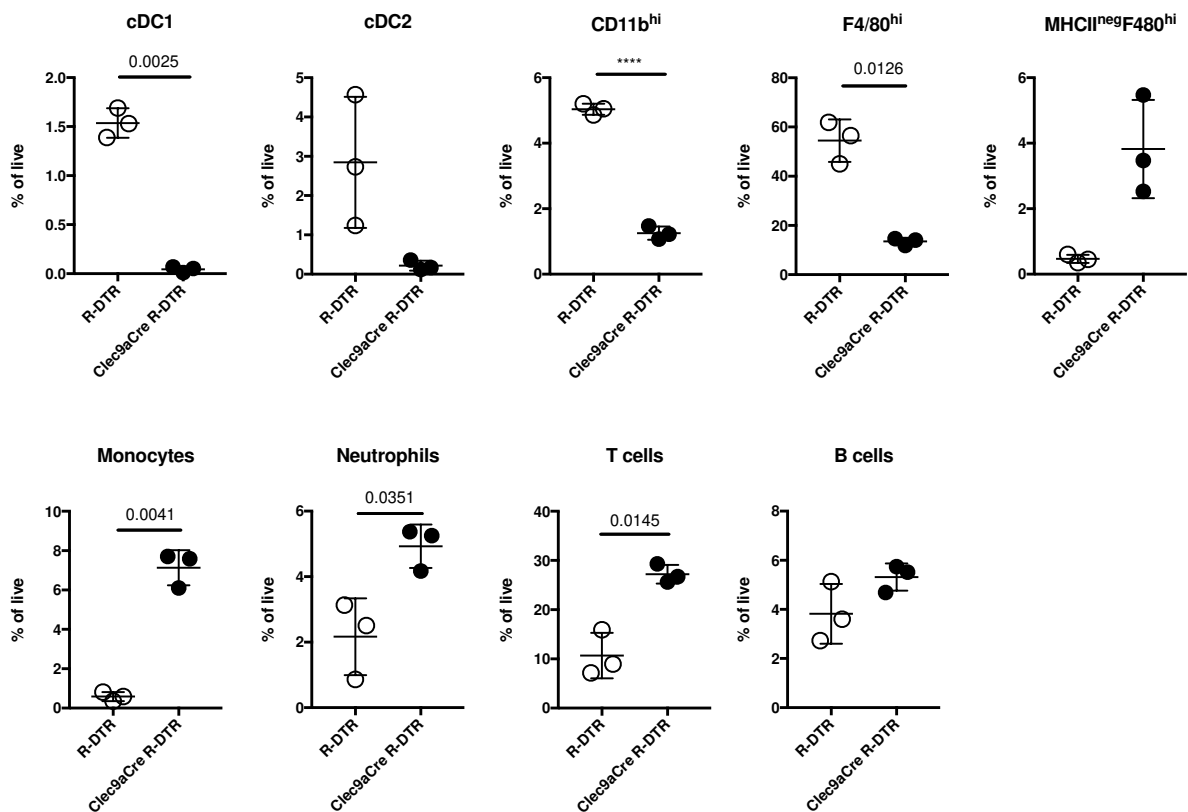


Figure 46. Quantification of lymphoid populations in the kidney after AKI in *Clec9a^{Cre}Rosa^{DTR}* mice. Number of renal leukocyte populations per kidney (A) isolated after cisplatin-induced AKI in *Clec9a^{Cre}Rosa^{DTR}* mice (black) or *Rosa^{DTR}* control mice (white) and

the population frequency among live cells (B). Each dot represents one mouse. Horizontal bars indicate mean, error bars indicate SD. **** p-value < 0.0001

As expected, injection of DT in *Clec9a^{Cre}Rosa^{DTR}* lead to a decrease of all cells with DC origin visible both in cell counts per kidney and more obvious in the frequency of these populations among leukocytes (Figure 46). Interestingly, cell counts indicated a higher number of MHCII^{neg}F4/80^{hi} cells, monocytes and T cells in kidneys from *Clec9a^{Cre}Rosa^{DTR}* mice despite no difference in disease severity (Figure 46).

To sum up, we could identify that depletion of DCs in *Clec9a^{Cre}Rosa^{DTR}* mice leads to a more severe disease progression with higher neutrophil counts, rapid weight loss and seemingly elevated levels of serum BUN and creatinine.

3.5. cDC1 are dispensable for cisplatin-induced acute kidney injury

3.5.1. Severity of acute kidney injury unchanged after depletion of XCR1⁺ cDC1

To start deciphering specific roles of DC subsets during kidney injury we chose to utilize *XCR1^{Venus-DTR}* mice and subjected them to cisplatin-induced AKI. These mice can be used to deplete cDC1 through injection of DT because XCR1 is specifically expressed in this population. We injected DT 24 h before induction of AKI and sacrificed mice 72 h after cisplatin injection. We harvested blood serum, kidneys and spleen for analysis. Serum Creatinine and BUN levels were used to assess kidney damage severity. We could not detect a significant difference in disease severity between control mice and mice with cDC1 depletion (Figure 47A). We also could not detect a difference in weight loss which could be another indicator of a more severe disease progression (Figure 47B).

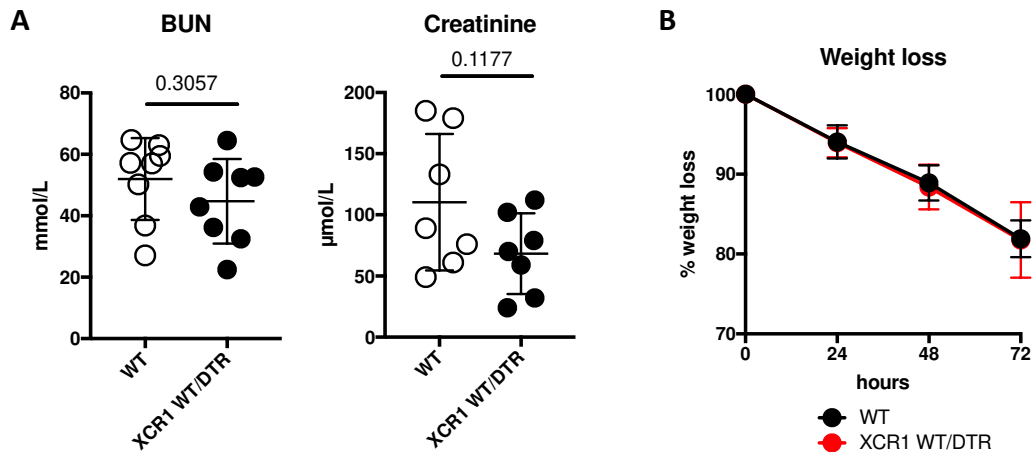


Figure 47. Serum creatinine and BUN levels 72h after AKI in $XCR1^{Venus-DTR}$ mice. (A) BUN and creatinine levels in blood serum isolated from DT treated WT or $XCR1^{Venus-DTR}$ mice 72h after cisplatin-induced AKI. Each dot represents one mouse. Horizontal bars indicate mean, error bars indicate SD. (B) Average weight loss in WT or $XCR1^{Venus-DTR}$ mice. Dots represent average weight loss at each time point, error bars indicate SD.

3.5.2. cDC1 numbers are still decreased in the spleen 96h after depletion

Since we did not perform repeated injections of DT, we wanted to make sure that cDC1 were still decreased 96 h after depletion. We analysed DCs in the spleen for $CD3^+Ly6G^-MHCII^+CD11c^+CD24^+XCR1^+$ cDC1 in $XCR1^{Venus-DTR}$ mice and DT-injected controls (Figure 48A and B). As expected, cDC1 were still clearly decreased in $XCR1^{Venus-DTR}$ mice compared to controls 96 h after depletion with DT (Figure 48B). Therefore, one-time depletion of cDC1 24 h before AKI induction is working model to study the role of these cells in early phases of kidney disease.

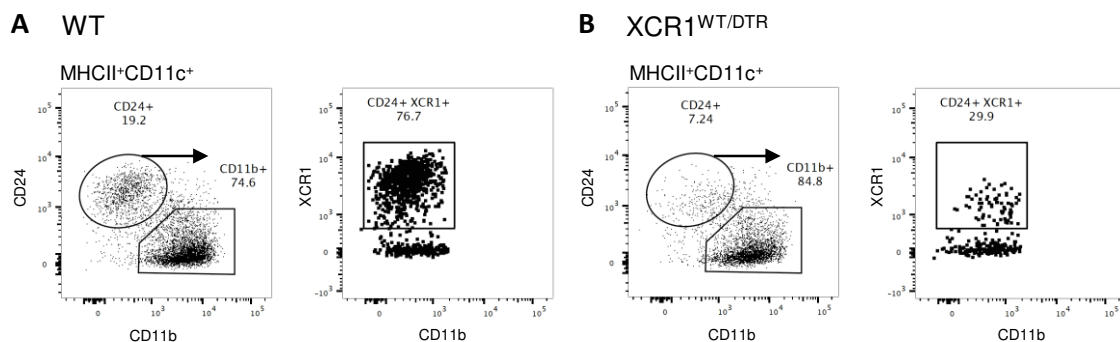


Figure 48. cDC1 are decreased in kidney and spleen 96h after DT injection in $XCR1^{Venus-DTR}$ mice. Representative analysis of $MHCII^+CD11c^+CD24^+XCR1^+$ cDC1 in splenocytes isolated from DT treated WT (A) or $XCR1^{Venus-DTR}$ (B) mice 72 h after cisplatin-induced AKI.

3.5.3. Mice with cDC1 depletion show a decreased infiltration of neutrophils

It was described that cDC1 have important functions during glomerular nephritis, e.g. dampening the influx of proinflammatory neutrophils (Brähler et al., 2017). Therefore, we wanted to analyse whether a comparable trend could be found in cisplatin-induced AKI. We profiled renal leukocyte populations using flow cytometry and found that, apart from cDC1, most populations were unchanged between control mice and $XCR1^{Venus-DTR}$ mice (Figure 49). However, we found that $XCR1^{Venus-DTR}$ mice had a less severe infiltration of neutrophils compared to controls (Figure 49).

This result was striking to us since a decreased neutrophil infiltration upon cDC1 depletion is completely opposite to what was detected in glomerular nephritis models (Brähler et al., 2017). Another function of cDC1 in kidney disease can be the induction of IL10-producing regulatory T cells (Tregs) during glomerular nephritis. Therefore, we wanted to see whether a depletion of cDC1 in cisplatin-induced AKI lead to differences in lymphoid populations. We devised another panel to identify $CD4^+/CD8^+$ T cells, $CD4^+Foxp3^+$ Tregs, $CD127^+$ innate lymphoid cells (ILCs) and the $Gata3^+$ subset of ILCs (Gating strategy Figure 50).

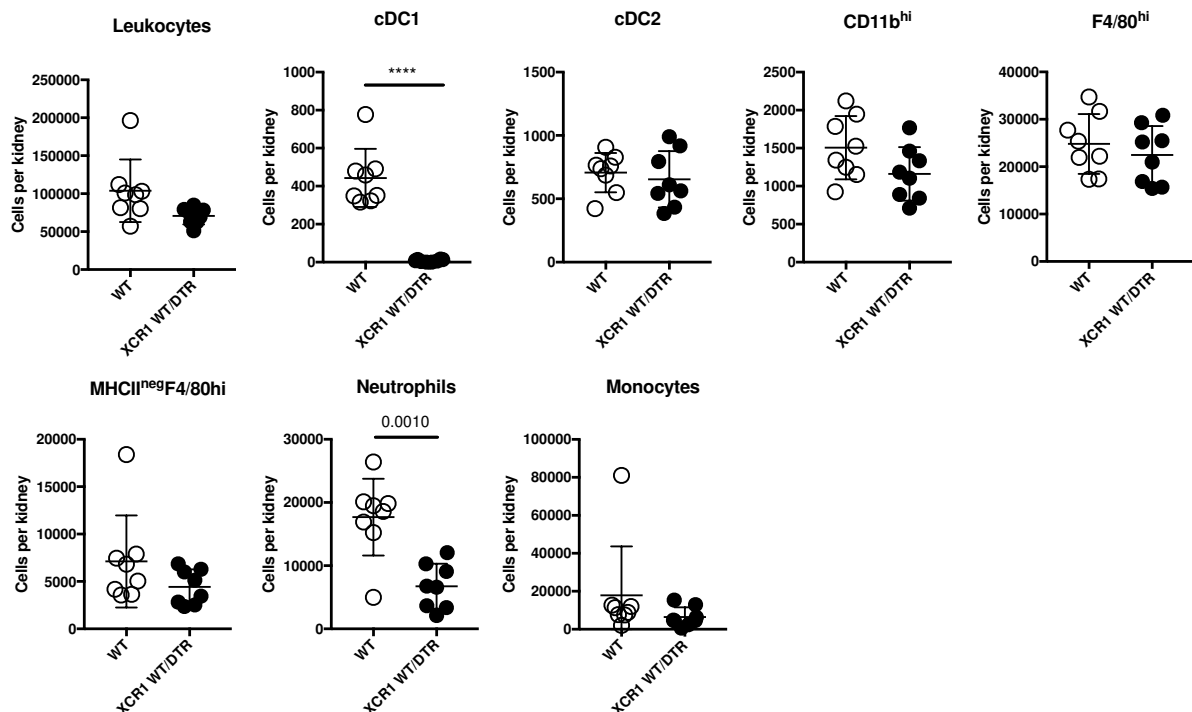


Figure 49. Myeloid populations in the kidney after AKI in $XCR1^{Venus-DTR}$ mice. Number of renal myeloid populations per kidney isolated after cisplatin-induced AKI (black) or from

control mice (white). Each dot represents one mouse. Horizontal bars indicate mean, error bars indicate SD. **** p-value < 0.0001

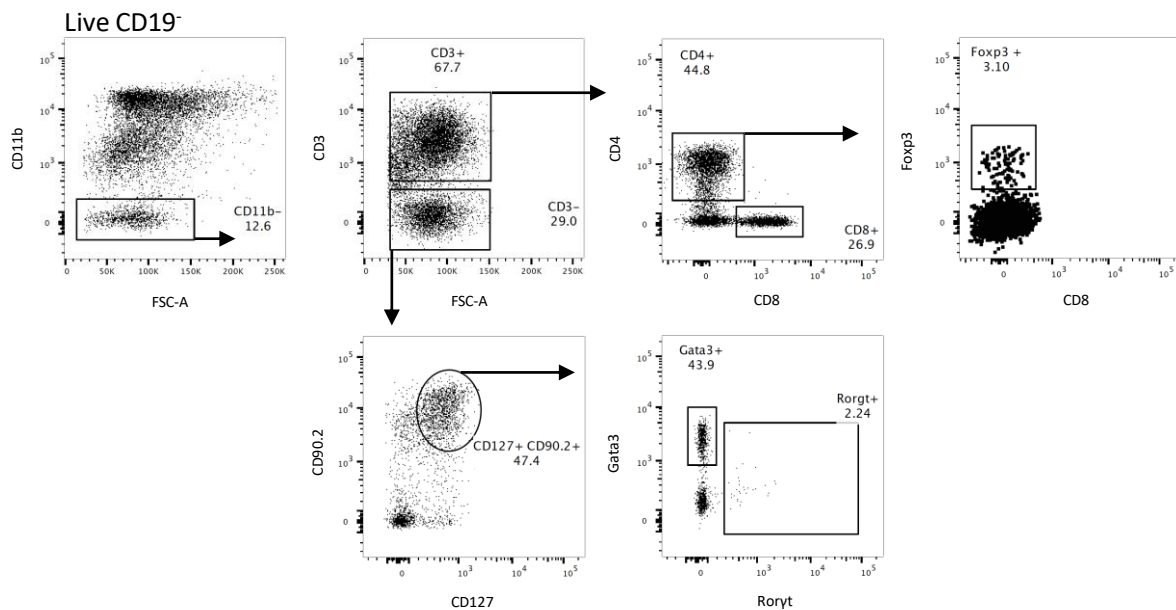


Figure 50. Gating strategy to identify T cell subsets and ILCs in the kidney. Representative flow cytometric analysis to identify T cells and ILCs in the kidney of *XCR1^{Venus-DTR}* mice. CD19⁺ and CD11b⁺ cells were excluded from live CD45.2⁺ cells to remove unwanted cells. Remaining cells were split into CD3⁺ and CD3⁻ cells. The latter contained CD127⁺CD90.2⁺ ILCs which harboured a prominent Gata3⁺ ILC2 population. CD3⁺ T cells were split into the CD8⁺ and CD4⁺ subsets. CD4⁺ T cells were analysed for Foxp3⁺ Tregs.

When we compared quantifications of these populations, we did not notice any changes between control mice and *XCR1^{Venus-DTR}* mice in cell counts (Figure 51) (data not shown). We did notice a slight increase of CD4⁺ T cells and ILCs in terms of frequency among live cells (Figure 52). Whether this difference has a consequence in later stages of cisplatin-induced AKI is not clear, but it did not influence the severity in early stages.

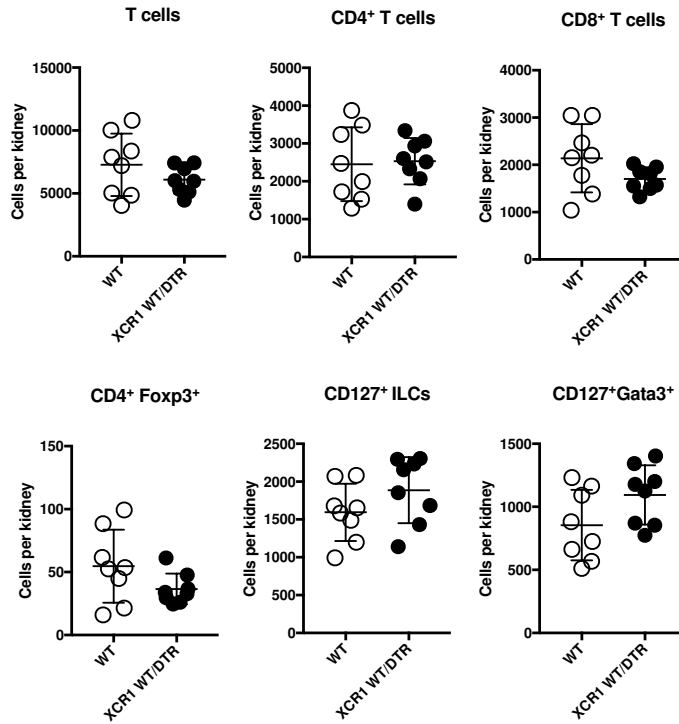


Figure 51. Quantification of lymphoid populations in the kidney after AKI in *XCR1^{Venus-DTR}* mice. Number of renal lymphoid populations per kidney isolated after cisplatin-induced AKI in *XCR1^{Venus-DTR}* (black) or WT mice (white). Each dot represents one mouse. Horizontal bars indicate mean, error bars indicate SD.

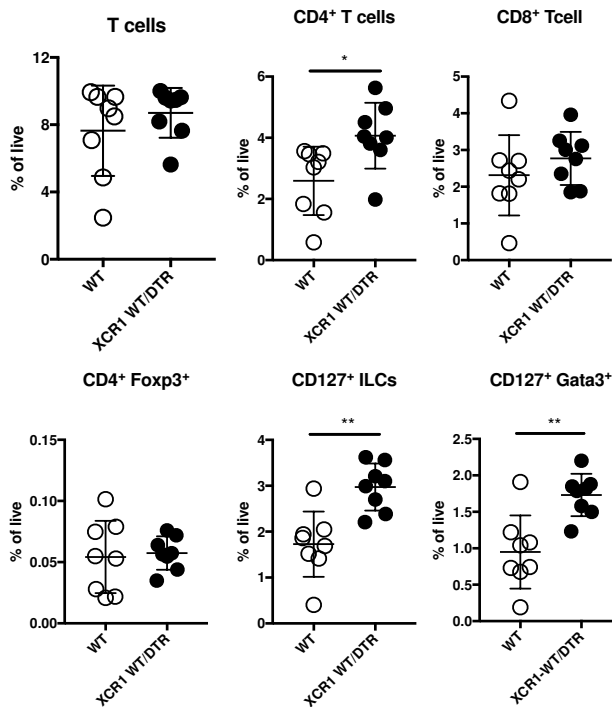


Figure 52. Frequency of lymphoid cells in the kidney after AKI in *XCR1^{Venus-DTR}* mice. Frequency of renal lymphoid populations among live cells isolated after cisplatin-induced AKI

in *XCR1*^{Venus-DTR} (black) or WT mice (white). Each dot represents one mouse. Horizontal bars indicate mean, error bars indicate SD. *p-value < 0.05, ** p-value < 0.01

All in all, we conclude that cDC1 play a minor role in cisplatin-induced AKI. While we did notice less infiltration of neutrophils which is usually a sign of lower kidney inflammation, we could not detect any differences in disease severity.

4. Discussion

4.1. Histo-Cytometry can be used to identify multiple DC subsets in the steady-state kidney

In this study we aimed to establish an image analysis technique called Histo-Cytometry. This method was first described by Gerner *et al.* in 2012 and is a powerful technique that allows identification of cells based on fluorescent values from a microscopic image all the while preserving positional information (Gerner *et al.*, 2012; W. Li *et al.*, 2017). We used a combination of techniques described by Gerner *et al.* and Li *et al.* to establish a working version of this method for DC subsets in the kidney (Gerner *et al.*, 2012; W. Li *et al.*, 2017). We found that segmentation of cells is the most crucial step with many variables to consider. Segmentation of cells based on nuclear signal is not feasible for renal DC subsets because of their dendritic morphology in the tissue leading to only minor overlap of membranous signal with the nucleus. Therefore, we employed a segmentation strategy using membrane signals combined with a cytoplasmic fluorescent reporter. A combination of multiple channels for the masking allowed a much higher efficiency for segmentation because less cells with irregular or weak membrane signals were excluded. However, it has to be considered that many cells were still not identified or were only partially identified and split into multiple selections. In addition, this approach worked best when cells were more or less evenly spread across the tissue with minor overlap. Cells with close neighbours tended to be combined to one big selection which led to exclusion based on size properties in the following analyses. For our approach we performed all downstream analysis on a 2D maximum projection from a thin z-stack. While this helped us with segmentation it should also be considered that many cells are lost using this approach because of their morphology. This approach allows for accurate cell identification but may miss some cells. Ideally segmentation should be performed in 3D from a thick z-stack, because otherwise cells which are only partially in the imaged plane will be excluded because of small size.

Renal F4/80^{hi} cells are MHCII⁻ in early life and mostly located in the medulla, but with age F4/80^{hi}MHCII⁺ enter the kidney and form a continuous network across the whole kidney (Berry *et al.*, 2017; Lever *et al.*, 2019; Salei *et al.*, 2020). However, localization of MHCII⁺ and MHCII⁻ F4/80^{hi} cells and DC subsets has not been addressed in detail. As a proof of concept for Histo-Cytometry we confirmed previous results that showed

F4/80^{hi} cells across the kidney with a high concentration in the medulla in adult kidney (Brähler et al., 2017; Hume & Gordon, 1983). To examine developmental changes in the localization of renal mononuclear phagocyte populations we isolated kidneys at PND2, PND14, PND28 and from adult mice. We isolated these kidneys from *Clec9a^{Cre/+}Rosa^{Tomato}* mice to also be able to identify cells with a DC origin. We used *Rosa^{Tomato}* mice for microscopic analyses because of the brightness and stability of Tomato in microscopic analyses (Shaner, Steinbach, & Tsien, 2005). However, it needs to be considered that labelling is much higher in *Rosa^{Tomato}* mice compared to *Rosa^{YFP}* mice caused by more efficient removal of the shorter *loxP-stop-loxP* cassette (Glaser, Anastassiadis, & Stewart, 2005). We therefore used mice heterozygous for *Cre* in the *Clec9a* locus then working with *Rosa^{Tomato}* mice to achieve comparable labelling in DCs then compared to the homozygous *Clec9a^{Cre/Cre}Rosa^{YFP}* mice we used for flow cytometric analyses. With Histo-Cytometry we confirmed that F4/80^{hi} cells are mostly MHCII^{neg} in the first two weeks of life (Lever et al., 2019; Salei et al., 2020). Between PND2 and PND14 MHCII⁺F4/80^{hi} cells arise and quickly become the dominant population in the kidney at PND28. We showed that MHCII^{neg}F4/80^{hi} cells are always confined to the renal medulla. Interestingly, MHCII⁺F4/80^{hi} cells can be found in equal numbers in the cortex and medulla at PND14. This could indicate that these cells enter the kidney preferentially in the cortex and then move to the medulla. Of course, it is also possible that F4/80^{hi} cells in the kidney upregulate MHCII based on signals present in the tissue microenvironment. To address this question, one could think about using mouse models with inducible CRE expression such as *Cx3cr1^{ERT2-Cre}* crossed to a fluorescent reporter and follow the MHCII expression of labelled F4/80^{hi} cells during early life.

4.2. Macrophages, monocytes or DCs – CD11b^{hi} cells and F4/80^{hi} cells in the kidney

We showed that *Cleca9^{Cre}Rosa^{YFP}* mice faithfully label DC populations but not other cell types in the kidney both in steady state and after AKI. Our bulk RNA sequencing data did not identify expression of CRE in F4/80^{hi} or CD11b^{hi} cells indicating that these cells do in fact have a DC origin (Schraml et al., 2013). However, these cells are still labelled to a significantly lower extent to cDC2. Studies using a novel monocyte fate-mapping mouse utilizing the expression of *Ms4a3* specific to the monocytes-lineage

showed that in adult mice at least a part of the F4/80^{hi} population is made up from cells with a monocyte-origin (Z. Liu et al., 2019). This would argue that F4/80^{hi} cells are a heterogeneous population with at least two ontogenetic sources. Other studies performing RNA sequencing identified low levels of *Clec9a* expression in F4/80^{hi} cells, however whether this expression is enough to create functional protein is not clear yet (Lever et al., 2019). Since F4/80^{hi} cells were shown to be long-lived and considering their slow accumulation of YFP labelling in *Clec9a^{Cre}Rosa^{YFP}* mice, it is possible that these cells are in fact macrophages and just acquire labelling with time due to baseline expression of *Clec9a* (Salei et al., 2020). Apart from YFP labelling in *Clec9a^{Cre}Rosa^{YFP}* mice, another DC-like characteristic of F4/80^{hi} cells their ability to activate CD4⁺ T cells in vitro (Schraml et al., 2013). Although it has to be mentioned that other studies claimed that F4/80^{hi} cells do in fact only possess very low potential to induce CD4⁺ T cell proliferation (Cao et al., 2016). Additional characteristics of these cells i.e. being long-lived, dependency on CSF1R signalling, expression of F4/80 and CD64 etc. would rather indicate that these cells are not DCs but macrophages. However, it was also shown that the tissue microenvironment can have a strong influence on phenotypic and transcriptional characteristics of immune cells (Lavin et al., 2014). Considering the special situation of the kidney with high salt concentrations in the tissue it is possible that F4/80^{hi} cells are a unique DC which adapted to the kidney environment by upregulation of macrophage markers and genes (Chessa et al., 2016). We showed that F4/80^{hi} cells possess a transcriptomic profile similar to other macrophages which is both demonstrated by their close relationship to red pulp macrophages in PCA but also by their expression of many genes out of a list of core-macrophage genes. F4/80^{hi} cells also clearly lacked expression of DC specific genes out of the core-DC signature compared to other cDCs. On the other hand, CD11b^{hi} cells and cDC2 also expressed genes from the core-macrophage signature. This illustrates the major flaw using core-signatures because gene expression in macrophages and DCs is strongly influenced by the tissue microenvironment and therefore a tissue-wide signature is often not specific enough (Lavin et al., 2014). All in all, despite their labelling in *Clec9a^{Cre}* fate-mapping mice, these cells possess both the phenotype and transcriptomic signature of macrophages.

We used Histo-Cytometry to identify cDC1, cDC2, CD11b^{hi} cells and F4/80^{hi} cells with a combination of CD11b, Tomato, CD64 and MHCII. All three subsets mentioned before localized in the cortex. Unfortunately, we were not able to identify differences

between CD11b^{hi} cells and cDC2, both populations were mostly located between the cortex and medulla and therefore differential localization cannot explain phenotypic differences between these populations. However, while their localization may be the same, using bulk RNA sequencing we showed that CD11b^{hi} cells and cDC2 differ in their transcriptional profile. We showed that CD11b^{hi} cells possess transcriptional characteristics of both macrophages and DCs. We identified differential expression of pattern-recognition receptors such as TLR7, TLR8 between these two populations which could hint at different functions during disease. Some targets were addressed in Salei *et al.* and there seems to be thickening evidence that cDC2 and CD11b^{hi} cells are indeed also functionally distinct cell types (Salei et al., 2020). In contrast, a study published by Zimmerman *et al.* performed single cell RNA sequencing of the renal myeloid cell compartment from mouse, rat, swine and human samples (Zimmerman et al., 2019). They identified cDC2 but were not able to find CD11b^{hi} cells. We performed our own analysis on this dataset but were also not able to distinguish these two populations (data not shown). However, a downside of single cell RNA sequencing is that the sequencing depth per cell is much lower compared to bulk RNA sequencing (Bacher & Kendzioriski, 2016). Because of this the number of genes detected may not be enough to distinguish populations that are as similar to each other as cDC2 and CD11b^{hi} cells (Bacher & Kendzioriski, 2016). Since CD11b^{hi} cells and cDC2 are only a small percentage of renal mononuclear phagocytes, it is also possible the number of sequenced cells by Zimmerman *et al.* was not high enough to distinguish between these closely related subsets.

All in all, we think that CD11b^{hi} cells should be considered a unique DC subset in the kidney rather than a type of cDC2 with expression of CD64 (Guilliams et al., 2016). We were not able to find traces of an ontogenetic relationship between F4/80^{hi} cells and other cDC subsets. With current evidence F4/80^{hi} cells seem to be a heterogeneous population with contributions from the monocyte-lineage as well as the DC lineage. Zimmerman *et al.* identified two populations of F4/80^{hi} cells. Whether these two populations correspond to F4/80^{hi} cells from medulla and cortex or to F4/80^{hi} cells from different ontogenetic sources is not clear.

4.3. F4/80^{hi} cells downregulate MHCII after acute kidney injury and may orchestrate recruitment of inflammatory cells to damaged areas

Recent studies showed that F4/80^{hi} cells downregulate MHCII upon IRI-induced kidney injury (Lever et al., 2019). This phenotypic switch was accompanied with transcriptional changes indicating a more developmental function of these cells after injury (Lever et al., 2019). Since IRI - and to some extent cisplatin-induced AKI - is also accompanied with a massive influx of inflammatory cells we aimed to address how DCs contribute to the early phase of IRI and whether MHCII^{neg}F4/80^{hi} cells are in fact F4/80^{hi} cells downregulating MHCII or rather inflammatory cells taking up this phenotype (L. Li et al., 2008). For this we used the *Clec9a^{Cre}Rosa^{YFP}* model which labels all cells with a DC origin and subjected it to IRI or cisplatin-induced AKI. We showed that the *Clec9a^{Cre}Rosa^{YFP}* stayed faithful to DC populations even during severe kidney injury, infiltrating cells were not labelled with YFP. We observed a clear difference in the dynamics of F4/80^{hi} cells between IRI and cisplatin-induced AKI. While F4/80^{hi} cells showed a gradual downregulation of MHCII in cisplatin-induced AKI after 72h, there was already a clear population devoid of MHCII expression present after the same time in the IRI model same as seen in the study by Lever *et al.* (Lever et al., 2019). Interestingly, F4/80^{hi} cells and MHCII^{neg}F4/80^{hi} cells were labelled with YFP to almost the same extent in cisplatin-induced AKI further indicating a downregulation of MHCII. On the contrary, after IRI the MHCII^{neg}F4/80^{hi} population seemed to be more heterogeneous and presented with lower frequency of YFP labelling compared to MHCII⁺F4/80^{hi} cells. This argues that in cisplatin-induced AKI the MHCII^{neg}F4/80^{hi} population are in fact MHCII⁺F4/80^{hi} cells downregulating MHCII while in IRI there is substantial contribution of infiltrating cells to this population.

To address a mechanism which could lead to downregulation of MHCII on renal F4/80^{hi} cells we sorted MHCII^{neg}F4/80^{hi} cells and MHCII⁺F4/80^{hi} cells 72h after cisplatin-induced AKI. We showed that MHCII^{neg}F4/80^{hi} cells and F4/80^{hi} cells are transcriptionally almost identical and the few differentially expressed genes between the two populations were mostly related to the antigen-presentation machinery. We found many more differentially expressed genes between F4/80^{hi} cells from control mice and F4/80^{hi} cells from mice with AKI. For this comparison we did not distinguish between MHCII⁺ and MHCII^{neg}F4/80^{hi} cells. We showed that upon kidney injury many chemokines are differentially expressed which could indicate a role for F4/80^{hi} cells to

coordinate recruitment of inflammatory cells to specific sites in the injured tissue. In line with this observation we identified clusters of F4/80^{hi} cells around damaged areas in the renal cortex while non-damaged areas were almost devoid of myeloid cells. F4/80^{hi} cells are potentially recruited to damaged areas and are then able to guide inflammatory cells to the tissue via expression of specific cytokines. Among the upregulated cytokines we identified CCL17, CCL2, CCL7, CXCL2 and CXCL14. CCL17 was shown to be produced in a variety of lymphoid and non-lymphoid organs. It is important for recruitment of activated T cells (Alferink et al., 2003). CXCL14 binds to CXCR4 and is able to attract NK cells and immature DCs to the tissue in humans, but the function in mice less clear (Hara & Tanegashima, 2012). Studies in mice showed that CXCL14 is important for the uptake of CpG through TLR9 (Tanegashima et al., 2017). CCL2 and CCL7 are important cytokines for the recruitment of monocytes to the injured kidney (J. Gonzalez et al., 2013; Kashyap et al., 2018). Last but not least, CXCL2 is an important chemoattractant for neutrophils which was shown to be induced in cisplatin-induced AKI (Chan et al., 2014). All together F4/80^{hi} cells are able to attract or guide many different kinds of inflammatory cells to damaged areas in the kidney. This could indicate an important role of F4/80^{hi} cells in coordinating the immune response after acute kidney injury. Considering the fact that F4/80^{hi} cells were found close to damaged areas after cisplatin-induced AKI, another explanation of this observation could be that F4/80^{hi} cells are rather masking the damaged area from other immune cells and are thereby keeping the inflammatory response under control akin to what has been shown by Uderhardt *et al.* (Uderhardt, Martins, Tsang, Lämmermann, & Germain, 2019).

Among differentially expressed genes between F4/80^{hi} cells from healthy and injured kidneys we identified many genes associated to the regulation of MHCII expression. We showed that both positive regulators such as *Irf1*, *Stat1* but also negative regulators of MHCII expression such as *Ptger2* and *Cebpb* were differentially expressed in F4/80^{hi} cells after cisplatin-induced AKI. Previous studies identified a role of PGE2 signalling on the expression of MHCII mediated by the inhibition of *Ciita* function through rising cellular cAMP levels (Aronoff et al., 2004; Ivashkiv et al., 1994; G. Li et al., 2001). Intriguingly, another study also confirmed that PGE2 expression is induced upon AKI, making PGE2 signalling a likely initiator of MHCII downregulation on F4/80^{hi} cells upon kidney injury (Jia et al., 2011). However, this remains a theory for now as this study did not perform any assays to confirm this hypothesis. A possible

option to address the relevancy hypothesis could be a conditional knockout of PGE2 signalling in DCs or other cell types and subjecting these mice to AKI.

To sum up, this study confirmed previous results which showed downregulation of MHCII on renal F4/80^{hi} cells upon IRI. These findings were also observed in cisplatin-induced AKI, however in contrast to IRI MHCII^{neg}F4/80^{hi} cells in cisplatin-induced AKI seem to be a much more homogeneous population and not diluted by inflammatory cells. This observation offers many possibilities for future studies to discern a mechanism and the functional consequences of MHCII downregulation on renal F4/80^{hi} cells. Moreover, this study provided bulk RNA sequencing data of F4/80^{hi} cells isolated from healthy and injured kidneys which could provide a valuable tool for future functional studies.

4.4. Specific depletion of DCs with *Clec9a^{Cre}Rosa^{DTR}* may increase disease severity after cisplatin-induced AKI

In contrast to *XCR1^{Venus-DTR}* mice we saw a clear effect on cisplatin-induced AKI after depletion of all cells with a DC origin using *Clec9a^{Cre}Rosa^{DTR}* mice as expected. We demonstrated that 96 h after DT injection all four DC populations were still clearly reduced compared to *Rosa^{DTR}* control mice. We noticed that DC depleted mice exhibited a higher weight loss compared to control mice and because of this the experiment had to be stopped after 48 h according to experimental regulations. DC depleted mice also showed a trend to higher disease induction compared to *Rosa^{DTR}* mice based on BUN, Creatinine and neutrophil infiltration, but results need to be confirmed with a higher number of biological replicates. We also noticed a higher number of monocytes after DC depletion. It should be considered that depletion of DCs for example with *CD11c^{DTR}* or other models lead to monocytosis and neutrophilia in different organs (Salvermoser et al., 2018; van Blijswijk et al., 2013). It is therefore possible that higher monocytes and neutrophil numbers in *Clec9a^{Cre}Rosa^{DTR}* mice are not correlating with disease induction but are rather lasting effects of DT mediated DC depletion. In general, our observations are in line with what was published by Tadagavadi *et al.* based on depletion using *CD11c^{DTR}* (Tadagavadi & Reeves, 2010b). It should be mentioned that we used a lower dose of cisplatin compared to other studies because disease induction with higher doses of cisplatin was too severe in our hands (data not shown). This could explain why BUN and Creatinine levels are lower

compared to Tadagavadi *et al.* (Tadagavadi & Reeves, 2010b). Moreover, we used mice homozygous for Cre which causes a complete knockout of *Clec9a* expression. *Clec9a* and its protein DNGR1 were shown to play a dampening role during *Candida* infection (Del Fresno *et al.*, 2018). Although it is unlikely that DNGR1 plays a role in our model of cisplatin-induced AKI, we cannot exclude effects of a DNGR1 knockout on cisplatin-induced AKI based on our experimental setup.

4.5. cDC1 are dispensable in cisplatin-induced AKI

To date the precise role of DC subsets remains ill-defined during acute kidney injury because of substantial phenotypic overlap between renal mononuclear phagocytes and a lack of subset specific studies. Therefore, this work aimed to utilize *XCR1^{Venus-DTR}* mice and *Clec9a^{Cre}Rosa^{DTR}* mice in combination with cisplatin-induced AKI to decipher the role of the DC lineage and cDC1 in particular during kidney disease. We showed that depletion of cDC1 was still visible 96 h after DT depletion but did not have an influence on disease severity or weight loss. Analysis of myeloid populations only showed a decrease in infiltrating neutrophils in *XCR1^{Venus-DTR}* mice. This could indicate less severe kidney damage since induction of kidney damage is usually followed by infiltration of neutrophils in cisplatin-induced AKI (Tadagavadi & Reeves, 2010b). cDC1 were implicated to have a protective role during glomerular nephritis through induction of IL10-producing Tregs and regulation of CXCL2 production by cDC2s (Brähler *et al.*, 2017; Evers *et al.*, 2016). On the other hand, induction of CD8⁺ T cells by CD103⁺ cDC1 during Adriamycin-induced kidney injury leads to an exacerbation of the disease (Cao *et al.*, 2016). Additionally, the study was based on a *Batf3^{-/-}* model to deplete cDC1. BATF3 is an important regulator in CD4⁺ T cells and *Batf3^{-/-}* mice were shown to have increased amounts of Tregs (W. Lee, Kim, Hwang, & Lee, 2017). Tregs were shown to be dampen kidney injury in a variety of diseases including cisplatin-induced AKI, IRI and glomerular nephritis (Alikhan, Huynh, Kitching, & Ooi, 2018; do Valle Duraes *et al.*, 2020; H. Lee *et al.*, 2010). We did not identify altered numbers of CD4⁺Foxp3⁺ in *XCR1^{Venus-DTR}* mice compared to WT controls 72 h after cisplatin-induce AKI and we also did not see changes of disease severity upon cDC1 depletion. We did find an increase of CD127⁺ ILCs among live cells and recent studies showed that expansion of ILC2s via injection of a combination of IL2 and IL33 protected from cisplatin-induced AKI (Stremaska *et al.*, 2017). Whether

cDC1 play a role in maintaining ILC populations in the kidney is currently unknown. It will be important for future studies to compare ILC numbers to non-cisplatin-injected control since it is possible that these populations are just decreased to a greater extent in WT mice due to a higher induction of kidney damage. Overall it seems that cDC1 do not play a role in cisplatin-induced AKI. Considering the ability of cDC1 to maintain Tregs it will be important to look at the consequences of cDC1 depletion on the recovery phase after kidney injury. To achieve this, cisplatin could be injected repeatedly at lower doses to induce non-lethal AKI or studies could be performed in established lower models studying the recovery process after kidney damage such as unilateral IRI (Rogers et al., 2014; Sharp & Siskind, 2017).

4.6. Outlook

Future studies should improve on the Histo-Cytometry workflow to make this method more reliable in tissue where cells of interest are in close contact with each other. Possible approaches could be to use segmentation algorithms in 3D space, which could help segmenting cells which would otherwise overlap in a 2D image. Furthermore, inclusion of additional markers should improve segmentation overall and would also allow mask creation on additional markers. Since the amount of markers in traditional imaging techniques are usually limited by spectral overlap, novel imaging techniques circumvent this problem by sequential immunostaining for different markers with intermittent washing steps to remove bound antibodies (Bolognesi et al., 2017).

In light of our transcriptional analysis on F4/80^{hi} cells after cisplatin-induced AKI, further studies should be performed to verify the role of F4/80^{hi} cells and PGE2 during kidney injury. In vitro cultures of F4/80^{hi} cells could address the role of PGE2 directly on these cells. Additionally, use of *Ptger4^{flox}Ptger2^{KO}* mice crossed to a DC specific CRE mouse line such as *Clec9a^{Cre}* could be used to elucidate the role of PGE2 signalling in DCs during kidney injury (Kennedy et al., 1999; Schneider et al., 2004). Lastly, the CDP origin of F4/80^{hi} cells needs to be confirmed to strengthen the observation that F4/80^{hi} cells are indeed DCs. To achieve this CDPs could be transferred to mice after depletion of F4/80^{hi} cells in *Clec9a^{Cre}Rosa^{DTR}* mice to ensure niche-availability.

References

- Akashi, K., Traver, D., Miyamoto, T., & Weissman, I. L. (2000). A clonogenic common myeloid progenitor that gives rise to all myeloid lineages. *Nature*, *404*(6774), 193–197. <http://doi.org/10.1038/35004599>
- Alferink, J., Lieberam, I., Reindl, W., Behrens, A., Weiss, S., Hüser, N., et al. (2003). Compartmentalized production of CCL17 in vivo: strong inducibility in peripheral dendritic cells contrasts selective absence from the spleen. *Journal of Experimental Medicine*, *197*(5), 585–599. <http://doi.org/10.1084/jem.20021859>
- Aliberti, J., Schulz, O., Pennington, D. J., Tsujimura, H., Reis e Sousa, C., Ozato, K., & Sher, A. (2003). Essential role for ICSBP in the in vivo development of murine CD8alpha + dendritic cells. *Blood*, *101*(1), 305–310. <http://doi.org/10.1182/blood-2002-04-1088>
- Alikhan, M. A., Huynh, M., Kitching, A. R., & Ooi, J. D. (2018). Regulatory T cells in renal disease. *Clinical & Translational Immunology*, *7*(1), e1004. <http://doi.org/10.1002/cti2.1004>
- Aronoff, D. M., Canetti, C., & Peters-Golden, M. (2004). Prostaglandin E2 inhibits alveolar macrophage phagocytosis through an E-prostanoid 2 receptor-mediated increase in intracellular cyclic AMP. *The Journal of Immunology*, *173*(1), 559–565. <http://doi.org/10.4049/jimmunol.173.1.559>
- Asselin-Paturel, C., Boonstra, A., Dalod, M., Durand, I., Yessaad, N., Dezutter-Dambuyant, C., et al. (2001). Mouse type I IFN-producing cells are immature APCs with plasmacytoid morphology. *Nature Immunology*, *2*(12), 1144–1150. <http://doi.org/10.1038/ni736>
- Auffray, C., Fogg, D. K., Narni-Mancinelli, E., Senechal, B., Trouillet, C., Saederup, N., et al. (2009). CX3CR1+ CD115+ CD135+ common macrophage/DC precursors and the role of CX3CR1 in their response to inflammation. *The Journal of Experimental Medicine*, *206*(3), 595–606. <http://doi.org/10.1084/jem.20081385>
- Austyn, J. M., & Gordon, S. (1981). F4/80, a monoclonal antibody directed specifically against the mouse macrophage. *European Journal of Immunology*, *11*(10), 805–815. <http://doi.org/10.1002/eji.1830111013>
- Bacher, R., & Kendzioriski, C. (2016). Design and computational analysis of single-cell RNA-sequencing experiments. *Genome Biology*, *17*(1), 63–14. <http://doi.org/10.1186/s13059-016-0927-y>
- Bajénoff, M., Glaichenhaus, N., & Germain, R. N. (2008). Fibroblastic reticular cells guide T lymphocyte entry into and migration within the splenic T cell zone. *Journal of Immunology (Baltimore, Md. : 1950)*, *181*(6), 3947–3954.
- Bao, Y.-W., Yuan, Y., Chen, J.-H., & Lin, W.-Q. (2018). Kidney disease models: tools to identify mechanisms and potential therapeutic targets. *Zoological Research*, *39*(2), 72–86. <http://doi.org/10.24272/j.issn.2095-8137.2017.055>
- Berry, M. R., Mathews, R. J., Ferdinand, J. R., Jing, C., Loudon, K. W., Wlodek, E., et al. (2017). Renal Sodium Gradient Orchestrates a Dynamic Antibacterial Defense Zone. *Cell*, *170*(5), 860–874.e19. <http://doi.org/10.1016/j.cell.2017.07.022>
- Bertrand, J. Y., Chi, N. C., Santoso, B., Teng, S., Stainier, D. Y. R., & Traver, D. (2010). Haematopoietic stem cells derive directly from aortic endothelium during development. *Nature*, *464*(7285), 108–111. <http://doi.org/10.1038/nature08738>
- Bolognesi, M. M., Manzoni, M., Scalia, C. R., Zannella, S., Bosisio, F. M., Faretta, M., & Cattoretti, G. (2017). Multiplex Staining by Sequential Immunostaining and Antibody Removal on Routine Tissue Sections. *The Journal of Histochemistry and Cytochemistry : Official Journal of the Histochemistry Society*, *65*(8), 431–444. <http://doi.org/10.1369/0022155417719419>
- Boss, J. M., & Jensen, P. E. (2003). Transcriptional regulation of the MHC class II antigen presentation pathway. *Current Opinion in Immunology*, *15*(1), 105–111. [http://doi.org/10.1016/s0952-7915\(02\)00015-8](http://doi.org/10.1016/s0952-7915(02)00015-8)
- Brasel, K., De Smedt, T., Smith, J. L., & Maliszewski, C. R. (2000). Generation of murine dendritic cells from flt3-ligand-supplemented bone marrow cultures. *Blood*, *96*(9), 3029–3039.
- Brähler, S., Zinselmeyer, B. H., Raju, S., Nitschke, M., Suleiman, H., Saunders, B. T., et al. (2017). Opposing Roles of Dendritic Cell Subsets in Experimental GN. *Journal of the American Society of Nephrology : JASN*, *29*(1), 138–154. <http://doi.org/10.1681/ASN.2017030270>
- Briseño, C. G., Satpathy, A. T., Davidson, J. T., Ferris, S. T., Durai, V., Bagadia, P., et al. (2018). Notch2-dependent DC2s mediate splenic germinal center responses. *Proceedings of the National Academy of Sciences of the United States of America*, *115*(42), 10726–10731. <http://doi.org/10.1073/pnas.1809925115>

- Buch, T., Heppner, F. L., Tertilt, C., Heinen, T. J. A. J., Kremer, M., Wunderlich, F. T., et al. (2005). A Cre-inducible diphtheria toxin receptor mediates cell lineage ablation after toxin administration. *Nature Methods*, 2(6), 419–426. <http://doi.org/10.1038/nmeth762>
- Caminschi, I., Proietto, A. I., Ahmet, F., Kitsoulis, S., Shin Teh, J., Lo, J. C. Y., et al. (2008). The dendritic cell subtype-restricted C-type lectin Clec9A is a target for vaccine enhancement. *Blood*, 112(8), 3264–3273. <http://doi.org/10.1182/blood-2008-05-155176>
- Cao, Q., Lu, J., Li, Q., Wang, C., Wang, X. M., Lee, V. W. S., et al. (2016). CD103+ Dendritic Cells Elicit CD8+ T Cell Responses to Accelerate Kidney Injury in Adriamycin Nephropathy. *Journal of the American Society of Nephrology : JASN*, 27(5), 1344–1360. <http://doi.org/10.1681/ASN.2015030229>
- Cao, Q., Wang, Y., Wang, X. M., Lu, J., Lee, V. W. S., Ye, Q., et al. (2015). Renal F4/80+ CD11c+ mononuclear phagocytes display phenotypic and functional characteristics of macrophages in health and in adriamycin nephropathy. *Journal of the American Society of Nephrology : JASN*, 26(2), 349–363. <http://doi.org/10.1681/ASN.2013121336>
- Caton, M. L., Smith-Raska, M. R., & Reizis, B. (2007). Notch-RBP-J signaling controls the homeostasis of CD8- dendritic cells in the spleen. *Journal of Experimental Medicine*, 204(7), 1653–1664. <http://doi.org/10.1084/jem.20062648>
- Cecchini, M. G., Dominguez, M. G., Mocci, S., Wetterwald, A., Felix, R., Fleisch, H., et al. (1994). Role of colony stimulating factor-1 in the establishment and regulation of tissue macrophages during postnatal development of the mouse. *Development*, 120(6), 1357–1372.
- Chan, A. J., Alikhan, M. A., Odobasic, D., Gan, P. Y., Khouri, M. B., Steinmetz, O. M., et al. (2014). Innate IL-17A-producing leukocytes promote acute kidney injury via inflammasome and Toll-like receptor activation. *The American Journal of Pathology*, 184(5), 1411–1418. <http://doi.org/10.1016/j.ajpath.2014.01.023>
- Chen, S., Fu, H., Wu, S., Zhu, W., Liao, J., Hong, X., et al. (2019). Tenascin-C protects against acute kidney injury by recruiting Wnt ligands. *Kidney International*, 95(1), 62–74. <http://doi.org/10.1016/j.kint.2018.08.029>
- Chessa, F., Mathow, D., Wang, S., Hielscher, T., Atzberger, A., Porubsky, S., et al. (2016). The renal microenvironment modifies dendritic cell phenotype. *Kidney International*, 89(1), 82–94. <http://doi.org/10.1038/ki.2015.292>
- Ciarimboli, G., Deuster, D., Knief, A., Sperling, M., Holtkamp, M., Edemir, B., et al. (2010). Organic cation transporter 2 mediates cisplatin-induced oto- and nephrotoxicity and is a target for protective interventions. *The American Journal of Pathology*, 176(3), 1169–1180. <http://doi.org/10.2353/ajpath.2010.090610>
- Cisse, B., Caton, M. L., Lehner, M., Maeda, T., Scheu, S., Locksley, R., et al. (2008). Transcription factor E2-2 is an essential and specific regulator of plasmacytoid dendritic cell development. *Cell*, 135(1), 37–48. <http://doi.org/10.1016/j.cell.2008.09.016>
- Clausen, B. E., Burkhardt, C., Reith, W., Renkawitz, R., & Förster, I. (1999). Conditional gene targeting in macrophages and granulocytes using LysMcre mice. *Transgenic Research*, 8(4), 265–277. <http://doi.org/10.1023/a:1008942828960>
- Côté, S. C., Pasvanis, S., Bounou, S., & Dumais, N. (2009). CCR7-specific migration to CCL19 and CCL21 is induced by PGE2 stimulation in human monocytes: Involvement of EP2/EP4 receptors activation. *Molecular Immunology*, 46(13), 2682–2693. <http://doi.org/10.1016/j.molimm.2008.08.269>
- Cronk, J. C., Filiano, A. J., Louveau, A., Marin, I., Marsh, R., Ji, E., et al. (2018). Peripherally derived macrophages can engraft the brain independent of irradiation and maintain an identity distinct from microglia. *The Journal of Experimental Medicine*, 215(6), 1627–1647. <http://doi.org/10.1084/jem.20180247>
- Crowley, M., Inaba, K., Witmer-Pack, M., & Steinman, R. M. (1989). The cell surface of mouse dendritic cells: FACS analyses of dendritic cells from different tissues including thymus. *Cellular Immunology*, 118(1), 108–125. [http://doi.org/10.1016/0008-8749\(89\)90361-4](http://doi.org/10.1016/0008-8749(89)90361-4)
- Dai, X.-M., Ryan, G. R., Hapel, A. J., Dominguez, M. G., Russell, R. G., Kapp, S., et al. (2002). Targeted disruption of the mouse colony-stimulating factor 1 receptor gene results in osteopetrosis, mononuclear phagocyte deficiency, increased primitive progenitor cell frequencies, and reproductive defects. *Blood*, 99(1), 111–120. <http://doi.org/10.1182/blood.v99.1.111>
- Dasari, S., & Tchounwou, P. B. (2014). Cisplatin in cancer therapy: molecular mechanisms of action. *European Journal of Pharmacology*, 740, 364–378. <http://doi.org/10.1016/j.ejphar.2014.07.025>
- Del Fresno, C., Saz-Leal, P., Enamorado, M., Wculek, S. K., Martínez-Cano, S., Blanco-Menéndez, N., et al. (2018). DNGR-1 in dendritic cells limits tissue damage by dampening neutrophil

- recruitment. *Science (New York, N.Y.)*, 362(6412), 351–356.
<http://doi.org/10.1126/science.aan8423>
- del Rio, M.-L., Rodriguez-Barbosa, J.-I., Kremmer, E., & Förster, R. (2007). CD103- and CD103+ bronchial lymph node dendritic cells are specialized in presenting and cross-presenting innocuous antigen to CD4+ and CD8+ T cells. *The Journal of Immunology*, 178(11), 6861–6866.
<http://doi.org/10.4049/jimmunol.178.11.6861>
- Deng, B., Lin, Y., Chen, Y., Ma, S., Cai, Q., Wang, W., et al. (2020). Plasmacytoid dendritic cells promote acute kidney injury by producing interferon- α . *Cellular & Molecular Immunology*, 386, 1465. <http://doi.org/10.1038/s41423-019-0343-9>
- do Valle Duraes, F., Lafont, A., Beibel, M., Martin, K., Darribat, K., Cuttat, R., et al. (2020). Immune cell landscaping reveals a protective role for regulatory T cells during kidney injury and fibrosis. *JCI Insight*, 5(3), S146. <http://doi.org/10.1172/jci.insight.130651>
- Dobin, A., Davis, C. A., Schlesinger, F., Drenkow, J., Zaleski, C., Jha, S., et al. (2013). STAR: ultrafast universal RNA-seq aligner. *Bioinformatics (Oxford, England)*, 29(1), 15–21.
<http://doi.org/10.1093/bioinformatics/bts635>
- Dong, X., Swaminathan, S., Bachman, L. A., Croatt, A. J., Nath, K. A., & Griffin, M. D. (2005). Antigen presentation by dendritic cells in renal lymph nodes is linked to systemic and local injury to the kidney. *Kidney International*, 68(3), 1096–1108. <http://doi.org/10.1111/j.1523-1755.2005.00502.x>
- Dong, X., Swaminathan, S., Bachman, L. A., Croatt, A. J., Nath, K. A., & Griffin, M. D. (2007). Resident dendritic cells are the predominant TNF-secreting cell in early renal ischemia-reperfusion injury. *Kidney International*, 71(7), 619–628. <http://doi.org/10.1038/sj.ki.5002132>
- Dorner, B. G., Dorner, M. B., Zhou, X., Opitz, C., Mora, A., Güttler, S., et al. (2009). Selective expression of the chemokine receptor XCR1 on cross-presenting dendritic cells determines cooperation with CD8+ T cells. *Immunity*, 31(5), 823–833.
<http://doi.org/10.1016/j.immuni.2009.08.027>
- Dudziak, D., Kamphorst, A. O., Heidkamp, G. F., Buchholz, V. R., Trumpfheller, C., Yamazaki, S., et al. (2007). Differential antigen processing by dendritic cell subsets in vivo. *Science (New York, N.Y.)*, 315(5808), 107–111. <http://doi.org/10.1126/science.1136080>
- Erblich, B., Zhu, L., Etgen, A. M., Dobrenis, K., & Pollard, J. W. (2011). Absence of colony stimulation factor-1 receptor results in loss of microglia, disrupted brain development and olfactory deficits. *PloS One*, 6(10), e26317. <http://doi.org/10.1371/journal.pone.0026317>
- Evers, B. D. G., Engel, D. R., Böhner, A. M. C., Tittel, A. P., Krause, T. A., Heuser, C., et al. (2016). CD103+ Kidney Dendritic Cells Protect against Crescentic GN by Maintaining IL-10-Producing Regulatory T Cells. *Journal of the American Society of Nephrology : JASN*, 27(11), 3368–3382.
<http://doi.org/10.1681/ASN.2015080873>
- Ferenbach, D. A., Sheldrake, T. A., Dhaliwal, K., Kipari, T. M. J., Marson, L. P., Kluth, D. C., & Hughes, J. (2012). Macrophage/monocyte depletion by clodronate, but not diphtheria toxin, improves renal ischemia/reperfusion injury in mice. *Kidney International*, 82(8), 928–933.
<http://doi.org/10.1038/ki.2012.207>
- Fogg, D. K., Sibon, C., Miled, C., Jung, S., Aucouturier, P., Littman, D. R., et al. (2006). A clonogenic bone marrow progenitor specific for macrophages and dendritic cells. *Science (New York, N.Y.)*, 311(5757), 83–87. <http://doi.org/10.1126/science.1117729>
- Gautier, E. L., Shay, T., Miller, J., Greter, M., Jakubzick, C., Ivanov, S., et al. (2012). Gene-expression profiles and transcriptional regulatory pathways that underlie the identity and diversity of mouse tissue macrophages. *Nature Immunology*, 13(11), 1118–1128. <http://doi.org/10.1038/ni.2419>
- Gentek, R., Molawi, K., & Sieweke, M. H. (2014). Tissue macrophage identity and self-renewal. *Immunological Reviews*, 262(1), 56–73. <http://doi.org/10.1111/imr.12224>
- Germain, R. N., Bajénoff, M., Castellino, F., Chieppa, M., Egen, J. G., Huang, A. Y. C., et al. (2008). Making friends in out-of-the-way places: how cells of the immune system get together and how they conduct their business as revealed by intravital imaging. *Immunological Reviews*, 221(1), 163–181. <http://doi.org/10.1111/j.1600-065X.2008.00591.x>
- Gerner, M. Y., Kastenmuller, W., Ifrim, I., Kabat, J., & Germain, R. N. (2012). Histo-cytometry: a method for highly multiplex quantitative tissue imaging analysis applied to dendritic cell subset microanatomy in lymph nodes. *Immunity*, 37(2), 364–376.
<http://doi.org/10.1016/j.immuni.2012.07.011>
- Ginhoux, F., Greter, M., Leboeuf, M., Nandi, S., See, P., Gokhan, S., et al. (2010). Fate mapping analysis reveals that adult microglia derive from primitive macrophages. *Science (New York, N.Y.)*, 330(6005), 841–845. <http://doi.org/10.1126/science.1194637>

- Ginhoux, F., Liu, K., Helft, J., Bogunovic, M., Greter, M., Hashimoto, D., et al. (2009). The origin and development of nonlymphoid tissue CD103+ DCs. *The Journal of Experimental Medicine*, 206(13), 3115–3130. <http://doi.org/10.1084/jem.20091756>
- Glaser, S., Anastassiadis, K., & Stewart, A. F. (2005). Current issues in mouse genome engineering. *Nature Genetics*, 37(11), 1187–1193. <http://doi.org/10.1038/ng1668>
- Gomez-Perdiguero, E., Klapproth, K., Schulz, C., Busch, K., Azzoni, E., Crozet, L., et al. (2015). Tissue-resident macrophages originate from yolk-sac-derived erythro-myeloid progenitors. *Nature*, 518(7540), 547–551. <http://doi.org/10.1038/nature13989>
- Gonzalez, J., Mouttalib, S., Delage, C., Calise, D., Maoret, J.-J., Pradère, J.-P., et al. (2013). Dual effect of chemokine CCL7/MCP-3 in the development of renal tubulointerstitial fibrosis. *Biochemical and Biophysical Research Communications*, 438(2), 257–263. <http://doi.org/10.1016/j.bbrc.2013.07.025>
- Grajales-Reyes, G. E., Iwata, A., Albring, J., Wu, X., Tussiwand, R., KC, W., et al. (2015). Batf3 maintains autoactivation of Irf8 for commitment of a CD8 α (+) conventional DC clonogenic progenitor. *Nature Immunology*, 16(7), 708–717. <http://doi.org/10.1038/ni.3197>
- Guilliams, M., Dutertre, C.-A., Scott, C. L., McGovern, N., Sichien, D., Chakarov, S., et al. (2016). Unsupervised High-Dimensional Analysis Aligns Dendritic Cells across Tissues and Species. *Immunity*, 45(3), 669–684. <http://doi.org/10.1016/j.immuni.2016.08.015>
- Guilliams, M., Ginhoux, F., Jakubzick, C., Naik, S. H., Onai, N., Schraml, B. U., et al. (2014). Dendritic cells, monocytes and macrophages: a unified nomenclature based on ontogeny. *Nature Reviews. Immunology*, 14(8), 571–578. <http://doi.org/10.1038/nri3712>
- Haan, den, J. M., Lehar, S. M., & Bevan, M. J. (2000). CD8(+) but not CD8(-) dendritic cells cross-prime cytotoxic T cells in vivo. *Journal of Experimental Medicine*, 192(12), 1685–1696. <http://doi.org/10.1084/jem.192.12.1685>
- Hacker, C., Kirsch, R. D., Ju, X.-S., Hieronymus, T., Gust, T. C., Kuhl, C., et al. (2003). Transcriptional profiling identifies Id2 function in dendritic cell development. *Nature Immunology*, 4(4), 380–386. <http://doi.org/10.1038/ni903>
- Hara, T., & Tanegashima, K. (2012). Pleiotropic functions of the CXC-type chemokine CXCL14 in mammals. *Journal of Biochemistry*, 151(5), 469–476. <http://doi.org/10.1093/jb/mvs030>
- Hashimoto, D., Chow, A., Noizat, C., Teo, P., Beasley, M. B., Leboeuf, M., et al. (2013). Tissue-resident macrophages self-maintain locally throughout adult life with minimal contribution from circulating monocytes. *Immunity*, 38(4), 792–804. <http://doi.org/10.1016/j.immuni.2013.04.004>
- Hettinger, J., Richards, D. M., Hansson, J., Barra, M. M., Joschko, A.-C., Krijgsveld, J., & Feuerer, M. (2013). Origin of monocytes and macrophages in a committed progenitor. *Nature Immunology*, 14(8), 821–830. <http://doi.org/10.1038/ni.2638>
- Hildner, K., Edelson, B. T., Purtha, W. E., Diamond, M., Matsushita, H., Kohyama, M., et al. (2008). Batf3 deficiency reveals a critical role for CD8 α + dendritic cells in cytotoxic T cell immunity. *Science (New York, N.Y.)*, 322(5904), 1097–1100. <http://doi.org/10.1126/science.1164206>
- Hoeffel, G., Chen, J., Lavin, Y., Low, D., Almeida, F. F., See, P., et al. (2015). C-Myb(+) erythro-myeloid progenitor-derived fetal monocytes give rise to adult tissue-resident macrophages. *Immunity*, 42(4), 665–678. <http://doi.org/10.1016/j.immuni.2015.03.011>
- Holditch, S. J., Brown, C. N., Lombardi, A. M., Nguyen, K. N., & Edelstein, C. L. (2019). Recent Advances in Models, Mechanisms, Biomarkers, and Interventions in Cisplatin-Induced Acute Kidney Injury. *International Journal of Molecular Sciences*, 20(12), 3011. <http://doi.org/10.3390/ijms20123011>
- Hume, D. A., & Gordon, S. (1983). Mononuclear phagocyte system of the mouse defined by immunohistochemical localization of antigen F4/80. Identification of resident macrophages in renal medullary and cortical interstitium and the juxtaglomerular complex. *Journal of Experimental Medicine*, 157(5), 1704–1709.
- Ichikawa, E., Hida, S., Omatsu, Y., Shimoyama, S., Takahara, K., Miyagawa, S., et al. (2004). Defective development of splenic and epidermal CD4+ dendritic cells in mice deficient for IFN regulatory factor-2. *Proceedings of the National Academy of Sciences of the United States of America*, 101(11), 3909–3914. <http://doi.org/10.1073/pnas.0400610101>
- Ivashkiv, L. B., Ayres, A., & Glimcher, L. H. (1994). Inhibition of IFN-gamma induction of class II MHC genes by cAMP and prostaglandins. *Immunopharmacology*, 27(1), 67–77.
- Jia, Z., Wang, N., Aoyagi, T., Wang, H., Liu, H., & Yang, T. (2011). Amelioration of cisplatin nephrotoxicity by genetic or pharmacologic blockade of prostaglandin synthesis. *Kidney International*, 79(1), 77–88. <http://doi.org/10.1038/ki.2010.331>

- Jung, S., Unutmaz, D., Wong, P., Sano, G.-I., De los Santos, K., Sparwasser, T., et al. (2002). In Vivo Depletion of CD11c+ Dendritic Cells Abrogates Priming of CD8+ T Cells by Exogenous Cell-Associated Antigens. *Immunity*, 17(2), 211–220. [http://doi.org/10.1016/S1074-7613\(02\)00365-5](http://doi.org/10.1016/S1074-7613(02)00365-5)
- Kashyap, S., Osman, M., Ferguson, C. M., Nath, M. C., Roy, B., Lien, K. R., et al. (2018). Ccl2 deficiency protects against chronic renal injury in murine renovascular hypertension. *Scientific Reports*, 8(1), 8598. <http://doi.org/10.1038/s41598-018-26870-y>
- Kawakami, T., Lichtnekert, J., Thompson, L. J., Karna, P., Bouabe, H., Hohl, T. M., et al. (2013). Resident renal mononuclear phagocytes comprise five discrete populations with distinct phenotypes and functions. *Journal of Immunology (Baltimore, Md. : 1950)*, 191(6), 3358–3372. <http://doi.org/10.4049/jimmunol.1300342>
- Kennedy, C. R., Zhang, Y., Brandon, S., Guan, Y., Coffee, K., Funk, C. D., et al. (1999). Salt-sensitive hypertension and reduced fertility in mice lacking the prostaglandin EP2 receptor. *Nature Medicine*, 5(2), 217–220. <http://doi.org/10.1038/5583>
- Kim, M.-G., Boo, C. S., Ko, Y. S., Lee, H. Y., Cho, W. Y., Kim, H. K., & Jo, S.-K. (2010). Depletion of kidney CD11c+ F4/80+ cells impairs the recovery process in ischaemia/reperfusion-induced acute kidney injury. *Nephrology, Dialysis, Transplantation : Official Publication of the European Dialysis and Transplant Association - European Renal Association*, 25(9), 2908–2921. <http://doi.org/10.1093/ndt/gfq183>
- Kingston, D., Schmid, M. A., Onai, N., Obata-Onai, A., Baumjohann, D., & Manz, M. G. (2009). The concerted action of GM-CSF and Flt3-ligand on in vivo dendritic cell homeostasis. *Blood*, 114(4), 835–843. <http://doi.org/10.1182/blood-2009-02-206318>
- Kissa, K., & Herbomel, P. (2010). Blood stem cells emerge from aortic endothelium by a novel type of cell transition. *Nature*, 464(7285), 112–115. <http://doi.org/10.1038/nature08761>
- Kondo, M., Weissman, I. L., & Akashi, K. (1997). Identification of clonogenic common lymphoid progenitors in mouse bone marrow. *Cell*, 91(5), 661–672. [http://doi.org/10.1016/S0092-8674\(00\)80453-5](http://doi.org/10.1016/S0092-8674(00)80453-5)
- Langlet, C., Tamoutounour, S., Henri, S., Luche, H., Ardouin, L., Grégoire, C., et al. (2012). CD64 expression distinguishes monocyte-derived and conventional dendritic cells and reveals their distinct role during intramuscular immunization. *Journal of Immunology (Baltimore, Md. : 1950)*, 188(4), 1751–1760. <http://doi.org/10.4049/jimmunol.1102744>
- Lavin, Y., Winter, D., Blecher-Gonen, R., David, E., Keren-Shaul, H., Merad, M., et al. (2014). Tissue-resident macrophage enhancer landscapes are shaped by the local microenvironment. *Cell*, 159(6), 1312–1326. <http://doi.org/10.1016/j.cell.2014.11.018>
- Lee, H., Nho, D., Chung, H.-S., Lee, H., Shin, M.-K., Kim, S.-H., & Bae, H. (2010). CD4+CD25+ regulatory T cells attenuate cisplatin-induced nephrotoxicity in mice. *Kidney International*, 78(11), 1100–1109. <http://doi.org/10.1038/ki.2010.139>
- Lee, W., Kim, H. S., Hwang, S. S., & Lee, G. R. (2017). The transcription factor Batf3 inhibits the differentiation of regulatory T cells in the periphery. *Experimental & Molecular Medicine*, 49(11), e393–e393. <http://doi.org/10.1038/emm.2017.157>
- Lever, J. M., Hull, T. D., Boddu, R., Pepin, M. E., Black, L. M., Adedoyin, O. O., et al. (2019). Resident macrophages reprogram toward a developmental state after acute kidney injury. *JCI Insight*, 4(2), 833. <http://doi.org/10.1172/jci.insight.125503>
- Lewis, K. L., Caton, M. L., Bogunovic, M., Greter, M., Grajkowska, L. T., Ng, D., et al. (2011). Notch2 receptor signaling controls functional differentiation of dendritic cells in the spleen and intestine. *Immunity*, 35(5), 780–791. <http://doi.org/10.1016/j.immuni.2011.08.013>
- Li, B., & Dewey, C. N. (2011). RSEM: accurate transcript quantification from RNA-Seq data with or without a reference genome. *BMC Bioinformatics*, 12(1), 323. <http://doi.org/10.1186/1471-2105-12-323>
- Li, G., Harton, J. A., Zhu, X., & Ting, J. P. (2001). Downregulation of CIITA function by protein kinase a (PKA)-mediated phosphorylation: mechanism of prostaglandin E, cyclic AMP, and PKA inhibition of class II major histocompatibility complex expression in monocytic lines. *Molecular and Cellular Biology*, 21(14), 4626–4635. <http://doi.org/10.1128/MCB.21.14.4626-4635.2001>
- Li, L., Huang, L., Sung, S.-S. J., Vergis, A. L., Rosin, D. L., Rose, C. E., et al. (2008). The chemokine receptors CCR2 and CX3CR1 mediate monocyte/macrophage trafficking in kidney ischemia-reperfusion injury. *Kidney International*, 74(12), 1526–1537. <http://doi.org/10.1038/ki.2008.500>
- Li, W., Germain, R. N., & Gerner, M. Y. (2017). Multiplex, quantitative cellular analysis in large tissue volumes with clearing-enhanced 3D microscopy (Ce3D). *Proceedings of the National Academy of Sciences of the United States of America*, 114(35), E7321–E7330. <http://doi.org/10.1073/pnas.1708981114>

- Liu, K., Victora, G. D., Schwickert, T. A., Guermonprez, P., Meredith, M. M., Yao, K., et al. (2009). In vivo analysis of dendritic cell development and homeostasis. *Science (New York, N.Y.)*, 324(5925), 392–397. <http://doi.org/10.1126/science.1170540>
- Liu, Z., Gu, Y., Chakarov, S., Bleriot, C., Kwok, I., Chen, X., et al. (2019). Fate Mapping via Ms4a3-Expression History Traces Monocyte-Derived Cells. *Cell*, 178(6), 1509–1525.e19. <http://doi.org/10.1016/j.cell.2019.08.009>
- Lu, L. H., Oh, D.-J., Dursun, B., He, Z., Hoke, T. S., Faubel, S., & Edelstein, C. L. (2008). Increased macrophage infiltration and fractalkine expression in cisplatin-induced acute renal failure in mice. *The Journal of Pharmacology and Experimental Therapeutics*, 324(1), 111–117. <http://doi.org/10.1124/jpet.107.130161>
- Lu, X., Rudemiller, N. P., Privratsky, J. R., Ren, J., Wen, Y., Griffiths, R., & Crowley, S. D. (2019). Classical Dendritic Cells Mediate Hypertension by Promoting Renal Oxidative Stress and Fluid Retention. *Hypertension (Dallas, Tex. : 1979)*, 10, HYPERTENSIONAHA11913667. <http://doi.org/10.1161/HYPERTENSIONAHA.119.13667>
- Madisen, L., Zwingman, T. A., Sunkin, S. M., Oh, S. W., Zariwala, H. A., Gu, H., et al. (2010). A robust and high-throughput Cre reporting and characterization system for the whole mouse brain. *Nature Neuroscience*, 13(1), 133–140. <http://doi.org/10.1038/nn.2467>
- Malek, M., & Nematbakhsh, M. (2015). Renal ischemia/reperfusion injury; from pathophysiology to treatment. *Journal of Renal Injury Prevention*, 4(2), 20–27. <http://doi.org/10.12861/jrip.2015.06>
- Maraskovsky, E., Brasel, K., Teepe, M., Roux, E. R., Lyman, S. D., Shortman, K., & McKenna, H. J. (1996). Dramatic increase in the numbers of functionally mature dendritic cells in Flt3 ligand-treated mice: multiple dendritic cell subpopulations identified. *Journal of Experimental Medicine*, 184(5), 1953–1962. <http://doi.org/10.1084/jem.184.5.1953>
- Marschner, J. A., Schäfer, H., Holderied, A., & Anders, H.-J. (2016). Optimizing Mouse Surgery with Online Rectal Temperature Monitoring and Preoperative Heat Supply. Effects on Post-Ischemic Acute Kidney Injury. *PloS One*, 11(2), e0149489. <http://doi.org/10.1371/journal.pone.0149489>
- McKenna, H. J., Stocking, K. L., Miller, R. E., Brasel, K., De Smedt, T., Maraskovsky, E., et al. (2000). Mice lacking flt3 ligand have deficient hematopoiesis affecting hematopoietic progenitor cells, dendritic cells, and natural killer cells. *Blood*, 95(11), 3489–3497.
- Merad, M., Sathe, P., Helft, J., Miller, J., & Mortha, A. (2013). The dendritic cell lineage: ontogeny and function of dendritic cells and their subsets in the steady state and the inflamed setting. *Annual Review of Immunology*, 31(1), 563–604. <http://doi.org/10.1146/annurev-immunol-020711-074950>
- Meredith, M. M., Liu, K., Darrasse-Jèze, G., Kamphorst, A. O., Schreiber, H. A., Guermonprez, P., et al. (2012). Expression of the zinc finger transcription factor zDC (Zbtb46, Btbd4) defines the classical dendritic cell lineage. *The Journal of Experimental Medicine*, 209(6), 1153–1165. <http://doi.org/10.1084/jem.20112675>
- Metlay, J. P., Witmer-Pack, M. D., Agger, R., Crowley, M. T., Lawless, D., & Steinman, R. M. (1990). The distinct leukocyte integrins of mouse spleen dendritic cells as identified with new hamster monoclonal antibodies. *Journal of Experimental Medicine*, 171(5), 1753–1771. <http://doi.org/10.1084/jem.171.5.1753>
- Metzger, D., Clifford, J., Chiba, H., & Chambon, P. (1995). Conditional site-specific recombination in mammalian cells using a ligand-dependent chimeric Cre recombinase. *Proceedings of the National Academy of Sciences of the United States of America*, 92(15), 6991–6995. <http://doi.org/10.1073/pnas.92.15.6991>
- Mildner, A., & Jung, S. (2014). Development and function of dendritic cell subsets. *Immunity*, 40(5), 642–656. <http://doi.org/10.1016/j.immuni.2014.04.016>
- Miller, J. C., Brown, B. D., Shay, T., Gautier, E. L., Jojic, V., Cohain, A., et al. (2012). Deciphering the transcriptional network of the dendritic cell lineage. *Nature Immunology*, 13(9), 888–899. <http://doi.org/10.1038/ni.2370>
- Moreno, S. G. (2018). Depleting Macrophages In Vivo with Clodronate-Liposomes. *Methods in Molecular Biology (Clifton, N.J.)*, 1784(Chapter 23), 259–262. http://doi.org/10.1007/978-1-4939-7837-3_23
- Munro, D. A. D., & Hughes, J. (2017). The Origins and Functions of Tissue-Resident Macrophages in Kidney Development. *Frontiers in Physiology*, 8, 837. <http://doi.org/10.3389/fphys.2017.00837>
- Munro, D. A., Wineberg, Y., Tarnick, J., Vink, C. S., Li, Z., Pridans, C., et al. (2019). Macrophages restrict the nephrogenic field and promote endothelial connections during kidney development. *eLife*, 8, 663. <http://doi.org/10.7554/eLife.43271>
- Muzaki, A. R. B. M., Tetlak, P., Sheng, J., Loh, S. C., Setiagani, Y. A., Poidinger, M., et al. (2016). Intestinal CD103(+)CD11b(-) dendritic cells restrain colitis via IFN-γ-induced anti-inflammatory

- response in epithelial cells. *Mucosal Immunology*, 9(2), 336–351. <http://doi.org/10.1038/mi.2015.64>
- Naik, S. H., Metcalf, D., van Nieuwenhuijze, A., Wicks, I., Wu, L., O'Keeffe, M., & Shortman, K. (2006). Intrasplenic steady-state dendritic cell precursors that are distinct from monocytes. *Nature Immunology*, 7(6), 663–671. <http://doi.org/10.1038/ni1340>
- Naik, S. H., Proietto, A. I., Wilson, N. S., Dakic, A., Schnorrer, P., Fuchsberger, M., et al. (2005). Cutting edge: generation of splenic CD8+ and CD8- dendritic cell equivalents in Fms-like tyrosine kinase 3 ligand bone marrow cultures. *The Journal of Immunology*, 174(11), 6592–6597. <http://doi.org/10.4049/jimmunol.174.11.6592>
- Nussenzweig, M. C., Steinman, R. M., Gutchinov, B., & Cohn, Z. A. (1980). Dendritic cells are accessory cells for the development of anti-trinitrophenyl cytotoxic T lymphocytes. *Journal of Experimental Medicine*, 152(4), 1070–1084. <http://doi.org/10.1084/jem.152.4.1070>
- Nussenzweig, M. C., Steinman, R. M., Unkeless, J. C., Witmer, M. D., Gutchinov, B., & Cohn, Z. A. (1981). Studies of the cell surface of mouse dendritic cells and other leukocytes. *Journal of Experimental Medicine*, 154(1), 168–187. <http://doi.org/10.1084/jem.154.1.168>
- Onai, N., Obata-Onai, A., Schmid, M. A., Ohteki, T., Jarrossay, D., & Manz, M. G. (2007). Identification of clonogenic common Flt3+M-CSFR+ plasmacytoid and conventional dendritic cell progenitors in mouse bone marrow. *Nature Immunology*, 8(11), 1207–1216. <http://doi.org/10.1038/ni1518>
- Ozkok, A., & Edelstein, C. L. (2014). Pathophysiology of cisplatin-induced acute kidney injury. *BioMed Research International*, 2014(91), 967826–17. <http://doi.org/10.1155/2014/967826>
- Pennini, M. E., Liu, Y., Yang, J., Croniger, C. M., Boom, W. H., & Harding, C. V. (2007). CCAAT/Enhancer-Binding Protein β and δ Binding to CIITA Promoters Is Associated with the Inhibition of CIITA Expression in Response to Mycobacterium tuberculosis 19-kDa Lipoprotein. *The Journal of Immunology*, 179(10), 6910–6918. <http://doi.org/10.4049/jimmunol.179.10.6910>
- Persson, E. K., Uronen-Hansson, H., Semmrich, M., Rivollier, A., Hägerbrand, K., Marsal, J., et al. (2013). IRF4 transcription-factor-dependent CD103(+)CD11b(+) dendritic cells drive mucosal T helper 17 cell differentiation. *Immunity*, 38(5), 958–969. <http://doi.org/10.1016/j.immuni.2013.03.009>
- Piva, L., Tetlak, P., Claser, C., Karjalainen, K., Renia, L., & Ruedl, C. (2012). Cutting edge: Clec9A+ dendritic cells mediate the development of experimental cerebral malaria. *Journal of Immunology (Baltimore, Md. : 1950)*, 189(3), 1128–1132. <http://doi.org/10.4049/jimmunol.1201171>
- Poltorak, M. P., & Schraml, B. U. (2015). Fate mapping of dendritic cells. *Frontiers in Immunology*, 6, 199. <http://doi.org/10.3389/fimmu.2015.00199>
- Poulin, L. F., Reyat, Y., Uronen-Hansson, H., Schraml, B. U., Sancho, D., Murphy, K. M., et al. (2012). DNGR-1 is a specific and universal marker of mouse and human Batf3-dependent dendritic cells in lymphoid and nonlymphoid tissues. *Blood*, 119(25), 6052–6062. <http://doi.org/10.1182/blood-2012-01-406967>
- Probst, H. C., Tschannen, K., Odermatt, B., Schwendener, R., Zinkernagel, R. M., & Van Den Broek, M. (2005). Histological analysis of CD11c-DTR/GFP mice after in vivo depletion of dendritic cells. *Clinical and Experimental Immunology*, 141(3), 398–404. <http://doi.org/10.1111/j.1365-2249.2005.02868.x>
- Puranik, A. S., Leaf, I. A., Jensen, M. A., Hedayat, A. F., Saad, A., Kim, K.-W., et al. (2018). Kidney-resident macrophages promote a proangiogenic environment in the normal and chronically ischemic mouse kidney. *Scientific Reports*, 8(1), 13948. <http://doi.org/10.1038/s41598-018-31887-4>
- Ramesh, G., & Reeves, W. B. (2002). TNF-alpha mediates chemokine and cytokine expression and renal injury in cisplatin nephrotoxicity. *The Journal of Clinical Investigation*, 110(6), 835–842. <http://doi.org/10.1172/JCI15606>
- Reis e Sousa, C., Hieny, S., Scharon-Kersten, T., Jankovic, D., Charest, H., Germain, R. N., & Sher, A. (1997). In vivo microbial stimulation induces rapid CD40 ligand-independent production of interleukin 12 by dendritic cells and their redistribution to T cell areas. *Journal of Experimental Medicine*, 186(11), 1819–1829. <http://doi.org/10.1084/jem.186.11.1819>
- Rogers, N. M., Ferenbach, D. A., Isenberg, J. S., Thomson, A. W., & Hughes, J. (2014). Dendritic cells and macrophages in the kidney: a spectrum of good and evil. *Nature Reviews. Nephrology*, 10(11), 625–643. <http://doi.org/10.1038/nrneph.2014.170>
- Saito, M., Iwawaki, T., Taya, C., Yonekawa, H., Noda, M., Inui, Y., et al. (2001). Diphtheria toxin receptor-mediated conditional and targeted cell ablation in transgenic mice. *Nature Biotechnology*, 19(8), 746–750. <http://doi.org/10.1038/90795>

- Salei, N.*, **Rambichler, S.***, Salvermoser, J., Papaioannou, N. E., Schuchert, R., Pakalniškytė, D., et al. (2020). The Kidney Contains Ontogenetically Distinct Dendritic Cell and Macrophage Subtypes throughout Development That Differ in Their Inflammatory Properties. *Journal of the American Society of Nephrology : JASN*, 126, ASN.2019040419. <http://doi.org/10.1681/ASN.2019040419>
- *equal contribution**
- Salvermoser, J., van Blijswijk, J., Papaioannou, N. E., Rambichler, S., Pasztoi, M., Pakalniškytė, D., et al. (2018). Clec9a-Mediated Ablation of Conventional Dendritic Cells Suggests a Lymphoid Path to Generating Dendritic Cells In Vivo. *Frontiers in Immunology*, 9, 699. <http://doi.org/10.3389/fimmu.2018.00699>
- Sancho, D., Mourão-Sá, D., Joffre, O. P., Schulz, O., Rogers, N. C., Pennington, D. J., et al. (2008). Tumor therapy in mice via antigen targeting to a novel, DC-restricted C-type lectin. *The Journal of Clinical Investigation*, 118(6), 2098–2110. <http://doi.org/10.1172/JCI34584>
- Satpathy, A. T., KC, W., Albring, J. C., Edelson, B. T., Kretzer, N. M., Bhattacharya, D., et al. (2012). Zbtb46 expression distinguishes classical dendritic cells and their committed progenitors from other immune lineages. *The Journal of Experimental Medicine*, 209(6), 1135–1152. <http://doi.org/10.1084/jem.20120030>
- Schindelin, J., Arganda-Carreras, I., Frise, E., Kaynig, V., Longair, M., Pietzsch, T., et al. (2012). Fiji: an open-source platform for biological-image analysis. *Nature Methods*, 9(7), 676–682. <http://doi.org/10.1038/nmeth.2019>
- Schlitzer, A., McGovern, N., Teo, P., Zelante, T., Atarashi, K., Low, D., et al. (2013). IRF4 transcription factor-dependent CD11b+ dendritic cells in human and mouse control mucosal IL-17 cytokine responses. *Immunity*, 38(5), 970–983. <http://doi.org/10.1016/j.immuni.2013.04.011>
- Schlitzer, A., Sivakamasundari, V., Chen, J., Sumatoh, H. R. B., Schreuder, J., Lum, J., et al. (2015). Identification of cDC1- and cDC2-committed DC progenitors reveals early lineage priming at the common DC progenitor stage in the bone marrow. *Nature Immunology*, 16(7), 718–728. <http://doi.org/10.1038/ni.3200>
- Schneider, A., Guan, Y., Zhang, Y., Magnuson, M. A., Pettepher, C., Loftin, C. D., et al. (2004). Generation of a conditional allele of the mouse prostaglandin EP4 receptor. *Genesis (New York, N.Y. : 2000)*, 40(1), 7–14. <http://doi.org/10.1002/gene.20048>
- Schraml, B. U., & Reis e Sousa, C. (2015). Defining dendritic cells. *Current Opinion in Immunology*, 32, 13–20. <http://doi.org/10.1016/j.coi.2014.11.001>
- Schraml, B. U., van Blijswijk, J., Zelenay, S., Whitney, P. G., Filby, A., Acton, S. E., et al. (2013). Genetic tracing via DNGR-1 expression history defines dendritic cells as a hematopoietic lineage. *Cell*, 154(4), 843–858. <http://doi.org/10.1016/j.cell.2013.07.014>
- Schulz, C., Gomez-Perdiguero, E., Chorro, L., Szabo-Rogers, H., Cagnard, N., Kierdorf, K., et al. (2012). A lineage of myeloid cells independent of Myb and hematopoietic stem cells. *Science (New York, N.Y.)*, 336(6077), 86–90. <http://doi.org/10.1126/science.1219179>
- Scott, C. L., T'Jonck, W., Martens, L., Todorov, H., Sichien, D., Soen, B., et al. (2018). The Transcription Factor ZEB2 Is Required to Maintain the Tissue-Specific Identities of Macrophages. *Immunity*, 49(2), 312–325.e5. <http://doi.org/10.1016/j.immuni.2018.07.004>
- See, P., Dutertre, C.-A., Chen, J., Günther, P., McGovern, N., Irac, S. E., et al. (2017). Mapping the human DC lineage through the integration of high-dimensional techniques. *Science (New York, N.Y.)*, 356(6342), eaag3009. <http://doi.org/10.1126/science.aag3009>
- Shaner, N. C., Steinbach, P. A., & Tsien, R. Y. (2005). A guide to choosing fluorescent proteins. *Nature Methods*, 2(12), 905–909. <http://doi.org/10.1038/nmeth819>
- Sharp, C. N., & Siskind, L. J. (2017). Developing better mouse models to study cisplatin-induced kidney injury. *American Journal of Physiology. Renal Physiology*, 313(4), F835–F841. <http://doi.org/10.1152/ajprenal.00285.2017>
- Shin, C., Han, J.-A., Choi, B., Cho, Y.-K., Do, Y., & Ryu, S. (2016). Intrinsic features of the CD8α(-) dendritic cell subset in inducing functional T follicular helper cells. *Immunology Letters*, 172, 21–28. <http://doi.org/10.1016/j.imlet.2016.01.009>
- Siegal, F. P., Kadowaki, N., Shodell, M., Fitzgerald-Bocarsly, P. A., Shah, K., Ho, S., et al. (1999). The nature of the principal type 1 interferon-producing cells in human blood. *Science (New York, N.Y.)*, 284(5421), 1835–1837.
- Soos, T. J., Sims, T. N., Barisoni, L., Lin, K., Littman, D. R., Dustin, M. L., & Nelson, P. J. (2006). CX3CR1+ interstitial dendritic cells form a contiguous network throughout the entire kidney. *Kidney International*, 70(3), 591–596. <http://doi.org/10.1038/sj.ki.5001567>

- Srinivas, S., Watanabe, T., Lin, C. S., William, C. M., Tanabe, Y., Jessell, T. M., & Costantini, F. (2001). Cre reporter strains produced by targeted insertion of EYFP and ECFP into the ROSA26 locus. *BMC Developmental Biology*, *1*(1), 4. <http://doi.org/10.1186/1471-213x-1-4>
- Stamatiades, E. G., Tremblay, M.-E., Bohm, M., Crozet, L., Bisht, K., Kao, D., et al. (2016). Immune Monitoring of Trans-endothelial Transport by Kidney-Resident Macrophages. *Cell*, *166*(4), 991–1003. <http://doi.org/10.1016/j.cell.2016.06.058>
- Steinman, R. M., & Cohn, Z. A. (1973). Identification of a novel cell type in peripheral lymphoid organs of mice. *Journal of Experimental Medicine*, *137*(5), 1142–1162. <http://doi.org/10.1084/jem.137.5.1142>
- Steinman, R. M., & Witmer, M. D. (1978). Lymphoid dendritic cells are potent stimulators of the primary mixed leukocyte reaction in mice. *Proceedings of the National Academy of Sciences of the United States of America*, *75*(10), 5132–5136. <http://doi.org/10.1073/pnas.75.10.5132>
- Stremaska, M. E., Jose, S., Sabapathy, V., Huang, L., Bajwa, A., Kinsey, G. R., et al. (2017). IL233, A Novel IL-2 and IL-33 Hybrid Cytokine, Ameliorates Renal Injury. *Journal of the American Society of Nephrology : JASN*, *28*(9), 2681–2693. <http://doi.org/10.1681/ASN.2016121272>
- Suzuki, S., Honma, K., Matsuyama, T., Suzuki, K., Toriyama, K., Akitoyo, I., et al. (2004). Critical roles of interferon regulatory factor 4 in CD11bhighCD8alpha- dendritic cell development. *Proceedings of the National Academy of Sciences of the United States of America*, *101*(24), 8981–8986. <http://doi.org/10.1073/pnas.0402139101>
- Tadagavadi, R. K., & Reeves, W. B. (2010a). Endogenous IL-10 attenuates cisplatin nephrotoxicity: role of dendritic cells. *Journal of Immunology (Baltimore, Md. : 1950)*, *185*(8), 4904–4911. <http://doi.org/10.4049/jimmunol.1000383>
- Tadagavadi, R. K., & Reeves, W. B. (2010b). Renal dendritic cells ameliorate nephrotoxic acute kidney injury. *Journal of the American Society of Nephrology : JASN*, *21*(1), 53–63. <http://doi.org/10.1681/ASN.2009040407>
- Tadagavadi, R. K., Gao, G., Wang, W. W., Gonzalez, M. R., & Reeves, W. B. (2015). Dendritic Cell Protection from Cisplatin Nephrotoxicity Is Independent of Neutrophils. *Toxins*, *7*(8), 3245–3256. <http://doi.org/10.3390/toxins7083245>
- Tamoutounour, S., Henri, S., Lelouard, H., de Bovis, B., de Haar, C., van der Woude, C. J., et al. (2012). CD64 distinguishes macrophages from dendritic cells in the gut and reveals the Th1-inducing role of mesenteric lymph node macrophages during colitis. *European Journal of Immunology*, *42*(12), 3150–3166. <http://doi.org/10.1002/eji.201242847>
- Tanegashima, K., Takahashi, R., Nuriya, H., Iwase, R., Naruse, N., Tsuji, K., et al. (2017). CXCL14 Acts as a Specific Carrier of CpG DNA into Dendritic Cells and Activates Toll-like Receptor 9-mediated Adaptive Immunity. *EBioMedicine*, *24*, 247–256. <http://doi.org/10.1016/j.ebiom.2017.09.012>
- Tussiwand, R., Everts, B., Grajales-Reyes, G. E., Kretzer, N. M., Iwata, A., Bagaitkar, J., et al. (2015). Klf4 expression in conventional dendritic cells is required for T helper 2 cell responses. *Immunity*, *42*(5), 916–928. <http://doi.org/10.1016/j.immuni.2015.04.017>
- Uderhardt, S., Martins, A. J., Tsang, J. S., Lämmermann, T., & Germain, R. N. (2019). Resident Macrophages Cloak Tissue Microlesions to Prevent Neutrophil-Driven Inflammatory Damage. *Cell*, *177*(3), 541–555.e17. <http://doi.org/10.1016/j.cell.2019.02.028>
- van Blijswijk, J., Schraml, B. U., & Reis e Sousa, C. (2013). Advantages and limitations of mouse models to deplete dendritic cells. *European Journal of Immunology*, *43*(1), 22–26. <http://doi.org/10.1002/eji.201243022>
- van Blijswijk, J., Schraml, B. U., Rogers, N. C., Whitney, P. G., Zelenay, S., Acton, S. E., & Reis e Sousa, C. (2015). Altered lymph node composition in diphtheria toxin receptor-based mouse models to ablate dendritic cells. *Journal of Immunology (Baltimore, Md. : 1950)*, *194*(1), 307–315. <http://doi.org/10.4049/jimmunol.1401999>
- van Furth, R. (1981). IDENTIFICATION OF MONONUCLEAR PHAGOCYTES: OVERVIEW AND DEFINITIONS. In *Methods for Studying Mononuclear Phagocytes* (pp. 243–251). Academic Press. <http://doi.org/10.1016/B978-0-12-044220-1.50033-7>
- Van Rooijen, N., & Sanders, A. (1994). Liposome mediated depletion of macrophages: mechanism of action, preparation of liposomes and applications. *Journal of Immunological Methods*, *174*(1-2), 83–93. [http://doi.org/10.1016/0022-1759\(94\)90012-4](http://doi.org/10.1016/0022-1759(94)90012-4)
- Volarevic, V., Djokovic, B., Jankovic, M. G., Harrell, C. R., Fellabaum, C., Djonov, V., & Arsenijevic, N. (2019). Molecular mechanisms of cisplatin-induced nephrotoxicity: a balance on the knife edge between renoprotection and tumor toxicity. *Journal of Biomedical Science*, *26*(1), 25–14. <http://doi.org/10.1186/s12929-019-0518-9>

- Vorhagen, S., Jackow, J., Mohor, S. G., Tanghe, G., Tanrikulu, L., Skazik-Vogt, C., & Tellkamp, F. (2015). Lineage tracing mediated by cre-recombinase activity. *The Journal of Investigative Dermatology*, *135*(1), 1–4. <http://doi.org/10.1038/jid.2014.472>
- Vremec, D., Zorbas, M., Scollay, R., Saunders, D. J., Ardavin, C. F., Wu, L., & Shortman, K. (1992). The surface phenotype of dendritic cells purified from mouse thymus and spleen: investigation of the CD8 expression by a subpopulation of dendritic cells. *Journal of Experimental Medicine*, *176*(1), 47–58. <http://doi.org/10.1084/jem.176.1.47>
- Wang, Y., Szretter, K. J., Vermi, W., Gilfillan, S., Rossini, C., Cella, M., et al. (2012). IL-34 is a tissue-restricted ligand of CSF1R required for the development of Langerhans cells and microglia. *Nature Immunology*, *13*(8), 753–760. <http://doi.org/10.1038/ni.2360>
- Waskow, C., Liu, K., Darrasse-Jèze, G., Guermonprez, P., Ginhoux, F., Merad, M., et al. (2008). The receptor tyrosine kinase Flt3 is required for dendritic cell development in peripheral lymphoid tissues. *Nature Immunology*, *9*(6), 676–683. <http://doi.org/10.1038/ni.1615>
- Weisheit, C. K., Engel, D. R., & Kurts, C. (2015). Dendritic Cells and Macrophages: Sentinels in the Kidney. *Clinical Journal of the American Society of Nephrology : CJASN*, *10*(10), 1841–1851. <http://doi.org/10.2215/CJN.07100714>
- Wu, L., D'Amico, A., Winkel, K. D., Suter, M., Lo, D., & Shortman, K. (1998). RelB is essential for the development of myeloid-related CD8alpha- dendritic cells but not of lymphoid-related CD8alpha+ dendritic cells. *Immunity*, *9*(6), 839–847. [http://doi.org/10.1016/s1074-7613\(00\)80649-4](http://doi.org/10.1016/s1074-7613(00)80649-4)
- Yamazaki, C., Sugiyama, M., Ohta, T., Hemmi, H., Hamada, E., Sasaki, I., et al. (2013). Critical roles of a dendritic cell subset expressing a chemokine receptor, XCR1. *Journal of Immunology (Baltimore, Md. : 1950)*, *190*(12), 6071–6082. <http://doi.org/10.4049/jimmunol.1202798>
- Yatim, K. M., Gosto, M., Humar, R., Williams, A. L., & Oberbarnscheidt, M. H. (2016). Renal dendritic cells sample blood-borne antigen and guide T-cell migration to the kidney by means of intravascular processes. *Kidney International*, *90*(4), 818–827. <http://doi.org/10.1016/j.kint.2016.05.030>
- Yona, S., Kim, K.-W., Wolf, Y., Mildner, A., Varol, D., Breker, M., et al. (2013). Fate mapping reveals origins and dynamics of monocytes and tissue macrophages under homeostasis. *Immunity*, *38*(1), 79–91. <http://doi.org/10.1016/j.immuni.2012.12.001>
- Zhang, B., Ramesh, G., Norbury, C. C., & Reeves, W. B. (2007). Cisplatin-induced nephrotoxicity is mediated by tumor necrosis factor-alpha produced by renal parenchymal cells. *Kidney International*, *72*(1), 37–44. <http://doi.org/10.1038/sj.ki.5002242>
- Zhu, A., Ibrahim, J. G., & Love, M. I. (2018). Heavy-tailed prior distributions for sequence count data: removing the noise and preserving large differences. *Bioinformatics (Oxford, England)*, *11*, R106. <http://doi.org/10.1093/bioinformatics/bty895>
- Zimmerman, K. A., Bentley, M. R., Lever, J. M., Li, Z., Crossman, D. K., Song, C. J., et al. (2019). Single-Cell RNA Sequencing Identifies Candidate Renal Resident Macrophage Gene Expression Signatures across Species. *Journal of the American Society of Nephrology : JASN*, *30*(5), 767–781. <http://doi.org/10.1681/ASN.2018090931>

Acknowledgements

First, I would like to thank Prof. Dr. Barbara Schraml for the opportunity to work in her group and for her excellent supervision, guidance and support during my project.

Furthermore, I would like to thank my thesis advisory committee, Prof. Dr. Gunnar Schotta and Prof. Dr. Christoph Scheiermann for their constructive feedback and guidance during my project.

Thank you to all group and institute members, especially Dalia Pakalniškytė, Nikolaos Papaioannou, Johanna Salvermoser and Vanessa Küntzel for their help and for making our lab a fun place to work in. Special thanks of course to Natallia Salei for making Team Kidney the best and most successful team in AG Schraml.

I also would like to thank the organizers of the SFB 914 and associated IRTG914 for financial support and excellent seminars, courses and retreats. In particular, I would like to thank Dr. Verena Kochan for all her help and her excellent coordination of the program.

Finally, I would like to thank Johanna, my family and my friends for support during my thesis. I may not have talked too much about work, but I always got the best advice and support when I needed it.

Appendix

Publications arising from this work:

Major parts of this thesis have been published in in the *Journal of the American Society of Nephrology*

Salei, N.*, **Rambichler, S.***, Salvermoser, J., Papaioannou, N. E., Schuchert, R., Pakalniškytė, D., et al. (2020). The Kidney Contains Ontogenetically Distinct Dendritic Cell and Macrophage Subtypes throughout Development That Differ in Their Inflammatory Properties. *Journal of the American Society of Nephrology : JASN*, 126, ASN.2019040419. <http://doi.org/10.1681/ASN.2019040419>
***equal contribution**

Other publications:

Salvermoser J, van Blijswijk J, Papaioannou NE, **Rambichler S**, et al. (2018). *Clec9a*-Mediated Ablation of Conventional Dendritic Cells Suggests a Lymphoid Path to Generating Dendritic Cells *In Vivo*. *Front Immunol*. 2018;9:699. <http://doi:10.3389/fimmu.2018.00699>

Kumaraswami K, Salei N, Beck S, **Rambichler S**, et al. (2020). A Simple and Effective Flow Cytometry-Based Method for Identification and Quantification of Tissue Infiltrated Leukocyte Subpopulations in a Mouse Model of Peripheral Arterial Disease. *Int J Mol Sci*. 2020;21(10):3593. <http://doi:10.3390/ijms21103593>



LUDWIG-
MAXIMILIANS-
UNIVERSITÄT
MÜNCHEN

Dean's Office
Medical Faculty



Affidavit

Rambichler, Stephan

Surname, first name

Street

Zip code, town

Germany

Country

I hereby declare, that the submitted thesis entitled

Localization and functional characterization of renal dendritic cell subsets during steady state and after acute kidney injury

is my own work. I have only used the sources indicated and have not made unauthorised use of services of a third party. Where the work of others has been quoted or reproduced, the source is always given.

I further declare that the submitted thesis or parts thereof have not been presented as part of an examination degree to any other university.

München, 22.07.2020

Place, date

Stephan Rambichler

Signature doctoral candidate



LUDWIG-
MAXIMILIANS-
UNIVERSITÄT
MÜNCHEN

Dean's Office
Medical Faculty



Confirmation of congruency between printed and electronic version of the doctoral thesis

Rambichler, Stephan

Surname, first name

Street

Zip code, town

Germany

Country

I hereby declare that the electronic version of the submitted thesis, entitled
Localization and functional characterization of renal dendritic cell subsets during steady state and after acute kidney injury

is congruent with the printed version both in content and format.

München, 22.07.2020

Place, date

Stephan Rambichler

Signature doctoral candidate